

# Higgs Scalars in the Minimal Non-minimal Supersymmetric Standard Model

C. Panagiotakopoulos<sup>a</sup> and A. Pilaftsis<sup>b</sup>

<sup>a</sup>*Physics Division, School of Technology, Aristotle University of Thessaloniki,  
54006 Thessaloniki, Greece*

<sup>b</sup>*Institut für Theoretische Physik, Universität Würzburg,  
Am Hubland, 97074 Würzburg, Germany*

## ABSTRACT

We consider the simplest and most economic version among the proposed non-minimal supersymmetric models, in which the  $\mu$ -parameter is promoted to a singlet superfield, whose all self-couplings are absent from the renormalizable superpotential. Such a particularly simple form of the renormalizable superpotential may be enforced by discrete  $R$ -symmetries which are extended to the gravity-induced non-renormalizable operators as well. We show explicitly that within the supergravity-mediated supersymmetry-breaking scenario, the potentially dangerous divergent tadpoles associated with the presence of the gauge singlet first appear at loop levels higher than 5 and therefore do not destabilize the gauge hierarchy. The model provides a natural explanation for the origin of the  $\mu$ -term, without suffering from the visible axion or the cosmological domain-wall problem. Focusing on the Higgs sector of this minimal non-minimal supersymmetric standard model, we calculate its effective Higgs potential by integrating out the dominant quantum effects due to stop squarks. We then discuss the phenomenological implications of the Higgs scalars predicted by the theory for the present and future high-energy colliders. In particular, we find that our new minimal non-minimal supersymmetric model can naturally accommodate a relatively light charged Higgs boson, with a mass close to the present experimental lower bound.

# 1 Introduction

In the well-established Standard Model (SM), the generation of gauge-invariant, renormalizable masses for the observable fermions, e.g. the electron and the  $t$  quark, and for the  $W$  and  $Z$  bosons is achieved through the so-called Higgs mechanism. Most interestingly, the Higgs mechanism itself predicts inevitably the existence of a fundamental scalar, known as the Higgs boson. Recently, experiments at LEP2 have intensified their searches for directly observing the yet-elusive Higgs boson. Their latest analyses show that its mass must be larger than 113.3 GeV at the 95% confidence level (CL) [1]. At the same time, electroweak precision data place an upper bound of the order of 240 GeV on the Higgs-boson mass [2].

So far, we have no much evidence to suggest that the underlying structure of the Higgs potential is indeed that of the SM or it already contains components of a more fundamental theory which is about to be unraveled in the next-round experiments. In particular, it is known that the SM cannot adequately address the problem of gauge hierarchy, which is related to the perturbative stability of radiative effects between the electroweak scale and the Planck or grand unification scale. An appealing solution to this problem may be achieved by means of supersymmetry (SUSY). In order that SUSY theories avoid reintroducing the problem of gauge hierarchy, they must be softly broken at a relatively low scale  $M_{\text{SUSY}} \sim m_t$  of the order of 1 TeV, in agreement with experimental observations.

The minimal supersymmetric extension of the SM, also called the Minimal Supersymmetric Standard Model (MSSM), predicts a very constrained two-Higgs-doublet potential at the tree level, whose quartic couplings are determined by the well-measured  $\text{SU}(2)_L$  and  $\text{U}(1)_Y$  gauge couplings  $g_w$  and  $g'$ . As a consequence, the lightest neutral Higgs boson is always lighter than the  $Z$  boson at the tree level. Nevertheless, radiative corrections to the effective Higgs potential are significant and extend the above mass upper bound to 110 (130) GeV for small (large) values of the ratio of Higgs vacuum expectation values (VEV's)  $\tan \beta \approx 2$  ( $> 15$ ) [3]. Thus, a large portion of the parameter space of the MSSM has been already excluded by the current LEP2 experiments at CERN. Moreover, the upgraded Tevatron collider at Fermilab will have a much higher reach in discovering heavier Higgs bosons with SM-type couplings and masses up to 140 GeV and therefore will provide a unique test for the viability of the MSSM.

On the basis of the above strong experimental bounds on the lightest Higgs-boson mass in the MSSM (especially for low values of  $\tan \beta$ ), it would be rather premature to infer that realizations of low-energy SUSY in nature have a rather limited range. In order to reach a more definite conclusion, it is very important to further analyze the Higgs sectors of minimally extended scenarios of the MSSM. An additional reason for going beyond the

MSSM is the so called  $\mu$ -problem. The superpotential of the MSSM contains a bilinear term  $-\mu\widehat{H}_1\widehat{H}_2$  involving the two Higgs-doublet superfields  $\widehat{H}_1$  and  $\widehat{H}_2$ , known as the  $\mu$ -term. Although  $\mu$  is naturally of the order of the Planck scale  $M_P$ , it is actually required to be many orders of magnitude smaller of order  $M_{\text{SUSY}}$  for a successful Higgs mechanism at the electroweak scale. Many scenarios have been proposed in the existing literature to account for the origin of the  $\mu$ -term, albeit all in extended settings [4].

A simple SUSY extension of the MSSM, which one might have thought of considering to address the  $\mu$ -problem, would be to elevate the  $\mu$ -parameter to a dynamical variable by means of a gauge-singlet chiral superfield  $\widehat{S}$ , couple the latter to  $\widehat{H}_1$  and  $\widehat{H}_2$  as  $\lambda\widehat{S}\widehat{H}_1\widehat{H}_2$  and arrange that  $\widehat{S}$  somehow develops a VEV of the order of  $M_{\text{SUSY}} \sim m_t$ . However, this minimally extended scenario possesses a global U(1) Peccei-Quinn (PQ) symmetry, whose spontaneous breakdown gives rise to a phenomenologically excluded axion. The most popular way in the literature of removing the unwanted PQ symmetry is to break the latter explicitly by adding the cubic self-coupling  $\frac{1}{3}\kappa\widehat{S}^3$  to the superpotential. The resulting model has been termed the Next-to-Minimal Supersymmetric Standard Model (NMSSM) [5]. Unfortunately, the NMSSM is also plagued by its own problems. The cubic self-coupling of  $\widehat{S}$  leaves invariant a subgroup of U(1)<sub>PQ</sub>, namely the discrete  $\mathcal{Z}_3$  symmetry, whose subsequent spontaneous breakdown gives rise to the formation of cosmologically catastrophic weak-scale domain walls [6,7].

Another well-known problem that a model of low-energy physics involving light gauge-singlets has to face is the destabilization of the gauge hierarchy through the generation of at least quadratically divergent tadpoles for the singlet [8]. In the context of  $N = 1$  supergravity, which is spontaneously broken by a set of hidden sector superfields, even if one assumes no other scale between  $M_{\text{SUSY}}$  and  $M_P$ , the simple presence of gravity-induced non-renormalizable operators in the superpotential and the Kähler potential is able to generate such tadpoles [9]. Using the Planck mass  $M_P$  as a physical cut-off energy, such divergences contribute tadpole terms of order  $(1/16\pi^2)^n M_P M_{\text{SUSY}}^2 S$  to the effective potential, where  $n$  indicates the loop level at which the tadpole divergence appears. It is obvious that for small values of  $n$ , e.g.  $n \leq 4$ , the generated tadpole terms lead generically to unacceptably large values for the VEV of  $S$  (the scalar component of  $\widehat{S}$ ), thereby destabilizing the gauge hierarchy.

In the case of the aforementioned extensions of the MSSM, the problem of destabilization does not occur as long as the U(1)<sub>PQ</sub> or  $\mathcal{Z}_3$  symmetries are imposed on the complete set of non-renormalizable operators as well. However, any attempt to break these unwanted symmetries through a subset of non-renormalizable operators would, as an immediate consequence, destabilize the weak scale. This aspect has been emphasized in Ref. [7,10], in

connection with the  $\mathcal{Z}_3$  symmetry of the NMSSM.

Recently, it has been realized that the unwanted  $\mathcal{Z}_3$  and  $U(1)_{\text{PQ}}$  symmetries present in the corresponding supersymmetric extensions of the MSSM could be effectively broken not by the non-renormalizable operators themselves, but rather by the tadpoles generated by them [11,12]. For the  $\mathcal{Z}_3$ -symmetric extension of the MSSM, harmless tadpole terms of order  $(1/16\pi^2)^n M_{\text{SUSY}}^3 S$ , with  $2 \leq n \leq 4$ , were sufficient for the breaking of the  $\mathcal{Z}_3$  symmetry. For the PQ-symmetric extension instead, it was necessary that the harmful tadpoles of order  $(1/16\pi^2)^n M_{\text{P}} M_{\text{SUSY}}^2 S$  (using  $M_{\text{P}}$  as a cut-off scale) be generated at a sufficiently high loop level  $n$ , with  $5 \leq n \leq 8$ . In the  $\mathcal{Z}_3$  case, the harmful tadpoles were forbidden by imposing on the operators of the non-renormalizable superpotential and Kähler potential the  $\mathcal{Z}_2$   $R$ -symmetry of the cubic superpotential, under which all superfields as well as the superpotential flip sign. However, the desirable form of the renormalizable superpotential was enforced by imposing a larger group, namely the product of the  $\mathcal{Z}_2$  matter parity with a  $\mathcal{Z}_4$   $R$ -symmetry [11]. In the  $U(1)_{\text{PQ}}$  case, a  $\mathcal{Z}_5$   $R$ -symmetry proved sufficient to enforce the desirable renormalizable superpotential and postpone the appearance of the harmful divergent tadpoles until the sixth loop order [12]. Thus, in both cases the breaking of the unwanted symmetries was successfully implemented without jeopardizing the stability of the electroweak scale and without generating new cosmological problems.

In the present paper, we shall study in detail the new minimal supersymmetric extension of the MSSM, in which the linear, quadratic and cubic terms involving the singlet superfield  $\hat{S}$  itself are absent from the renormalizable part of the superpotential. Hereafter, we shall call such a supersymmetric extension the Minimal Non-minimal Supersymmetric Standard Model (MNSSM). In particular, we shall explicitly show that with the imposition of the discrete  $\mathcal{Z}_5$  and  $\mathcal{Z}_7$   $R$ -symmetries on the complete superpotential and on the Kähler potential of the corresponding supergravity models, the potentially dangerous tadpole divergences first appear at the six- and seven- loop levels, respectively, and hence are naturally suppressed to the order of  $M_{\text{SUSY}}^3 S$ . Evidently, the resulting model constitutes the simplest and most economic version among the non-minimal supersymmetric models proposed in the literature. In order to properly study the properties of the Higgs bosons predicted by the theory, we will calculate the effective Higgs potential by taking into account the dominant stop-loop effects. Finally, we shall analyze the phenomenological implications of the MNSSM for direct Higgs-boson searches at the LEP2 and the upgraded Tevatron colliders.

The organization of the paper is as follows: in Section 2 we describe the Higgs sector of the MNSSM and show that harmful tadpole divergences first appear at the six- and seven- loop levels, after the aforementioned discrete  $\mathcal{Z}_5$  and  $\mathcal{Z}_7$   $R$ -symmetries are respectively imposed on the theory. Technical details of the argument are relegated to Appendix

A. In Section 3 we compute the effective Higgs potential by integrating out the dominant radiative effects due to stop squarks, from which we derive the CP-even and CP-odd Higgs-boson mass matrices. In Section 4 we investigate the theoretical differences of the Higgs-boson mass spectrum between the MNSSM under consideration and the frequently-discussed NMSSM. In Section 5 we present numerical estimates of the Higgs-boson masses and their couplings associated with the  $Z$  boson in these two models, and discuss the phenomenological implications of the MNSSM Higgs sector for the direct Higgs-boson searches at LEP2 and for the upcoming searches at the upgraded Tevatron collider. Section 6 contains our conclusions.

## 2 MNSSM: Symmetries and stability of the electroweak scale

In this section we shall consider the simplest extension of the MSSM, the MNSSM, within the context of  $N = 1$  supergravity spontaneously broken by a set of hidden sector fields at an intermediate scale. In the MNSSM, the  $\mu$ -parameter is promoted to a dynamical chiral superfield,\* with the linear, quadratic and cubic terms involving only the singlet superfield  $\hat{S}$  being absent from the renormalizable superpotential. Such a particularly simple form of the superpotential may be enforced by discrete  $R$ -symmetries, e.g.  $\mathcal{Z}_5^R$  and  $\mathcal{Z}_7^R$ , which are extended to the non-renormalizable parts of the superpotential and the Kähler potential as well. Adopting the standard power counting rules [9,10], we shall show that in such  $N = 1$  supergravity scenarios, the potentially dangerous tadpole divergences are suppressed by loop factors  $1/(16\pi^2)^n$  of order  $n = 6$  and higher, and therefore do not destabilize the gauge hierarchy. Technical details are given in Appendix A.

The renormalizable superpotential of the MNSSM under discussion is given by

$$W_{\text{ren}} = h_l \hat{H}_1^T i\tau_2 \hat{L} \hat{E} + h_d \hat{H}_1^T i\tau_2 \hat{Q} \hat{D} + h_u \hat{Q}^T i\tau_2 \hat{H}_2 \hat{U} + \lambda \hat{S} \hat{H}_1^T i\tau_2 \hat{H}_2, \quad (2.1)$$

where  $\tau_2$  is the usual  $2 \times 2$  Pauli matrix. In Eq. (2.1), the Higgs superfields,  $\hat{H}_1$  and  $\hat{H}_2$ , as well as the quark and lepton chiral multiplets,  $\hat{Q}$  and  $\hat{L}$ , are  $SU(2)_L$ -doublets, while the remaining superfields  $\hat{S}$ ,  $\hat{U}$ ,  $\hat{D}$  and  $\hat{E}$  are singlets under  $SU(2)_L$ . The chiral multiplets also carry the following hypercharges:

$$U(1)_Y : \quad \hat{H}_1(-1), \hat{H}_2(1), \hat{S}(0), \hat{Q}(1/3), \hat{U}(-4/3), \hat{D}(2/3), \hat{L}(-1), \hat{E}(2), \quad (2.2)$$

---

\*An earlier suggestion along these lines was discussed in [13].

where the hypercharge of each superfield is indicated within the parentheses. In addition to the baryon (B) and lepton (L) numbers, the renormalizable superpotential  $W_{\text{ren}}$  respects the global U(1) PQ and  $R$  symmetries:

$$\begin{aligned} \text{U}(1)_{\text{PQ}} &: \widehat{H}_1(1), \widehat{H}_2(1), \widehat{S}(-2), \widehat{Q}(-1), \widehat{U}(0), \widehat{D}(0), \widehat{L}(-1), \widehat{E}(0); \\ \text{U}(1)_R &: \widehat{H}_1(0), \widehat{H}_2(0), \widehat{S}(2), \widehat{Q}(1), \widehat{U}(1), \widehat{D}(1), \widehat{L}(1), \widehat{E}(1), W_{\text{ren}}(2). \end{aligned} \quad (2.3)$$

Note that  $W_{\text{ren}}$  has charge 2 under  $\text{U}(1)_R$ . The symmetry group  $\text{U}(1)_R$  is non-anomalous with respect to QCD interactions, but gets broken by the soft SUSY-breaking trilinear couplings down to its maximal non- $R$   $\mathbb{Z}_2$  subgroup which becomes the known matter-parity. Instead, the anomalous symmetry  $\text{U}(1)_{\text{PQ}}$  remains unbroken by the soft SUSY-breaking terms. Neglecting QCD-instanton effects,  $\text{U}(1)_{\text{PQ}}$  will remain unbroken, unless a gravity-induced tadpole operator linear in  $S$  gets generated from the non-renormalizable sector of the theory. The tadpole operator generically contributes to the effective potential a term

$$V_{\text{tad}} \sim \frac{1}{(16\pi^2)^n} M_{\text{P}} M_{\text{SUSY}}^2 S + \text{h.c.}, \quad (2.4)$$

where  $n$  is the loop level at which the tadpole divergence occurs, using the Planck mass  $M_{\text{P}}$  as an energy cut-off. The tadpole term  $V_{\text{tad}}$  together with the soft SUSY-breaking mass term  $M_{\text{SUSY}}^2 S^* S$  lead to a VEV for the singlet field  $S$  of order  $(1/16\pi^2)^n M_{\text{P}}$ . To avoid destabilizing the gauge hierarchy, one must require [12] that  $\langle S \rangle \sim M_{\text{SUSY}} \sim (1/16\pi^2)^n M_{\text{P}}$ , with  $M_{\text{SUSY}} \sim 1$  TeV. This requirement can only be fulfilled for sufficiently high values of  $n$ , i.e. for  $n \geq 5$ . Finally, we should remark that the full renormalizable Lagrangian, including the tadpole term, preserves the B and L numbers. However, the quantum numbers B and L may be violated by certain non-renormalizable operators, which are hopefully of sufficiently high order in order not to upset the laboratory limits on proton instability. We can therefore conclude that the renormalizable superpotential  $W_{\text{ren}}$  of Eq. (2.1) supplemented with a sufficiently suppressed tadpole for the singlet  $S$  leads to a model without any obvious phenomenological or cosmological problem.

One may now wonder whether there exists a symmetry giving rise to the above-described model that includes a tadpole term for  $S$  of the desirable order. To address this question, let us consider the global symmetry defined as a linear combination  $R' = 3R + \text{PQ}$  of  $\text{U}(1)_R$  and  $\text{U}(1)_{\text{PQ}}$ , with

$$\text{U}(1)_{R'} : \widehat{H}_1(1), \widehat{H}_2(1), \widehat{S}(4), \widehat{Q}(2), \widehat{U}(3), \widehat{D}(3), \widehat{L}(2), \widehat{E}(3), W_{\text{ren}}(6). \quad (2.5)$$

Observe that the imposition of  $\text{U}(1)_{R'}$  is sufficient to ensure the form (2.1) for  $W_{\text{ren}}$ . We should now examine whether  $\text{U}(1)_{R'}$  also allows the generation of a tadpole term. The

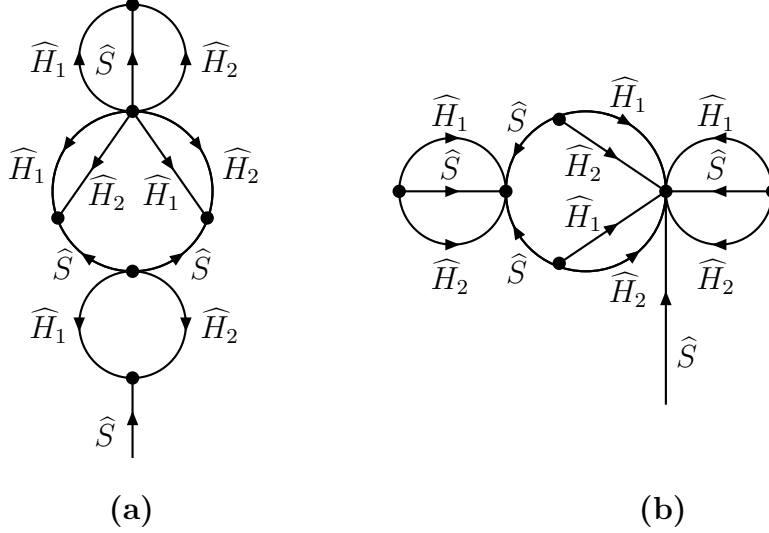


Figure 1: Typical harmful tadpole divergences at the (a) six- and (b) seven- loop levels.

symmetry group  $U(1)_{R'}$  is explicitly broken by the trilinear soft SUSY-breaking interactions down to its maximal non- $R$  subgroup  $\mathcal{Z}_6$  which is isomorph (equivalent) to the product group  $\mathcal{Z}_2 \times \mathcal{Z}_3$ . The symmetry  $\mathcal{Z}_2$  is essentially the ordinary matter-parity, under which the tadpole remains invariant. Instead, the symmetry  $\mathcal{Z}_3$  is broken by the tadpole of  $S$ . Consequently, a tadpole term can only be generated if the whole symmetry group  $U(1)_{R'}$  or one of its subgroups that includes  $\mathcal{Z}_3$  is violated by the higher-order non-renormalizable operators.

The above arguments seem to suggest that the symmetry we are looking for is likely to be a subgroup of  $U(1)_{R'}$  which is sufficiently large to enforce the form of  $W_{\text{ren}}$  given by Eq. (2.1), but does not contain the  $\mathcal{Z}_3$  subgroup of  $U(1)_{R'}$ . Subgroups of  $U(1)_{R'}$  obeying the above criteria are the discrete  $R$ -symmetries  $\mathcal{Z}_5^R$  [12] and  $\mathcal{Z}_7^R$ .

Let us first consider the  $\mathcal{Z}_5^R$  case. Under  $\mathcal{Z}_5^R$ , the chiral multiplets as well as the superpotential  $W_{\text{ren}}$  transform as follows:

$$\begin{aligned} \mathcal{Z}_5^R : (\widehat{H}_1, \widehat{H}_2) &\rightarrow \omega (\widehat{H}_1, \widehat{H}_2), \quad (\widehat{Q}, \widehat{L}) \rightarrow \omega^2 (\widehat{Q}, \widehat{L}), \quad (\widehat{U}, \widehat{D}, \widehat{E}) \rightarrow \omega^3 (\widehat{U}, \widehat{D}, \widehat{E}), \\ \widehat{S} &\rightarrow \omega^4 \widehat{S}, \quad W_{\text{ren}} \rightarrow \omega W_{\text{ren}}, \end{aligned} \quad (2.6)$$

with  $\omega = \exp(2\pi i/5)$  and  $\omega^5 = 1$ . The discrete  $R$ -symmetry  $\mathcal{Z}_5^R$  is imposed on the complete superpotential and Kähler potential. By means of standard power counting rules governing the harmful tadpole divergences, it can be shown that harmful tadpoles first appear at the six-loop level. As can be seen from Fig. 1(a), a typical harmful six-loop tadpole diagram

can be induced by appropriately combining the non-renormalizable operators of the Kähler potential

$$K_2 = \kappa_2 \frac{\widehat{S}^2 (\widehat{H}_1^T i\tau_2 \widehat{H}_2)}{M_{\text{P}}^2} + \text{h.c.}, \quad K_5 = \kappa_5 \frac{\widehat{S} (\widehat{H}_1^T i\tau_2 \widehat{H}_2)^3}{M_{\text{P}}^5} + \text{h.c.}, \quad (2.7)$$

and four times the renormalizable term  $\lambda \widehat{S} \widehat{H}_1^T i\tau_2 \widehat{H}_2$  of the superpotential (2.1). The analytic steps of the argument are presented in Appendix A. Thus, the induced harmful divergent tadpole term has the form

$$V_{\text{tad}} \sim \frac{\kappa_2 \kappa_5 \lambda^4}{(16\pi^2)^6} M_{\text{P}} M_{\text{SUSY}}^2 S + \text{h.c.} \quad (2.8)$$

From Eq. (2.8), it is easy to see that the tadpole term is of order  $(1 \text{ TeV})^3$ , e.g. for  $\kappa_2 \sim \kappa_5 \sim 0.1$ ,  $\lambda \sim 0.6$  and  $M_{\text{SUSY}} \sim 1 \text{ TeV}$ , and does not destabilize the gauge hierarchy.

In the  $\mathcal{Z}_7^R$  case, the harmful tadpole divergence occurs at one loop-order higher, namely at the seven-loop level, so the generated tadpole terms can naturally be as low as  $(100 \text{ GeV})^3$ . In detail, under this new discrete  $R$ -symmetry, the superfields and  $W_{\text{ren}}$  transform in the following way:

$$\begin{aligned} \mathcal{Z}_7^R : (\widehat{H}_1, \widehat{H}_2) &\rightarrow \omega (\widehat{H}_1, \widehat{H}_2), \quad (\widehat{Q}, \widehat{L}) \rightarrow \omega^2 (\widehat{Q}, \widehat{L}), \quad (\widehat{U}, \widehat{D}, \widehat{E}) \rightarrow \omega^3 (\widehat{U}, \widehat{D}, \widehat{E}), \\ \widehat{S} &\rightarrow \omega^4 \widehat{S}, \quad W_{\text{ren}} \rightarrow \omega^6 W_{\text{ren}}, \end{aligned} \quad (2.9)$$

with  $\omega = \exp(2\pi i/7)$  and  $\omega^7 = 1$ . Following the same line of steps as above, we impose the discrete  $R$ -symmetry  $\mathcal{Z}_7^R$  on the complete superpotential and Kähler potential. Based on standard power counting rules, we show in Appendix A that the potentially harmful tadpole divergences first appear at the seven-loop level. A typical harmful tadpole diagram at seven loops is displayed in Fig. 1(b), and can be obtained by combining the non-renormalizable operators of the Kähler potential

$$K_3^{(1)} = \kappa_3^{(1)} \frac{\widehat{S}^3 (\widehat{H}_1^T i\tau_2 \widehat{H}_2)}{M_{\text{P}}^3} + \text{h.c.}, \quad K_6 = \kappa_6 \frac{\widehat{S}^2 (\widehat{H}_1^T i\tau_2 \widehat{H}_2)^3}{M_{\text{P}}^6} + \text{h.c.}, \quad (2.10)$$

and four times the renormalizable term  $\lambda \widehat{S} \widehat{H}_1^T i\tau_2 \widehat{H}_2$  of  $W_{\text{ren}}$ . The size of the so-generated tadpole term may be estimated as

$$V_{\text{tad}} \sim \frac{\kappa_3^{(1)} \kappa_6 \lambda^4}{(16\pi^2)^7} M_{\text{P}} M_{\text{SUSY}}^2 S + \text{h.c.} \sim (1 \text{ TeV}) \times M_{\text{SUSY}}^2 S + \text{h.c.}, \quad (2.11)$$

for  $\kappa_3^{(1)} \sim \kappa_6 \sim 1$  and  $\lambda \sim 0.6$ . If  $\kappa_3^{(1)} \sim \kappa_6 \sim 0.1$  and  $M_{\text{SUSY}} \sim 1 \text{ TeV}$ , the size of  $V_{\text{tad}}$  can be as low as  $(0.2 \text{ TeV})^3$ .



We conclude this section by noticing that although the discrete  $R$ -symmetries  $\mathcal{Z}_5^R$  and  $\mathcal{Z}_7^R$  do not contain the usual  $\mathcal{Z}_2$  matter parity, they still prohibit the presence of all dimension  $d = 4$  B- and L- violating operators as well as the dangerous B- and L- violating operators  $\widehat{Q}\widehat{Q}\widehat{Q}\widehat{L}$  and  $\widehat{U}\widehat{U}\widehat{D}\widehat{E}$  of dimension 5. However, the symmetries  $\mathcal{Z}_5^R$  and  $\mathcal{Z}_7^R$  allow the L-violating operator  $\widehat{L}\widehat{L}\widehat{H}_2\widehat{H}_2$  of  $d = 5$ , which is able to generate Majorana masses for the light left-handed neutrinos. Moreover,  $\mathcal{Z}_5^R$  allows the  $d = 5$  L-violating operators  $\widehat{S}\widehat{S}\widehat{L}\widehat{H}_2$ ,  $\widehat{S}\widehat{L}\widehat{L}\widehat{E}$  and  $\widehat{S}\widehat{L}\widehat{Q}\widehat{D}$ , whereas  $\mathcal{Z}_7^R$  allows the  $d = 5$  B-violating operator  $\widehat{S}\widehat{U}\widehat{D}\widehat{D}$ . Although these last operators are unable to lead by themselves to an observable proton decay, they still render the lightest supersymmetric particle (LSP) unstable. However, estimates based on naive dimensional analysis show that the LSP is very long lived with a lifetime larger than the age of the Universe and therefore safely qualifies to be a dark-matter candidate. Of course, the LSP can be made absolutely stable by the additional imposition of the  $\mathcal{Z}_2$  matter parity.

### 3 The Higgs sector of the MNSSM

In this section we shall study the low-energy Higgs sector of the MNSSM. After discussing its tree-level structure, we will then calculate the one-loop effective Higgs potential by integrating out the dominant loop effects due to stop/top quarks, from which we derive analytic expressions for the Higgs-boson masses and their respective mixing angles. We shall then focus on the gaugino-Higgsino sector of the MNSSM, and briefly discuss possible laboratory limits on the would-be  $\mu$ -parameter due to the presence of a light quasi-singlet neutralino state. Finally, for our forthcoming phenomenological discussion in Section 5, we shall present the effective Higgs-boson couplings to the  $W$  and  $Z$  bosons.

#### 3.1 Higgs-boson masses at the tree level

In addition to terms proportional to  $S$ , another effect of the tadpole supergraphs of Fig. 1 is the generation of terms proportional to  $F_S$ , namely to the auxiliary scalar component of  $\widehat{S}$ . As a consequence, the effective renormalizable Higgs superpotential of the MNSSM reads

$$W_{\text{Higgs}}^{\text{eff}} = \lambda \widehat{S} \widehat{H}_1^T i\tau_2 \widehat{H}_2 + \xi_F M_{\text{SUSY}}^2 \widehat{S}, \quad (3.1)$$

where  $\xi_F$  is a model-dependent constant. Moreover, the Lagrangian describing the soft SUSY-breaking Higgs sector is given by

$$-\mathcal{L}_{\text{soft}} = \left( \xi_S M_{\text{SUSY}}^3 S + \text{h.c.} \right) + m_1^2 \widetilde{\Phi}_1^\dagger \widetilde{\Phi}_1 + m_2^2 \Phi_2^\dagger \Phi_2 + m_S^2 S^* S$$

$$+ \left( \lambda A_\lambda S \tilde{\Phi}_1^\dagger i \tau_2 \Phi_2 + \text{h.c.} \right), \quad (3.2)$$

where  $\tilde{\Phi}_1 = i \tau_2 \Phi_1^*$  and  $\Phi_2$  are the physical bosonic degrees of freedom of  $\widehat{H}_1$  and  $\widehat{H}_2$ , respectively. After including the relevant  $F$ - and  $D$ -term contributions in addition to the soft SUSY-breaking terms, we obtain the complete renormalizable Higgs potential of the model of interest

$$\begin{aligned} -\mathcal{L}_V^0 = & \left( t_S S + \text{h.c.} \right) + m_1^2 \Phi_1^\dagger \Phi_1 + m_2^2 \Phi_2^\dagger \Phi_2 + m_S^2 S^* S + \left( m_{12}^2 \Phi_1^\dagger \Phi_2 + \text{h.c.} \right) \\ & + \left( \lambda A_\lambda S \Phi_1^\dagger \Phi_2 + \text{h.c.} \right) - \lambda_1 (\Phi_1^\dagger \Phi_1)^2 - \lambda_2 (\Phi_2^\dagger \Phi_2)^2 - \lambda_3 (\Phi_1^\dagger \Phi_1) (\Phi_2^\dagger \Phi_2) \\ & - (\lambda_4 - \lambda^2) (\Phi_1^\dagger \Phi_2) (\Phi_2^\dagger \Phi_1) + \lambda^2 S^* S (\Phi_1^\dagger \Phi_1 + \Phi_2^\dagger \Phi_2), \end{aligned} \quad (3.3)$$

with

$$\begin{aligned} t_S &= \xi_S M_{\text{SUSY}}^3, & m_{12}^2 &= \lambda \xi_F M_{\text{SUSY}}^2, \\ \lambda_1 &= \lambda_2 = -\frac{g_w^2 + g'^2}{8}, & \lambda_3 &= -\frac{g_w^2 - g'^2}{4}, & \lambda_4 &= \frac{g_w^2}{2}. \end{aligned} \quad (3.4)$$

Here,  $g_w$  ( $g'$ ) is the coupling constant of the gauge group  $\text{SU}(2)_L$  ( $\text{U}(1)_Y$ ). As was discussed in the previous section, the tadpole prefactor  $\xi_S$  in Eq. (3.4) is of order unity. However, the size of  $\xi_F$  crucially depends on the VEVs of the scalar components of the hidden-sector superfields that break SUSY [9]. The VEVs remain unconstrained by the requirement that the breaking of SUSY takes place at some intermediate scale in the hidden sector, in which the  $F$ -terms of the respective hidden-sector superfields are involved. In case that some of the hidden-sector fields acquire VEVs of order  $M_P$ , the tadpole prefactors  $|\xi_F|$  and  $|\xi_S|$  could be comparable. Otherwise, it is  $|\xi_F| \ll |\xi_S|$ . In the following, we shall treat the ratio  $|\xi_F| / |\xi_S|$  as a free parameter which is always less than unity.

We shall now derive the minimization conditions of the Higgs potential in Eq. (3.3). Throughout the paper, we shall assume that CP is a good symmetry of the theory. Under this assumption, we can perform the following linear expansions of the Higgs fields about their VEV's:

$$\begin{aligned} \Phi_1 &= \begin{pmatrix} \phi_1^+ \\ \frac{1}{\sqrt{2}}(v_1 + \phi_1 + i a_1) \end{pmatrix}, & \Phi_2 &= \begin{pmatrix} \phi_2^+ \\ \frac{1}{\sqrt{2}}(v_2 + \phi_2 + i a_2) \end{pmatrix}, \\ S &= \frac{1}{\sqrt{2}}(v_S + \phi_S + i a_S). \end{aligned} \quad (3.5)$$

The minimization conditions are then determined by the vanishing of the tadpole parameters

$$T_{\phi_1} \equiv \left\langle \frac{\partial \mathcal{L}_V}{\partial \phi_1} \right\rangle = -v_1 \left[ m_1^2 + \left( \frac{1}{\sqrt{2}} \lambda A_\lambda v_S + m_{12}^2 \right) t_\beta - \lambda_1 v_1^2 \right]$$

$$-\frac{1}{2}(\lambda_3 + \lambda_4 - \lambda^2)v_2^2 + \frac{1}{2}\lambda^2 v_S^2 \Big], \quad (3.6)$$

$$T_{\phi_2} \equiv \left\langle \frac{\partial \mathcal{L}_V}{\partial \phi_2} \right\rangle = -v_2 \left[ m_2^2 + \left( \frac{1}{\sqrt{2}} \lambda A_\lambda v_S + m_{12}^2 \right) t_\beta^{-1} - \lambda_2 v_2^2 - \frac{1}{2}(\lambda_3 + \lambda_4 - \lambda^2)v_1^2 + \frac{1}{2}\lambda^2 v_S^2 \right], \quad (3.7)$$

$$T_{\phi_S} \equiv \left\langle \frac{\partial \mathcal{L}_V}{\partial \phi_S} \right\rangle = -v_S \left( m_S^2 + \lambda A_\lambda \frac{v_1 v_2}{\sqrt{2} v_S} + \frac{1}{2}\lambda^2 v^2 + \frac{\sqrt{2} t_S}{v_S} \right), \quad (3.8)$$

with  $v = \sqrt{v_1^2 + v_2^2} = 2M_W/g_w$  and  $t_\beta = v_2/v_1$ . Our earlier assumption of CP invariance entails that all kinematic parameters involved, e.g.  $\lambda$  and  $A_\lambda$ , are real, namely there are no explicit sources of CP violation in the theory. Also, it is important to remark that based on Romao's no-go theorem [14], CP invariance cannot be broken spontaneously at the tree level in the MNSSM.<sup>†</sup>

It proves now convenient to perform a change of the weak basis for the charged and CP-odd scalars:

$$\begin{pmatrix} \phi_1^+ \\ \phi_2^+ \end{pmatrix} = \begin{pmatrix} c_\beta & -s_\beta \\ s_\beta & c_\beta \end{pmatrix} \begin{pmatrix} G^+ \\ H^+ \end{pmatrix}, \quad \begin{pmatrix} a_1 \\ a_2 \end{pmatrix} = \begin{pmatrix} c_\beta & -s_\beta \\ s_\beta & c_\beta \end{pmatrix} \begin{pmatrix} G^0 \\ a \end{pmatrix}, \quad (3.9)$$

where  $s_\beta = v_2/v$  and  $c_\beta = v_1/v$ , such that  $H^+$  becomes the mass eigenstate of the charged Higgs boson, and  $G^+$  and  $G^0$  are the would-be Goldstone bosons which constitute the longitudinal degrees of freedom of the  $W^+$  and  $Z$  bosons, respectively.

Let us first consider the charged Higgs sector. In the newly defined weak basis of Eq. (3.9), the tree-level mass of the charged Higgs boson may easily be computed by

$$M_{H^+}^{2(0)} = \frac{1}{s_\beta c_\beta} (\mu A_\lambda - m_{12}^2) + M_W^2 - \frac{1}{2}\lambda^2 v^2, \quad (3.10)$$

where

$$\mu = -\frac{1}{\sqrt{2}}\lambda v_S \quad (3.11)$$

is the would-be  $\mu$ -parameter of the MSSM. Here and in the following, we adhere the superscript (0) to a specific kinematic quantity in order to emphasize its tree-level origin, e.g.  $M_{H^+}^{2(0)}$ .

Since the would-be Goldstone boson  $G^0$  does not mix with other fields, the tree-level CP-odd mass matrix takes on the simple form in the reduced weak basis  $\{a, a_S\}$ :

$$M_P^{2(0)} = \begin{pmatrix} M_a^{2(0)} & \frac{v}{v_S} (s_\beta c_\beta M_a^{2(0)} + m_{12}^2) \\ \frac{v}{v_S} (s_\beta c_\beta M_a^{2(0)} + m_{12}^2) & \frac{v^2}{v_S^2} s_\beta c_\beta (s_\beta c_\beta M_a^{2(0)} + m_{12}^2) + \frac{\lambda t_S}{\mu} \end{pmatrix}, \quad (3.12)$$

---

<sup>†</sup>We find that this property persists, even if CP-conserving radiative effects mediated by large stop mixing are included in our model.

with

$$M_a^{2(0)} = M_{H^+}^{2(0)} - M_W^2 + \frac{1}{2} \lambda^2 v^2. \quad (3.13)$$

In deriving the above form of  $M_P^{2(0)}$ , we have also considered the tadpole constraints given by Eqs. (3.6)–(3.8). In the MSSM limit, which is obtained for  $v_S \approx -\sqrt{2} t_S / m_S^2 \gg v$  with the would-be  $\mu$ -parameter being kept fixed ( $\lambda \rightarrow 0$ ), the mass eigenvalues of the CP-odd mass matrix can easily be approximated by

$$M_{A_1}^{2(0)} \approx M_a^{2(0)}, \quad M_{A_2}^{2(0)} \approx \frac{\lambda t_S}{\mu}, \quad (3.14)$$

with  $\lambda t_S / \mu > M_a^{2(0)}$ . Furthermore, in the limit, in which the tadpole parameters  $m_{12}^2$  and  $t_S$  vanish, the CP-odd mass matrix contains a massless state, i.e. a PQ axion, as a result of the spontaneous breakdown of the symmetry group  $U(1)_{\text{PQ}}$ .

Taking into account the tadpole constraints of Eqs. (3.6)–(3.8), the tree-level CP-even mass matrix may be expressed in the weak basis  $\{\phi_1, \phi_2, \phi_S\}$  as follows:

$$\begin{aligned} (M_S^{2(0)})_{11} &= c_\beta^2 M_Z^2 + s_\beta^2 M_a^{2(0)}, \\ (M_S^{2(0)})_{12} &= (M_S^{2(0)})_{21} = -s_\beta c_\beta (M_a^{2(0)} + M_Z^2 - \lambda^2 v^2), \\ (M_S^{2(0)})_{13} &= (M_S^{2(0)})_{31} = -\frac{v}{v_S} (s_\beta^2 c_\beta M_a^{2(0)} - 2c_\beta \mu^2 + s_\beta m_{12}^2), \\ (M_S^{2(0)})_{22} &= s_\beta^2 M_Z^2 + c_\beta^2 M_a^{2(0)}, \\ (M_S^{2(0)})_{23} &= (M_S^{2(0)})_{32} = -\frac{v}{v_S} (s_\beta c_\beta^2 M_a^{2(0)} - 2s_\beta \mu^2 + c_\beta m_{12}^2), \\ (M_S^{2(0)})_{33} &= \frac{v^2}{v_S^2} s_\beta c_\beta (s_\beta c_\beta M_a^{2(0)} + m_{12}^2) + \frac{\lambda t_S}{\mu}, \end{aligned} \quad (3.15)$$

with  $M_Z = \sqrt{g_w^2 + g'^2} v / 2$ . In the MSSM limit, in which  $v_S \approx -\sqrt{2} t_S / m_S^2 \gg v$  with  $\mu$  fixed, the Higgs-singlet components decouple from the tree-level CP-even mass matrix  $M_S^{2(0)}$ . In this case, the heaviest Higgs boson  $H_3$  is predominantly singlet and has a squared mass  $M_{H_3}^{2(0)} \approx \lambda t_S / \mu$ ;  $H_3$  becomes mass degenerate with  $A_2$  (cf. Eq. (3.14)).

Apart from the MSSM limit mentioned above, there exists a novel non-trivial decoupling limit for the heavy Higgs sector in the MNSSM. This decoupling limit is obtained for large values of the tadpole parameter  $|t_S|$ , where all other kinematic parameters are kept fixed. In this case, the Higgs states  $A_2$  and  $H_3$  are singlets, i.e.  $A_2 \equiv a_S$  and  $H_3 \equiv \phi_S$ , and so decouple from the remaining Higgs sector while being degenerate in mass, i.e.  $M_{A_2}^{2(0)} \approx M_{H_3}^{2(0)} \approx \lambda t_S / \mu$ . An immediate consequence of this is the relation

$$M_{A_1}^{2(0)} \approx M_a^{2(0)}, \quad (3.16)$$

where  $M_a^{2(0)}$  is defined in Eq. (3.13). Most importantly, in this limit the structure of the low-energy Higgs sector, although reminiscent of, is *not* identical to that of the MSSM. For example, as opposed to the MSSM limit, the terms proportional to  $\lambda^2 v^2$ , which occur in the CP-odd and CP-even mass matrices of Eqs. (3.12) and (3.15), do not necessarily vanish in the decoupling limit due to a large tadpole. Thus, contrary to the MSSM, Eq. (3.16) implies that for large values of  $\lambda$ , e.g.  $\lambda \sim g_w$ , the charged Higgs-boson mass  $M_{H^+}^{(0)}$  can become even smaller than the mass  $M_{A_1}^{(0)}$  of the non-decoupled CP-odd scalar. As we will see in Section 5, this last fact plays a very important rôle in lowering the mass of the MNSSM charged Higgs boson up to its experimental lower bound, i.e. up to  $M_{H^+} \sim 80$  GeV [1,15]. Moreover, in Section 4 we shall see that this new non-trivial decoupling limit due to a large tadpole parameter  $\lambda t_S/\mu$  is only attainable in the MNSSM, and no analogue of this exists in the NMSSM.

As in the MSSM [16], an upper bound on the mass of the lightest CP-even Higgs boson in the MNSSM with large  $|t_S|$  may easily be derived in the decoupling limit of a heavy charged Higgs boson, i.e. for

$$\frac{\lambda t_S}{\mu} \gg M_{H^+}^{2(0)} \gg M_Z^2. \quad (3.17)$$

In this limit, in addition to  $A_2$  and  $H_3$ , the Higgs scalars  $A_1$  and  $H_2$  decouple from the lightest Higgs sector as well, and are almost mass degenerate with the charged Higgs boson  $H^+$ . After taking into consideration the heavy  $H^+$ -decoupling limit of Eq. (3.17), the mass of the lightest CP-even Higgs state  $H_1$  is found to satisfy the inequality

$$M_{H_1}^{2(0)} \leq M_Z^2 \left( \cos^2 2\beta + \frac{2\lambda^2}{g_w^2 + g'^2} \sin^2 2\beta \right). \quad (3.18)$$

Note that as opposed to the MSSM where  $\lambda = 0$ ,  $M_{H_1}^{(0)}$  can be larger than  $M_Z$  in the MNSSM, especially for small values of  $\tan \beta$ . This prediction is very similar to the one obtained in the frequently-discussed NMSSM [5]. However, as  $\tan \beta$  increases, e.g. for  $\tan \beta \gtrsim 5$ , the  $\lambda$ -dependent term in Eq. (3.18) becomes negligible. Thus, in the large- $\tan \beta$  case, the upper bound on the  $H_1$ -boson mass is almost identical to the one obtained in the MSSM. Finally, an important property of the MNSSM is that the tree-level neutral Higgs-boson masses satisfy the equality

$$M_{H_1}^{2(0)} + M_{H_2}^{2(0)} + M_{H_3}^{2(0)} = M_Z^2 + M_{A_1}^{2(0)} + M_{A_2}^{2(0)}. \quad (3.19)$$

It is interesting to notice the striking similarity of the above mass sum rule with the corresponding one in the MSSM [16], in which case the mass terms  $M_{H_3}^{2(0)}$  and  $M_{A_2}^{2(0)}$  are not present in Eq. (3.19). The above observation allows us to advocate that the structure of

the MNSSM Higgs sector departs indeed minimally from that of the MSSM. Nevertheless, exactly as happens in the MSSM [3], the tree-level Higgs sector receives sizeable quantum corrections due to stop squarks, leading to a violation of the mass sum rule (3.19).

### 3.2 One-loop effective potential

We shall now calculate the dominant one-loop corrections to the effective potential due to top ( $t$ ) and scalar-top ( $\tilde{t}$ ) quarks. As a good approximation, we neglect the one-loop  $D$ -term contributions as well as bottom ( $b$ ) and scalar-bottom ( $\tilde{b}$ ) quark effects by assuming a vanishing  $b$ -quark Yukawa coupling, i.e.  $h_b = 0$ . The above approximations are reasonable for relatively small values of  $\tan\beta$ , e.g.  $\tan\beta \leq 10$ , where the MNSSM predictions for the lightest Higgs sector are expected to deviate considerably from the ones obtained in the MSSM.

The interaction Lagrangians relevant for the computation of the one-loop effective potential are given by

$$\begin{aligned} -\mathcal{L}_{\text{fermion}} &= h_t \bar{Q}_L i\tau_2 \Phi_2^* t_R + \text{h.c.}, \\ -\mathcal{L}_F &= h_t^2 |\Phi_2^T i\tau_2 \tilde{Q}_L|^2 + \left( \lambda h_t S \tilde{Q}_L^\dagger i\tau_2 \Phi_1^* \tilde{t}_R + \text{h.c.} \right) + h_t^2 \tilde{t}_R \Phi_2^\dagger \Phi_2 \tilde{t}_R^*, \\ -\mathcal{L}_{\text{soft}} &= \tilde{M}_Q^2 \tilde{Q}_L^\dagger \tilde{Q}_L + \tilde{M}_t^2 \tilde{t}_R^* \tilde{t}_R + \left( h_t A_t \tilde{Q}_L^\dagger i\tau_2 \Phi_2^* \tilde{t}_R + \text{h.c.} \right), \end{aligned} \quad (3.20)$$

where  $\tilde{Q}_L = (\tilde{t}_L, \tilde{b}_L)^T$  and  $Q_L = (t_L, b_L)^T$  are the bosonic and fermionic degrees of freedom of the third-generation left-handed quark superfield.

Equipped with the Lagrangians in Eq. (3.20), we can now derive the Higgs-dependent  $t$  and  $\tilde{t}$  masses. Thus, the squared  $t$ -quark mass in the Higgs background is given by

$$\bar{m}_t^2 = h_t^2 \Phi_2^\dagger \Phi_2. \quad (3.21)$$

The corresponding background-dependent stop masses may be determined from the  $3 \times 3$  squark mass matrix, which is expressed in the weak basis  $\{\tilde{Q}_L, \tilde{t}_R\}$  as:

$$\tilde{\mathcal{M}}^2 = \begin{pmatrix} \tilde{M}_Q^2 \mathbf{1}_2 + h_t^2 (\Phi_2^\dagger \Phi_2 \mathbf{1}_2 - \Phi_2 \Phi_2^\dagger) & h_t A_t i\tau_2 \Phi_2^* + \lambda h_t S i\tau_2 \Phi_1^* \\ -h_t A_t \Phi_2^T i\tau_2 - \lambda h_t S^* \Phi_1^T i\tau_2 & \tilde{M}_t^2 + h_t^2 \Phi_2^\dagger \Phi_2 \end{pmatrix}. \quad (3.22)$$

The squared squark-mass matrix  $\tilde{\mathcal{M}}^2$  has three mass eigenvalues. For  $\phi_{1,2}^\pm = 0$ , these are given by the two squared Higgs-dependent  $\tilde{t}$ -quark masses

$$\tilde{m}_{t_1(t_2)}^2 = \frac{1}{2} \left( \tilde{M}_Q^2 + \tilde{M}_t^2 + 2h_t^2 |\phi_2^0|^2 + (-) \sqrt{(\tilde{M}_Q^2 - \tilde{M}_t^2)^2 + 4h_t^2 |A_t \phi_2^0 + \lambda S^* \phi_1^0|^2} \right) \quad (3.23)$$

and by the squared left-handed sbottom mass  $m_{b_L}^2 = \widetilde{M}_Q^2$ , where  $\phi_{1,2}^0 = (v_{1,2} + \phi_{1,2} + ia_{1,2})/\sqrt{2}$  are the neutral parts of  $\Phi_{1,2}$ .

In the  $\overline{\text{MS}}$  scheme, the one-loop Coleman–Weinberg effective potential [17] may be expressed in terms of the relevant squared Higgs-dependent masses  $\bar{m}_t^2$ ,  $\bar{m}_{t_1}^2$ ,  $\bar{m}_{t_2}^2$  and  $\bar{m}_{b_L}^2$  as follows:

$$-\mathcal{L}_V = -\mathcal{L}_V^0 + \frac{3}{32\pi^2} \left[ \sum_{k=t_1, t_2, b_L} \bar{m}_k^4 \left( \ln \frac{\bar{m}_k^2}{Q^2} - \frac{3}{2} \right) - 2\bar{m}_t^4 \left( \ln \frac{\bar{m}_t^2}{Q^2} - \frac{3}{2} \right) \right], \quad (3.24)$$

where  $-\mathcal{L}_V^0$  is the bare Higgs potential given by Eq. (3.3). With the help of  $\mathcal{L}_V$ , we can now compute the radiatively corrected mass of the charged Higgs boson by means of the relation

$$\begin{aligned} M_{H^+}^2 &= \frac{1}{s_\beta c_\beta} \left\langle \frac{\partial^2 \mathcal{L}_V}{\partial \phi_1^+ \partial \phi_2^-} \right\rangle = M_{H^+}^{2(0)} + \Delta M_{H^+}^2 \\ &= M_{H^+}^{2(0)} - \frac{3}{16\pi^2 s_\beta c_\beta} \left[ \sum_{k=t_1, t_2, b_L} \left\langle \frac{\partial^2 \bar{m}_k^2}{\partial \phi_1^+ \partial \phi_2^-} \right\rangle m_k^2 \left( \ln \frac{m_k^2}{Q^2} - 1 \right) \right], \end{aligned} \quad (3.25)$$

where  $M_{H^+}^{2(0)}$  is the tree-level contribution and  $\langle \bar{m}_k^2 \rangle = m_k^2$ . Following the procedure outlined in [18],<sup>‡</sup> we find

$$\begin{aligned} \left\langle \frac{\partial^2 \bar{m}_{t_1(t_2)}^2}{\partial \phi_1^+ \partial \phi_2^-} \right\rangle &= -(+) \frac{h_t^2 \mu A_t}{m_{t_1}^2 - m_{t_2}^2} + (-) \frac{h_t^4 \mu^2 v_1 v_2}{2(m_{t_1(t_2)}^2 - m_{b_L}^2)(m_{t_1}^2 - m_{t_2}^2)}, \\ \left\langle \frac{\partial^2 \bar{m}_{b_L}^2}{\partial \phi_1^+ \partial \phi_2^-} \right\rangle &= \frac{h_t^4 \mu^2 v_1 v_2}{2(m_{t_1}^2 - m_{b_L}^2)(m_{t_2}^2 - m_{b_L}^2)}. \end{aligned} \quad (3.26)$$

Then, the one-loop correction to  $M_{H^+}^2$ ,  $\Delta M_{H^+}^2$ , is given by

$$\Delta M_{H^+}^2 = \frac{3h_t^2 \mu A_t}{32\pi^2 s_\beta c_\beta} \left[ \ln \left( \frac{m_{t_1}^2 m_{t_2}^2}{Q^4} \right) + g(m_{t_1}^2, m_{t_2}^2) \right] + \delta_{\text{rem}}, \quad (3.27)$$

with

$$g(m_1^2, m_2^2) = \frac{m_1^2 + m_2^2}{m_1^2 - m_2^2} \ln \left( \frac{m_1^2}{m_2^2} \right) - 2. \quad (3.28)$$

In Eq. (3.27), the quantity  $\delta_{\text{rem}}$  summarizes the remaining  $Q^2$ -independent corrections:

$$\begin{aligned} \delta_{\text{rem}} &= \frac{3h_t^4 \mu^2 v^2}{64\pi^2} \left[ \frac{m_{b_L}^2}{(m_{t_1}^2 - m_{b_L}^2)(m_{t_2}^2 - m_{b_L}^2)} \ln \left( \frac{m_{t_1}^2 m_{t_2}^2}{m_{b_L}^4} \right) \right. \\ &\quad \left. - \frac{1}{m_{t_1}^2 - m_{t_2}^2} \left( \frac{m_{t_1}^2}{m_{t_1}^2 - m_{b_L}^2} + \frac{m_{t_2}^2}{m_{t_2}^2 - m_{b_L}^2} \right) \ln \left( \frac{m_{t_1}^2}{m_{t_2}^2} \right) \right] \\ &\approx -\frac{3h_t^4}{32\pi^2} \frac{\mu^2 v^2}{m_{t_1}^2 + m_{t_2}^2}. \end{aligned} \quad (3.29)$$

---

<sup>‡</sup>A similar procedure was also followed in [19].

As we will see below, the presence of  $\delta_{\text{rem}}$  gives rise to a modification of the tree-level relation between  $M_{H^+}^2$  and  $M_a^2$  in Eq. (3.13). Nevertheless, it can be estimated from Eq. (3.29) that this modification, which scales quadratically with the  $\mu$ -parameter, is insignificant for almost all relevant values of  $\mu$  of interest to us, i.e. for  $|\mu/m_{\tilde{t}_1}| \lesssim 2$ .

We now calculate the one-loop radiative shift  $\Delta M_P^2$  to the CP-odd Higgs-boson mass matrix. The analytic result may be completely expressed in terms of  $\Delta M_a^2 = \Delta M_{H^+}^2 - \delta_{\text{rem}}$  as

$$\Delta M_P^2 = \Delta M_a^2 \begin{pmatrix} 1 & \frac{v}{v_S} s_\beta c_\beta \\ \frac{v}{v_S} s_\beta c_\beta & \frac{v^2}{v_S^2} s_\beta^2 c_\beta^2 \end{pmatrix}. \quad (3.30)$$

It is easy to see that the one-loop radiative shift may be entirely absorbed into the tree-level mass matrix in Eq. (3.12), after performing an one-loop re-definition of  $M_a^{2(0)}$ , namely  $M_a^2 = M_a^{2(0)} + \Delta M_a^2$ . After this re-definition, the tree-level mass relation in Eq. (3.13) gets radiatively corrected as follows:

$$M_a^2 = M_{H^+}^2 - M_W^2 + \frac{1}{2} \lambda^2 v^2 - \delta_{\text{rem}}. \quad (3.31)$$

The one-loop Born-improved CP-odd mass matrix,  $M_P^2 = M_P^{2(0)} + \Delta M_P^2$ , may be diagonalized through an orthogonal transformation of the weak fields

$$\begin{pmatrix} a \\ a_S \end{pmatrix} = O^A \begin{pmatrix} A_1 \\ A_2 \end{pmatrix}, \quad \text{with} \quad O^A = \begin{pmatrix} \cos \theta_A & \sin \theta_A \\ -\sin \theta_A & \cos \theta_A \end{pmatrix}. \quad (3.32)$$

The CP-odd fields  $A_1$  and  $A_2$  are the mass eigenstates of  $M_P^2$ , with squared masses

$$M_{A_1(A_2)}^2 = \frac{1}{2} \left( \text{Tr} M_P^2 - (+) \sqrt{\text{Tr}^2 M_P^2 - 4 \det M_P^2} \right). \quad (3.33)$$

The mixing angle  $\theta_A$  relating the weak to the mass eigenstates is uniquely determined by

$$\cos \theta_A = \frac{|(M_P^2)_{12}|}{\sqrt{(M_P^2)_{12}^2 + [(M_P^2)_{11} - M_{A_1}^2]^2}}, \quad \sin \theta_A = \frac{|(M_P^2)_{11} - M_{A_1}^2|}{\sqrt{(M_P^2)_{12}^2 + [(M_P^2)_{11} - M_{A_1}^2]^2}}. \quad (3.34)$$

Finally, we calculate the radiative corrections  $\Delta M_S^2$  to the CP-even Higgs-boson mass matrix. The individual matrix elements of  $\Delta M_S^2$  are given by

$$\begin{aligned} (\Delta M_S^2)_{11} &= s_\beta^2 \Delta M_a^2 - \frac{3h_t^4 v_2^2}{16\pi^2} \frac{\mu^2 X_t^2}{(m_{\tilde{t}_1}^2 - m_{\tilde{t}_2}^2)^2} g(m_{\tilde{t}_1}^2, m_{\tilde{t}_2}^2), \\ (\Delta M_S^2)_{12} &= (\Delta M_S^2)_{21} = -s_\beta c_\beta \Delta M_a^2 - \frac{3h_t^4 v_2^2}{16\pi^2} \left[ \frac{\mu X_t}{m_{\tilde{t}_1}^2 - m_{\tilde{t}_2}^2} \ln \left( \frac{m_{\tilde{t}_1}^2}{m_{\tilde{t}_2}^2} \right) \right] \end{aligned}$$



$$\begin{aligned}
& - \frac{\mu A_t X_t^2}{(m_{t_1}^2 - m_{t_2}^2)^2} g(m_{t_1}^2, m_{t_2}^2) \Big], \\
(\Delta M_S^2)_{13} &= (\Delta M_S^2)_{31} = -\frac{v}{v_S} s_\beta^2 c_\beta \left[ \Delta M_a^2 + \frac{3h_t^4 v^2}{16\pi^2} \frac{\mu^2 X_t^2}{(m_{t_1}^2 - m_{t_2}^2)^2} g(m_{t_1}^2, m_{t_2}^2) \right] \\
& + \frac{3h_t^2}{16\pi^2} \left( \frac{vc_\beta}{v_S} \right) \mu^2 \left[ \ln \left( \frac{m_{t_1}^2 m_{t_2}^2}{Q^4} \right) + g(m_{t_1}^2, m_{t_2}^2) \right], \\
(\Delta M_S^2)_{22} &= c_\beta^2 \Delta M_a^2 + \frac{3h_t^4 v^2}{16\pi^2} \left[ \ln \left( \frac{m_{t_1}^2 m_{t_2}^2}{m_t^4} \right) + \frac{2A_t X_t}{m_{t_1}^2 - m_{t_2}^2} \ln \left( \frac{m_{t_1}^2}{m_{t_2}^2} \right) \right. \\
& \left. - \frac{A_t^2 X_t^2}{(m_{t_1}^2 - m_{t_2}^2)^2} g(m_{t_1}^2, m_{t_2}^2) \right], \\
(\Delta M_S^2)_{23} &= (\Delta M_S^2)_{32} = -\frac{v}{v_S} s_\beta c_\beta^2 \left[ \Delta M_a^2 + \frac{3h_t^4 v^2}{16\pi^2} \frac{t_\beta \mu X_t}{m_{t_1}^2 - m_{t_2}^2} \ln \left( \frac{m_{t_1}^2}{m_{t_2}^2} \right) \right. \\
& \left. - \frac{3h_t^4 v^2}{16\pi^2} \frac{t_\beta \mu A_t X_t^2}{(m_{t_1}^2 - m_{t_2}^2)^2} g(m_{t_1}^2, m_{t_2}^2) \right], \\
(\Delta M_S^2)_{33} &= \frac{v^2}{v_S^2} s_\beta^2 c_\beta^2 \left[ \Delta M_a^2 - \frac{3h_t^4 v^2}{16\pi^2} \frac{\mu^2 X_t^2}{(m_{t_1}^2 - m_{t_2}^2)^2} g(m_{t_1}^2, m_{t_2}^2) \right], \tag{3.35}
\end{aligned}$$

where  $X_t = A_t - \mu/t_\beta$ . Again, we find that almost the entire  $Q^2$ -dependence of the radiatively-corrected CP-even mass matrix given in Eq. (3.35) can be absorbed into  $M_a^2$  by an one-loop re-definition of  $M_a^{2(0)}$ . An exception to this is the mass-matrix element  $(\Delta M_S^2)_{13}$ . The  $Q^2$ -dependence of the  $\{13\}$  element can be eliminated by the  $\Phi_2$ -wave-function counter term (CT) which is contained in the  $\lambda$ -parameter.

To make this last point explicit, we shall apply the non-renormalization theorem of the superpotential to the coupling  $\lambda \widehat{S} \widehat{H}_1^T i \tau_2 \widehat{H}_2$  in Eq. (3.1). Since this operator does not receive any ultra-violet (UV) infinite radiative corrections to all orders, the wave-functions of  $\widehat{S}$ ,  $\widehat{H}_1$  and  $\widehat{H}_2$ , denoted as  $Z_{\widehat{S}}$ ,  $Z_{\widehat{H}_1}$  and  $Z_{\widehat{H}_2}$  must cancel against the CT of  $\lambda$ ,  $\delta\lambda$ , that is

$$\delta\lambda = \left( Z_{\widehat{S}}^{-1/2} Z_{\widehat{H}_1}^{-1/2} Z_{\widehat{H}_2}^{-1/2} - 1 \right) \lambda = -\frac{1}{2} \left( \delta Z_{\widehat{S}} + \delta Z_{\widehat{H}_1} + \delta Z_{\widehat{H}_2} \right) \lambda \tag{3.36}$$

where  $Z_z^{1/2} = 1 + \frac{1}{2} \delta Z_z$ , with  $z = \widehat{S}$ ,  $\widehat{H}_1$ , and  $\widehat{H}_2$ . Since only the wave-function of  $\widehat{H}_2$  receives quantum corrections due to top quarks, Eq. (3.36) becomes

$$\delta\lambda = -\frac{1}{2} \delta Z_{\widehat{H}_2} \lambda = -\frac{3\lambda h_t^2}{32\pi^2} \ln \left( \frac{m_t^2}{Q^2} \right). \tag{3.37}$$

Here, we have implicitly assumed that the coupling  $\lambda$  is renormalized at the scale  $Q^2 = m_t^2$ . Returning now to the bare Higgs potential in Eq. (3.3), we see that the operator  $\lambda^2 (S^* S)(\Phi_1^\dagger \Phi_1)$  induces the CT  $2\lambda\delta\lambda$ , which gives rise to a corresponding CT in the tree-

level mass-matrix element  $(M_S^2)_{13}$ ,

$$(\delta M_S^2)_{13} = 4 \left( \frac{vc_\beta}{v_S} \right) \left( \frac{\delta\lambda}{\lambda} \right) \mu^2 = - \frac{3h_t^2}{8\pi^2} \left( \frac{vc_\beta}{v_S} \right) \mu^2 \ln \left( \frac{m_t^2}{Q^2} \right). \quad (3.38)$$

Adding the CT  $(\delta M_S^2)_{13}$  to the one-loop result  $(\Delta M_S^2)_{13}$ , we readily see that  $Q^2$  gets substituted by  $m_t^2$ . Finally, it is not difficult to convince ourselves that there are no analogous  $\delta\lambda$ -dependent CTs for the operators  $\lambda^2 (S^* S)(\Phi_2^\dagger \Phi_2)$  and  $\lambda^2 (\Phi_1^\dagger \Phi_1)(\Phi_2^\dagger \Phi_2)$ , as they are exactly canceled by the wave-function renormalization of  $\Phi_2$ .

The one-loop radiatively corrected CP-even mass matrix,  $M_S^2 = M_S^{2(0)} + \Delta M_S^2$ , is diagonalized by means of a  $3 \times 3$  orthogonal matrix  $O^H$ , i.e.

$$(O^H)^T M_S^2 O^H = \text{diag} \left( M_{H_1}^2, M_{H_2}^2, M_{H_3}^2 \right), \quad (3.39)$$

with  $M_{H_1}^2 \leq M_{H_2}^2 \leq M_{H_3}^2$ . Under this orthogonal transformation, the weak states are related to the mass eigenstates through

$$\begin{pmatrix} \phi_1 \\ \phi_2 \\ \phi_S \end{pmatrix} = O^H \begin{pmatrix} H_1 \\ H_2 \\ H_3 \end{pmatrix}. \quad (3.40)$$

The entries of  $O^H$  can be calculated analytically by solving the third-order characteristic equation of  $M_S^2$ . The procedure of deriving analytic expressions for the elements of  $O^H$  is very similar to the one presented in Appendix B of [18], and we will not repeat it here.

### 3.3 The Higgsino sector

In addition to the Higgs sector, the Higgsino (or neutralino) sector of the MSSM gets minimally extended in the MNSSM due to the presence of the neutral SUSY partner of the complex scalar singlet  $S$ , the singlino  $\tilde{s}$ . Instead, the tree-level chargino sector is identical to that of the MSSM. In the weak basis

$$\Psi_0^T = (\tilde{B}, \tilde{W}_3, \tilde{h}_1, \tilde{h}_2, \tilde{s}), \quad (3.41)$$

the Lagrangian describing the neutralino mass matrix in the MNSSM is given by

$$\mathcal{L}_{\text{mass}}^0 = -\frac{1}{2} \Psi_0^T \mathcal{M}_0 \Psi_0 + \text{h.c.}, \quad (3.42)$$

where

$$\mathcal{M}_0 = \begin{pmatrix} m_{\tilde{B}} & 0 & -M_Z s_w c_\beta & M_Z s_w s_\beta & 0 \\ 0 & m_{\tilde{W}} & M_Z c_w c_\beta & -M_Z c_w s_\beta & 0 \\ -M_Z s_w c_\beta & M_Z c_w c_\beta & 0 & -\mu & -\frac{v}{v_S} s_\beta \mu \\ M_Z s_w s_\beta & -M_Z c_w s_\beta & -\mu & 0 & -\frac{v}{v_S} c_\beta \mu \\ 0 & 0 & -\frac{v}{v_S} s_\beta \mu & -\frac{v}{v_S} c_\beta \mu & 0 \end{pmatrix}, \quad (3.43)$$

with  $c_w = \sqrt{1 - s_w^2} = M_W/M_Z$ . In Eq. (3.41),  $\tilde{B}$  and  $\tilde{W}_3$  are the  $U(1)_Y$  and  $SU(2)_L$  neutral gauginos, respectively, and  $\tilde{h}_1$ ,  $\tilde{h}_2$  and  $\tilde{s}$  are the corresponding Higgsino states of the chiral multiplets  $\widehat{H}_1$ ,  $\widehat{H}_2$  and  $\widehat{S}$ .

The neutralino mass matrix of the MNSSM given in Eq. (3.43) predicts a relatively light state, with mass smaller than 70 GeV. Since the neutralino mass matrix is identical to that of the PQ-symmetric extension of the MSSM, we call this light state axino  $\tilde{a}$ . The axino is predominantly a singlet field for values of the  $\mu$ -parameter in the phenomenologically relevant range, i.e. for  $|\mu| \gtrsim 120$  GeV. In order to have a first estimate of the axino mass, we assume that the gaugino mass parameters  $m_{\tilde{B}}$  and  $m_{\tilde{W}}$  are very large, e.g. of order 500 GeV and higher, such that the gauginos  $\tilde{B}$  and  $\tilde{W}_3$  decouple practically from the neutralino sector. The reduced  $3 \times 3$  Higgsino-mass matrix, which is expressed in the subspace spanned by  $\tilde{h}_1$ ,  $\tilde{h}_2$  and  $\tilde{s}$ , can then be expanded in terms of  $v/v_S$ , thus yielding the axino mass

$$m_{\tilde{a}} \approx \frac{v^2}{v_S^2} |\mu \sin 2\beta| = \frac{2\lambda^2}{g_w^2} \frac{M_W^2}{|\mu|} |\sin 2\beta|. \quad (3.44)$$

This last formula proves to be a good approximation for  $|\mu| \gtrsim 200$  GeV.

There are strict collider limits on the axino-related parameters, which come from LEP2 and especially from the invisible width of the  $Z$  boson [15], in which case a new invisible decay channel for the  $Z$  boson into axino pairs opens up kinematically when  $m_{\tilde{a}} \lesssim M_Z/2$ . Assuming that the gauginos are decoupled from the neutralino mass matrix  $\mathcal{M}_0$ , we find numerically that the axino mass is smaller than 45 GeV for values of  $|\mu| \gtrsim 150$  GeV and  $\lambda \approx g_w \approx 0.65$ . Of course, such a numerical estimate crucially depends on the values of  $m_{\tilde{B}}$  and  $m_{\tilde{W}}$ . For example, for relatively low values of  $m_{\tilde{B}}$  and  $m_{\tilde{W}}$  in the range 200–300 GeV, gaugino-Higgsino mixing effects can no longer be neglected, and the upper limit on the  $\mu$ -parameter is estimated to increase by 40–50 GeV.

On the other hand, the upper bound on the branching ratio of the  $Z$ -boson invisible width due to a new-physics decay mode imposes the constraint [15]

$$B(Z \rightarrow \tilde{a}\tilde{a}) = \frac{\alpha_w}{24 c_w^2} \frac{M_Z}{\Gamma_Z} |g_{\tilde{a}\tilde{a}Z}|^2 < 1. \times 10^{-3}, \quad (3.45)$$

at the 90% CL, where  $\alpha_w = g_w^2/(4\pi)$  is the  $SU(2)_L$  weak fine structure constant and  $\Gamma_Z = 2.49$  GeV is the total width of the  $Z$  boson. Moreover, in the seesaw-type approximation the  $\tilde{a}\tilde{a}Z$ -coupling is readily found to be

$$g_{\tilde{a}\tilde{a}Z} \approx \frac{v^2}{v_S^2} (s_\beta^2 - c_\beta^2) = \frac{2\lambda^2}{g_w^2} \frac{M_W^2}{\mu^2} (s_\beta^2 - c_\beta^2). \quad (3.46)$$

The constraint in Eq. (3.45), together with Eq. (3.46), leads to

$$\frac{2\lambda^2}{g_w^2} \frac{M_W^2}{\mu^2} |\cos 2\beta| < 0.122. \quad (3.47)$$

This last inequality can be translated into the following bound on the  $\mu$ -parameter:

$$|\mu| \gtrsim 250 \text{ GeV}, \quad (3.48)$$

for  $\lambda \approx g_w$  and  $\tan \beta \approx 2$ . The above exercise shows that in the MNSSM the LEP limits on the  $Z$ -boson invisible width give rise to a new exclusion range of  $\mu$  values:  $200 \lesssim |\mu| \lesssim 250$  GeV, for  $\lambda \approx 0.65$ . However, this additional exclusion range of  $\mu$  exhibits a quadratic dependence on  $\lambda$  and completely disappears for values of  $\lambda \lesssim 0.45$ .

### 3.4 Effective Higgs-boson couplings

Apart from the Higgs-boson masses, the effective couplings of the CP-even and CP-odd Higgs scalars to the  $W^\pm$  and  $Z$  bosons are very essential for our phenomenological discussion in Section 5. These effective couplings are given by the interaction Lagrangians

$$\mathcal{L}_{\text{HVV}} = g_w M_W \sum_{i=1}^3 g_{H_i VV} \left( H_i W_\mu^+ W^{-,\mu} + \frac{1}{c_w^2} H_i Z_\mu Z^\mu \right), \quad (3.49)$$

$$\mathcal{L}_{\text{HAZ}} = \frac{g_w}{2 c_w} \sum_{i=1}^3 \sum_{j=1}^2 g_{H_i A_j Z} (H_i \overleftrightarrow{\partial}_\mu A_j) Z^\mu, \quad (3.50)$$

where  $\overleftrightarrow{\partial}_\mu \equiv \overrightarrow{\partial}_\mu - \overleftarrow{\partial}_\mu$  and

$$g_{H_i VV} = c_\beta O_{1i}^H + s_\beta O_{2i}^H, \quad (3.51)$$

$$g_{H_i A_j Z} = O_{1j}^A \left( c_\beta O_{2i}^H - s_\beta O_{1i}^H \right). \quad (3.52)$$

Here, we wish to remind the reader that the orthogonal matrix  $O^A$  ( $O^H$ ) is related to the mixing of the CP-odd (CP-even) scalars and is defined in Eq. (3.32) ((3.40)).

It is now worth remarking that the effective couplings  $H_i VV$  (with  $V = Z, W$ ) and  $H_i A_j Z$  satisfy the unitarity relations [20]

$$\sum_{i=1}^3 g_{H_i VV}^2 = 1, \quad \sum_{i=1}^3 \sum_{j=1}^2 g_{H_i A_j Z}^2 = 1. \quad (3.53)$$

In particular, in the limit in which  $A_2$  and  $H_3$  decouple as singlets, which is obtained for large  $|t_S|$  with the remaining parameters kept fixed, one recovers the known MSSM complementarity relations among the effective Higgs-boson couplings [16]:

$$g_{H_1 VV}^2 = g_{H_2 A_1 Z}^2 \quad \text{and} \quad g_{H_2 VV}^2 = g_{H_1 A_1 Z}^2. \quad (3.54)$$

As an obvious consequence of the above decoupling limit, all couplings of the heavy Higgs scalars  $A_2$  and  $H_3$  to the  $W$  and  $Z$  bosons go to zero.

Another very important relation which involves the CP-even Higgs-boson masses and the respective couplings to the  $W$  and  $Z$  bosons is

$$\begin{aligned}
\sum_{i=1}^3 g_{H_i V V}^2 M_{H_i}^2 &= c_\beta^2 (M_S^2)_{11} + 2s_\beta c_\beta (M_S^2)_{12} + s_\beta^2 (M_S^2)_{22} \\
&= M_Z^2 \left( \cos^2 2\beta + \frac{2\lambda^2}{g_w^2 + g'^2} \sin^2 2\beta \right) \\
&\quad + \frac{3h_t^4 v^2 s_\beta^4}{16\pi^2} \left[ \ln \left( \frac{m_{\tilde{t}_1}^2 m_{\tilde{t}_2}^2}{m_t^4} \right) + \frac{2X_t^2}{m_{\tilde{t}_1}^2 - m_{\tilde{t}_2}^2} \ln \left( \frac{m_{\tilde{t}_1}^2}{m_{\tilde{t}_2}^2} \right) - \frac{X_t^4 g(m_{\tilde{t}_1}^2, m_{\tilde{t}_2}^2)}{(m_{\tilde{t}_1}^2 - m_{\tilde{t}_2}^2)^2} \right]. \quad (3.55)
\end{aligned}$$

This mass-coupling sum rule is very analogous to the one derived in [21] for the MSSM, where the RHS of Eq. (3.55) is the squared lightest Higgs-boson mass in the decoupling limit of a heavy charged Higgs boson (see also Eq. (3.17)). In this limit, only the  $H_1$  boson has non-vanishing couplings to the  $W$  and  $Z$  bosons [16]. As can be seen from Eq. (3.55), the mass-coupling sum rule is independent of the charged Higgs boson mass, while it only weakly depends on  $\mu$  at the one-loop order. The relations (3.53) and (3.55), which are obviously valid for the case of the NMSSM as well, are very useful to reduce the number of independent effective Higgs-boson couplings and so achieve a better control on the numerical predictions for the Higgs-boson masses and couplings.

## 4 MNSSM versus NMSSM

Here, we shall compare the generic predictions for the Higgs-boson mass spectrum in the NMSSM, which includes the cubic singlet-superfield coupling, with those obtained in the MNSSM. For this purpose, we shall only focus on the tree-level structure of the Higgs sector of the NMSSM, as the dominant stop/top-radiative effects are identical for both models and have already been computed in Section 3.2.

The often-discussed NMSSM is based on the Higgs superpotential

$$W_{\text{Higgs}} = \lambda \widehat{S} \widehat{H}_1^T i\tau_2 \widehat{H}_2 + \frac{\kappa}{3} \widehat{S}^3. \quad (4.1)$$

As usual, the complete tree-level Higgs potential is obtained by adding the relevant  $F$ - and  $D$ -term contributions to the soft SUSY-breaking terms induced by the superpotential:

$$\begin{aligned}
- \mathcal{L}_V^0 &= m_1^2 \Phi_1^\dagger \Phi_1 + m_2^2 \Phi_2^\dagger \Phi_2 + m_S^2 S^* S + \left( \lambda A_\lambda S \Phi_1^\dagger \Phi_2 + \text{h.c.} \right) + \left( \frac{\kappa}{3} A_\kappa S^3 + \text{h.c.} \right) \\
&\quad - \lambda_1 (\Phi_1^\dagger \Phi_1)^2 - \lambda_2 (\Phi_2^\dagger \Phi_2)^2 - \lambda_3 (\Phi_1^\dagger \Phi_1) (\Phi_2^\dagger \Phi_2) - (\lambda_4 - \lambda^2) (\Phi_1^\dagger \Phi_2) (\Phi_2^\dagger \Phi_1) \\
&\quad + \lambda^2 S^* S (\Phi_1^\dagger \Phi_1 + \Phi_2^\dagger \Phi_2) + \kappa^2 (S^* S)^2 + \left[ \lambda \kappa S^{*2} (\Phi_1^\dagger \Phi_2) + \text{h.c.} \right]. \quad (4.2)
\end{aligned}$$

Furthermore, the minimization conditions are determined by requiring that the following tadpole parameters vanish:

$$T_{\phi_1} \equiv \left\langle \frac{\partial \mathcal{L}_V}{\partial \phi_1} \right\rangle = -v_1 \left[ m_1^2 + \left( \frac{1}{\sqrt{2}} \lambda A_\lambda v_S + \frac{1}{2} \lambda \kappa v_S^2 \right) t_\beta - \lambda_1 v_1^2 - \frac{1}{2} (\lambda_3 + \lambda_4 - \lambda^2) v_2^2 + \frac{1}{2} \lambda^2 v_S^2 \right], \quad (4.3)$$

$$T_{\phi_2} \equiv \left\langle \frac{\partial \mathcal{L}_V}{\partial \phi_2} \right\rangle = -v_2 \left[ m_2^2 + \left( \frac{1}{\sqrt{2}} \lambda A_\lambda v_S + \frac{1}{2} \lambda \kappa v_S^2 \right) t_\beta^{-1} - \lambda_2 v_2^2 - \frac{1}{2} (\lambda_3 + \lambda_4 - \lambda^2) v_1^2 + \frac{1}{2} \lambda^2 v_S^2 \right], \quad (4.4)$$

$$T_{\phi_S} \equiv \left\langle \frac{\partial \mathcal{L}_V}{\partial \phi_S} \right\rangle = -v_S \left( m_S^2 + \lambda A_\lambda \frac{v_1 v_2}{\sqrt{2} v_S} + \frac{1}{2} \lambda^2 v^2 + \kappa A_\kappa \frac{v_S}{\sqrt{2}} + \kappa^2 v_S^2 + \lambda \kappa v_1 v_2 \right). \quad (4.5)$$

We should remark again that spontaneous CP violation is absent in the NMSSM at the tree level [14,22]. Also, CP appears to be still a good symmetry of the NMSSM, even if (CP-conserving) large radiative stop-mixing effects were to be taken into account [22].

Considering the vanishing of the tadpole parameters given in Eqs. (4.3)–(4.5), it is not difficult to compute the charged Higgs-boson mass, and the CP-odd and CP-even mass matrices. More explicitly, the squared charged Higgs-boson mass is given by

$$M_{H^+}^{2(0)} = \frac{1}{s_\beta c_\beta} \left( \mu A_\lambda - \frac{\kappa}{\lambda} \mu^2 \right) + M_W^2 - \frac{1}{2} \lambda^2 v^2, \quad (4.6)$$

where the would-be  $\mu$ -parameter is defined in Eq. (3.11). The entries of the tree-level CP-odd mass matrix  $M_P^{2(0)}$  are found to be

$$\begin{aligned} (M_P^{2(0)})_{11} &= M_a^{2(0)}, \\ (M_P^{2(0)})_{12} &= (M_P^{2(0)})_{21} = \frac{v}{v_S} \left( s_\beta c_\beta M_a^{2(0)} + 3 \frac{\kappa}{\lambda} \mu^2 \right), \\ (M_P^{2(0)})_{22} &= \frac{v^2}{v_S^2} s_\beta c_\beta \left( s_\beta c_\beta M_a^{2(0)} - 3 \frac{\kappa}{\lambda} \mu^2 \right) + 3 \frac{\kappa}{\lambda} \mu A_\kappa, \end{aligned} \quad (4.7)$$

where  $M_a^{2(0)}$  is given by Eq. (3.13). Finally, the entries of CP-even mass matrix  $M_S^{2(0)}$  read

$$\begin{aligned} (M_S^{2(0)})_{11} &= c_\beta^2 M_Z^2 + s_\beta^2 M_a^{2(0)}, \\ (M_S^{2(0)})_{12} &= (M_S^{2(0)})_{21} = -s_\beta c_\beta \left( M_a^{2(0)} + M_Z^2 - \lambda^2 v^2 \right), \\ (M_S^{2(0)})_{13} &= (M_S^{2(0)})_{31} = -\frac{v}{v_S} \left( s_\beta^2 c_\beta M_a^{2(0)} - 2 c_\beta \mu^2 - \frac{\kappa}{\lambda} s_\beta \mu^2 \right), \\ (M_S^{2(0)})_{22} &= s_\beta^2 M_Z^2 + c_\beta^2 M_a^{2(0)}, \end{aligned}$$

$$\begin{aligned}
(M_S^{2(0)})_{23} &= (M_S^{2(0)})_{32} = -\frac{v}{v_S} \left( s_\beta c_\beta^2 M_a^{2(0)} - 2s_\beta \mu^2 - \frac{\kappa}{\lambda} c_\beta \mu^2 \right), \\
(M_S^{2(0)})_{33} &= \frac{v^2}{v_S^2} s_\beta c_\beta \left( s_\beta c_\beta M_a^{2(0)} + \frac{\kappa}{\lambda} \mu^2 \right) - \frac{\kappa}{\lambda} \mu A_\kappa + 4 \frac{\kappa^2}{\lambda^2} \mu^2.
\end{aligned} \tag{4.8}$$

From the above analytic expressions for  $M_{H^\pm}^{2(0)}$ , and the CP-odd and CP-even Higgs-boson mass matrices,  $M_P^{2(0)}$  and  $M_S^{2(0)}$ , it is now evident that the MSSM limit of the NMSSM is obtained for  $\kappa, \lambda \rightarrow 0$ , while holding  $\kappa/\lambda$ ,  $\mu$ ,  $A_\lambda$  and  $A_\kappa$  fixed.

Parenthetically, we should remark that the Higgsino sector of the NMSSM is also different from the corresponding one in the MNSSM. Because of the presence of the operator  $\frac{\kappa}{3} \hat{S}^3$  in the superpotential (4.1), the  $\{55\}$ -matrix element of the neutralino mass matrix in Eq. (3.43) receives the additional contribution:

$$(\mathcal{M}_0)_{55} = -2 \frac{\kappa}{\lambda} \mu. \tag{4.9}$$

Note that if  $(\mathcal{M}_0)_{55} < 0$  with  $\mu < 0$ ,<sup>§</sup> this additional contribution to the predominantly singlet state in the NMSSM is constructive, rendering its mass larger than the axino mass in the MNSSM. However, for small positive values of  $\kappa$ , e.g.  $\kappa \lesssim 0.1$ , and  $|\mu| \lesssim 200$  GeV, with  $\mu < 0$  and  $\lambda \approx 0.65$ , the  $\{55\}$ -matrix element  $(\mathcal{M}_0)_{55}$  is positive and its contribution to the would-be axino mass is destructive, leading to light singlet masses smaller than  $m_{\tilde{a}}$ .

It is now important to notice that unlike the MNSSM case, the decoupled CP-even and CP-odd scalar singlets are no longer degenerate in the MSSM limit of the NMSSM. This fact is a manifestation of the violation of the mass sum rule (3.19) in the case of the NMSSM. Specifically, in the NMSSM we find that

$$\sum_{i=1}^3 M_{H_i}^{2(0)} - \sum_{i=1}^2 M_{A_i}^{2(0)} - M_Z^2 = 4 \frac{\kappa}{\lambda} \mu^2 \left( \frac{v^2}{v_S^2} s_\beta c_\beta + \frac{\kappa}{\lambda} - \frac{A_\kappa}{\mu} \right). \tag{4.10}$$

It is obvious that the mass sum rule (3.19) can be sizeably violated in the NMSSM for relatively large values of  $|\kappa|$  and  $|\mu|$  or  $|A_\kappa|$ . In such cases, the violation of the mass sum rule becomes much larger than the one caused by radiative stop effects.

The analytic expressions of the Higgs-boson masses in the NMSSM coincide with those of the MNSSM only in the PQ-symmetric limit, where  $\kappa/\lambda$ ,  $t_S$ ,  $m_{12}^2 \rightarrow 0$ . Although this limit is unphysical as it leads to a theory with a visible axion, its vicinity, however, could define an acceptable region of parameter space where the predictions of the two models exhibit reasonable agreement.

---

<sup>§</sup>Our choice of a negative  $\mu$ -parameter is mainly dictated by the fact that  $b \rightarrow s\gamma$  imposes a stronger lower limit on positive values of  $\mu$  [23] for relatively small charged Higgs-boson masses, close to the present experimental bound, i.e. for  $M_{H^\pm} \sim 80$  GeV [15]. Instead, for negative values of  $\mu$ , the bound on  $\mu$  can be dramatically relaxed up to the present LEP2 limit:  $|\mu| \gtrsim 90$  GeV [15].

An interesting property of the tree-level CP-even mass matrix  $M_S^{2(0)}$  in the PQ-symmetric limit is that the interval of the allowed  $\mu^2$  values is rather small. This interval may be determined by requiring that the determinant of  $M_S^{2(0)}$ ,

$$\begin{aligned} \det(M_S^{2(0)}) = & -\frac{v^2}{v_S^2} \left\{ 4 \left[ M^2 + \left( \frac{1}{2} \lambda^2 v^2 - M_Z^2 \right) \cos^2 2\beta \right] \mu^4 - 2 \sin^2 2\beta M^2 M_a^{2(0)} \mu^2 \right. \\ & \left. + \frac{1}{4} \sin^4 2\beta M^2 M_a^{2(0)} \left( M_a^{2(0)} - \frac{1}{2} \lambda^2 v^2 \right) \right\}, \end{aligned} \quad (4.11)$$

with  $M^2 = M_a^{2(0)} + M_Z^2 - \frac{1}{2} \lambda^2 v^2 = M_{H^+}^{2(0)} + M_Z^2 - M_W^2$ , be positive. Neglecting terms proportional to  $(\frac{1}{2} \lambda^2 v^2 - M_Z^2) \cos^2 2\beta$  next to  $M^2$  in Eq. (4.11), we may approximate the determinant  $\det(M_S^{2(0)})$  as

$$\det(M_S^{2(0)}) \approx -\frac{v^2}{v_S^2} M^2 \left[ 4\mu^4 - 2 \sin^2 2\beta M_a^{2(0)} \mu^2 + \frac{1}{4} \sin^4 2\beta M_a^{2(0)} \left( M_a^{2(0)} - \frac{1}{2} \lambda^2 v^2 \right) \right]. \quad (4.12)$$

Requiring now that  $\det(M_S^{2(0)})$  be positive gives the allowed  $\mu^2$  interval:

$$\frac{1}{4} \sin^2 2\beta M_a^{2(0)} (1 - \delta) \lesssim \mu^2 \lesssim \frac{1}{4} \sin^2 2\beta M_a^{2(0)} (1 + \delta) \quad (4.13)$$

with

$$\delta = \sqrt{\frac{\lambda^2 v^2}{2M_a^{2(0)}}}. \quad (4.14)$$

Here, it is understood that  $\delta \leq 1$  or, equivalently,  $M_{H^+}^{2(0)} \geq M_W^2$ . Especially for  $M_{H^+}^{2(0)} = M_W^2$ , for which the terms proportional to  $(\frac{1}{2} \lambda^2 v^2 - M_Z^2) \cos^2 2\beta$  are no longer negligible with respect to  $M^2 = M_Z^2$ , the allowed range of  $\mu^2$  becomes

$$0 < \mu^2 < \frac{1}{2} \sin^2 2\beta M_a^{2(0)} \left( 1 + \frac{\frac{1}{2} \lambda^2 v^2 - M_Z^2}{M_Z^2} \cos^2 2\beta \right)^{-1}. \quad (4.15)$$

Further insight into the predictions of the PQ-symmetric limit may be gained by analyzing the kinematic situation where  $M_{H^+}^{2(0)} \gg M_W^2$  (i.e.  $\delta \ll 1$ ) and  $\mu^2 = \mu_{\text{mid}}^2 = s_\beta^2 c_\beta^2 M_a^{2(0)}$  which is approximately the middle point of the allowed  $\mu^2$ -interval. In this case, we obtain (see also Appendix B)

$$\begin{aligned} M_{H_1}^{2(0)} &\approx \frac{1}{2} \lambda^2 v^2 \sin^2 2\beta, & M_{H_2}^{2(0)} &\approx M_Z^2 \cos^2 2\beta + \frac{1}{2} \lambda^2 v^2 \sin^2 2\beta, \\ M_{H_3}^{2(0)} &\approx M_a^{2(0)} + \frac{1}{2} \lambda^2 v^2 \cos^2 2\beta - \left( \frac{1}{2} \lambda^2 v^2 - M_Z^2 \right) \sin^2 2\beta, \\ M_{A_1}^{2(0)} &\approx 0, & M_{A_2}^{2(0)} &\approx M_a^{2(0)} + \frac{1}{2} \lambda^2 v^2 \end{aligned} \quad (4.16)$$

and

$$g_{H_2 ZZ}^2 \approx g_{H_3 A_2 Z}^2 \approx 1. \quad (4.17)$$



Thus, the light  $H_1$  and  $A_1$  scalars decouple from the gauge bosons, whilst the  $H_2$  boson couples maximally to them with SM strength. Moreover, according to the mass-coupling sum rule (3.55), the  $H_2$ -boson mass saturates the mass upper bound obeyed by the SM-like Higgs boson. Given that the length of the allowed  $\mu^2$ -interval is very small relative to  $\mu_{\text{mid}}^2$  for  $\delta \ll 1$ , one does not expect serious changes regarding the heaviest Higgs-boson masses  $M_{H_3}$  and  $M_{A_2}$  and the qualitative features of the Higgs to gauge-boson couplings as  $\mu$  takes all other allowed values.

A minimal deviation from the PQ-symmetric limit, in which the NMSSM could easily be compared with the MNSSM, is the limit  $\kappa \rightarrow 0$ , with  $\lambda$ ,  $\mu$ ,  $A_\lambda$  and  $\kappa A_\kappa$  held fixed. In fact, in this limit, the coupling  $\lambda$  could be the largest, thereby allowing for the largest possible value for the lightest Higgs-boson mass  $M_{H_1}$ . By the same token, the unwanted  $U(1)_{\text{PQ}}$  symmetry gets broken by the trilinear soft SUSY-breaking self-coupling  $\kappa A_\kappa$  of the singlet  $S$ . A corresponding limit of the MNSSM, which has the same number of independent parameters as in the NMSSM, is the one with  $m_{12}^2 \rightarrow 0$ , but  $\lambda$ ,  $\mu$ ,  $A_\lambda$  and  $t_S$  fixed. We should also bear in mind that vanishing of  $t_S$  entails vanishing of  $m_{12}^2$  as well which eliminates the possibility of  $t_S \rightarrow 0$ , with  $m_{12}^2$  fixed. In this way, we compare essentially two models which only differ in soft operators of dimensionality  $d \leq 3$ . An additional reason that renders such a comparison very interesting is the fact that the dimensionful parameters, such as  $A_\kappa$  and  $t_S$ , remain unconstrained by perturbativity arguments, and hence could severely affect the structure of the mass matrices.

The aforementioned physical limit allows for more direct comparisons of the NMSSM with the MNSSM. Equating the tadpole parameters  $T_{\phi_1}$ ,  $T_{\phi_2}$  and  $T_{\phi_S}$  pertinent to the two models yields, in this limit, the simple relation

$$\frac{\lambda t_S}{\mu} = \frac{\kappa}{\lambda} \mu A_\kappa. \quad (4.18)$$

Moreover, in the same limit, except for  $(M_P^{2(0)})_{22}$  and  $(M_S^{2(0)})_{33}$ , all other elements of the mass matrices coincide as well. In the MNSSM  $\lambda t_S/\mu$  enters the elements  $(M_P^{2(0)})_{22}$  and  $(M_S^{2(0)})_{33}$  in exactly the same way, whereas in the NMSSM the corresponding parameter  $(\kappa \mu A_\kappa)/\lambda$  appears in these two matrix elements with different coefficients, and most importantly, with different signs reflecting the violation of the tree-level mass sum rule (3.19). The fact that the determinants of the CP-odd Higgs-boson mass matrices in the MNSSM and NMSSM are proportional to  $\lambda t_S/\mu$  and  $(\kappa \mu A_\kappa)/\lambda$  necessitates that the two parameters must be both positive. As a result of this, the matrix element  $(M_S^{2(0)})_{33}$  will be enhanced in the MNSSM, but reduced in the NMSSM. In addition, it is not difficult to see that the determinant of the tree-level CP-even mass matrix,  $\det(M_S^{2(0)})$ , is a monotonically increasing function of  $(M_S^{2(0)})_{33}$  and is already negative if  $(M_S^{2(0)})_{33}$  vanishes. This last property

relies on the fact that the upper-left  $2 \times 2$  submatrix is positive definite. Therefore, the larger the mass  $M_{A_1}$  of the lightest CP-odd scalar is the larger (smaller)  $\det(M_S^{2(0)})$  is in the MNSSM (NMSSM). On the other hand, a very small value for  $\lambda t_S/\mu$  or  $(\kappa\mu A_\kappa)/\lambda$ , which amounts to having a very light  $A_1$ , does not seriously affect  $M_S^{2(0)}$ , and hence no essential difference in the predictions for the Higgs spectrum between the MNSSM and NMSSM can be observed. In this region, both models are close to the PQ-symmetric limit. However, the difference between the two models becomes appreciable, once the parameters  $\lambda t_S/\mu$  and  $(\kappa\mu A_\kappa)/\lambda$  become large. The first parameter has no upper bound, whereas the second one is limited by the fact that  $(M_S^{2(0)})_{33}$  should be positive. Thus, only in the MNSSM case a significant departure from the PQ-symmetric limit is possible, which may change the situation drastically. For example, a  $\mu$ -independent contribution to  $(M_S^{2(0)})_{33}$ , say  $T^2$ , changes the coefficient of  $\mu^2$  in the expression (4.11) for  $\det(M_S^{2(0)})$ , and as a consequence, the allowed interval for  $\mu^2$  can now expand (or further shrink) for  $T^2$  positive (negative). For the particular case that  $M_{H^+}^{2(0)} = M_W^2$ , the interval of  $\mu^2$  increases (decreases) by a factor  $1 + T^2/(\lambda^2 v^2 \sin^2 2\beta)$ . As we just observed, such an unconstrained (constrained) positive (negative) contribution is available in the MNSSM (NMSSM), i.e.  $T^2 \equiv \lambda t_S/\mu$  ( $T^2 \equiv -(\kappa\mu A_\kappa)/\lambda$ ), where  $t_S$  ( $A_\kappa$ ) should be regarded as a  $\mu$ -dependent parameter.

At this point, it should be stressed that our discussion of the NMSSM in the limit  $\kappa \rightarrow 0$ , with  $\lambda$ ,  $\mu$ ,  $A_\lambda$  and  $\kappa A_\kappa$  being kept fixed, by no means exhausts all possible predictions that the model offers for viable scenarios. Being close to the above limit requires that  $|\kappa/\lambda| \ll 1 \ll |A_\kappa/\mu|$ . However, it is possible to considerably depart from this limit, even if  $|\kappa/\lambda|$  is very small but non-zero, while avoiding the known problem associated with the presence of a visible axion. In order to better investigate alternative scenarios that avoid the presence of a visible axion, we compute the exact determinant of the CP-odd Higgs-scalar mass matrix

$$\det(M_P^{2(0)}) = 3 \frac{\kappa}{\lambda} \left( \mu A_\kappa - \frac{3}{4} \sin 2\beta \lambda^2 v^2 - 3 \frac{\kappa}{\lambda} \delta^2 \mu^2 \right) M_a^{2(0)}. \quad (4.19)$$

We shall now examine other possible deviations from the PQ-symmetric limit, for which the  $\mu$  values, however, are not very different from those determined by the allowed  $\mu$  interval in Eq. (4.13). Under this assumption and the fact that  $|\kappa/\lambda|$  is considered to be adequately small, the third term on the RHS of Eq. (4.19) remains always subdominant; it actually diminishes the size of  $\det(M_P^{2(0)})$  irrespectively of the sign of  $\kappa/\lambda$ . For  $|A_\kappa/\mu| \gg 1$ , the first term  $\mu A_\kappa$  on the RHS of Eq. (4.19) becomes dominant. In this case, this term should have the same sign as  $\kappa/\lambda$ , in compliance with our earlier requirement that  $(\kappa\mu A_\kappa)/\lambda$  be positive. However, as  $|A_\kappa/\mu|$  is getting smaller, the second term  $\frac{3}{4} \sin 2\beta \lambda^2 v^2$  within the parentheses on the RHS of Eq. (4.19) will then start playing an important rôle. For  $\kappa/\lambda > 0$  ( $\kappa/\lambda < 0$ ),

this second term provides a lower (upper) bound on  $\mu A_\kappa$ , which should not be saturated. In fact, the mass of the lightest CP-odd scalar depends crucially on the difference between these two first terms on the RHS of Eq. (4.19). It is then obvious that if  $\kappa/\lambda$  is negative,  $\mu A_\kappa$  could be negative, zero or even a positive quantity which is bounded from above.

Having gained some insight from the above discussion, let us now consider the most general case without resorting to specific assumptions or kinematic approximations. Then, the requirement that  $\det(M_P^{2(0)})$  in Eq. (4.19) be positive implies the constraint

$$\mu_- < \mu < \mu_+ \quad (4.20)$$

with

$$\mu_\pm = \left(6\frac{\kappa}{\lambda}\delta^2\right)^{-1} \left[ A_\kappa \pm \text{sign}\left(\frac{\kappa}{\lambda}\right) \sqrt{A_\kappa^2 - 9\sin 2\beta \delta^2 \kappa \lambda v^2} \right], \quad (4.21)$$

where  $A_\kappa^2 > 9\sin 2\beta \delta^2 \kappa \lambda v^2$ . We see again that  $A_\kappa = 0$  is only allowed for  $\kappa/\lambda < 0$ . In this case,  $\mu^2$  is constrained to be in the range:

$$0 < \mu^2 < -\frac{\lambda}{2\kappa} \sin 2\beta M_a^{2(0)}. \quad (4.22)$$

Here, it is also important to reiterate the fact that the requirement for a positive  $\det(M_P^{2(0)})$  constrains by itself the  $\{33\}$ -element of  $M_S^{2(0)}$ :

$$(M_S^{2(0)})_{33} < \frac{v^2}{v_S^2} s_\beta c_\beta \left( s_\beta c_\beta M_a^{2(0)} - 2\frac{\kappa}{\lambda} \mu^2 \right) + (4 - 3\delta^2) \frac{\kappa^2}{\lambda^2} \mu^2. \quad (4.23)$$

The constraint in Eq. (4.23) seems to favour negative values of  $\kappa/\lambda$ , as the upper limit on  $(M_S^{2(0)})_{33}$  gets larger in this case. Furthermore, saturation of the upper bound in Eq. (4.23) leads to  $M_{A_1}^{2(0)} = 0$ .

As the key parameter  $|\kappa/\lambda|$  increases, the situation is getting more involved since new terms start playing a rôle. In particular, a term which deserves special attention is the one proportional to  $\kappa^2 \mu^2 / \lambda^2$  that occurs in Eq. (4.23). This term becomes very important for larger values of  $M_{H^+}^{2(0)}$  which lead to smaller values of  $\delta$  and to larger values of  $\mu^2$  in accordance with Eqs. (4.13) and (4.14). In such a case, we may hope for an enlargement of the allowed interval of  $\mu^2$  values, for which  $\det(M_S^{2(0)})$  is positive. Therefore, it would be interesting to investigate to which extent such a situation can indeed be realized, especially for low values of  $M_{H^+}^{2(0)}$  for which  $\delta$  is not very small and  $(M_S^{2(0)})_{33}$  appears to be more severely constrained. To this end, we shall consider the special case where  $M_{H^+}^{2(0)} = M_W^2$ , i.e.  $\delta = 1$ . Then, after taking into account the constraint in Eq. (4.23) and making use of the fact that  $\det(M_S^{2(0)})$  increases monotonically with  $(M_S^{2(0)})_{33}$ , the following inequality

may be derived:

$$\det(M_S^{2(0)}) < -\lambda^2 v^2 M_Z^2 \left[ 2 \left( 1 + \frac{\kappa}{\lambda} \sin 2\beta + \frac{\frac{1}{2} \lambda^2 v^2 - M_Z^2}{M_Z^2} \cos^2 2\beta \right) \mu^2 - \sin^2 2\beta M_a^{2(0)} \right]. \quad (4.24)$$

Assuming that the corresponding upper bound in Eq. (4.23) is saturated (i.e.  $M_{A_1}^{2(0)} = 0$ ), then Eq. (4.24) and the fact that  $\det(M_S^{2(0)}) > 0$  lead to

$$0 < \mu^2 < \frac{1}{2} \sin^2 2\beta M_a^{2(0)} \left( 1 + \frac{\kappa}{\lambda} \sin 2\beta + \frac{\frac{1}{2} \lambda^2 v^2 - M_Z^2}{M_Z^2} \cos^2 2\beta \right)^{-1}. \quad (4.25)$$

It is easy to see that for  $|\kappa/\lambda| \ll 1$ , the double inequality in Eq. (4.25) reduces to our previous result found in Eq. (4.15). We observe now that for  $\kappa/\lambda > 0$ , the allowed interval of  $\mu^2$  given by Eq. (4.25) shrinks as  $|\kappa/\lambda|$  increases. Instead, for  $\kappa/\lambda < 0$  with  $|\kappa/\lambda|$  increasing, the allowed interval gets larger and, especially for values of  $|\kappa/\lambda|$  close to unity, it may even become infinitely large. Of course, at this critical kinematic region, radiative corrections are expected to play the dominant rôle. Notwithstanding this fact, our tree-level results should still be indicative of the various tendencies which govern the kinematic parameters of the theory. As we will see below, however, values of  $|\kappa/\lambda| \sim 1$  are not compatible with the largest possible value for  $\lambda$  and hence with the largest value of the lightest Higgs-boson mass  $M_{H_1}$ .

The Yukawa-type couplings  $\kappa$  and  $\lambda$  cannot be arbitrarily large, if we wish to preserve the good property of SUSY that perturbation theory be applicable up to the gauge unification scale  $M_U \sim 10^{16}$  GeV [24]. Therefore, upper limits on  $|\lambda|$  and  $|\kappa|$  can be obtained by studying their renormalization-group (RG) evolution along with the corresponding ones of the strong coupling constant  $g_s$  and the  $t$ -quark Yukawa coupling  $h_t$  [25,19,26]:

$$\begin{aligned} 16\pi^2 \frac{dg_s}{dt} &= -\frac{3}{2} g_s^3, \\ 16\pi^2 \frac{dh_t}{dt} &= h_t \left( 3h_t^2 + \frac{1}{2} \lambda^2 - \frac{8}{3} g_s^2 \right), \\ 16\pi^2 \frac{d\lambda}{dt} &= \lambda \left( \kappa^2 + 2\lambda^2 + \frac{3}{2} h_t^2 \right), \\ 16\pi^2 \frac{d\kappa}{dt} &= 3\kappa (\kappa^2 + \lambda^2), \end{aligned} \quad (4.26)$$

where  $t = \ln(Q^2/M_t^2)$ . In writing the RG equations (4.26), we have ignored possible mass threshold effects of the SUSY particles while running from the  $t$ -quark-pole mass  $M_t = 175$  GeV up to  $M_U \sim 10^{16}$  GeV. In the RG analysis, we use the value for the strong fine-structure constant  $\alpha_s(M_t) = g_s^2(M_t)/(4\pi) \approx 0.109$ . Furthermore, the running  $t$ -quark Yukawa coupling  $h_t$  is determined by

$$h_t(M_t) = \frac{m_t(M_t)}{v(M_t) s_\beta(M_t)}, \quad (4.27)$$

where  $v(M_t) = 174.1$  GeV and

$$m_t(M_t) = \frac{M_t}{1 + \frac{4}{3\pi} \alpha_s(M_t)} \quad (4.28)$$

is the known relation between the on-shell  $\overline{\text{MS}}$  mass and  $M_t$ . For  $3 \lesssim \tan \beta(M_t) < 10$ , we find the approximate upper bounds

$$|\lambda(M_t)| \lesssim 0.70, 0.63, 0.57, 0.44, 0.22, \quad \text{for } |\kappa(M_t)| = 0, 0.3, 0.4, 0.5 \text{ and } 0.6, \quad (4.29)$$

respectively. Correspondingly, for  $\tan \beta \approx 2$ , we obtain

$$|\lambda(M_t)| \lesssim 0.65, 0.59, 0.54, 0.42, 0.21. \quad (4.30)$$

The results in Eqs. (4.29) and (4.30) are in good agreement with Ref. [19,26]. From the above analysis, it is obvious that the largest value for  $|\lambda(M_t)|$  is more naturally attained in the MNSSM (corresponding to  $\kappa(M_t) = 0$ ) rather than in the NMSSM, as one would generically expect  $\lambda(M_t) \sim \kappa(M_t) \neq 0$ . This is another important difference between these two models. In particular, this implies that the MNSSM generically predicts higher masses for the lightest Higgs boson than the NMSSM.

In the next section, we shall study the Higgs sector of the MNSSM more quantitatively and also compare our numerical predictions with those obtained in the NMSSM.

## 5 Phenomenological discussion

In this section, we shall discuss the phenomenology of the Higgs bosons in the MNSSM, and make comparisons of our predictions with those obtained in the NMSSM.

At LEP2, the CP-even and CP-odd Higgs scalars,  $H_{1,2,3}$  and  $A_{1,2}$ , are mainly produced through the Higgs-strahlung process  $e^+e^- \rightarrow Z^* \rightarrow ZH_i$  or in pairs via  $e^+e^- \rightarrow Z^* \rightarrow H_i A_j$ . Analogous Higgs-boson production mechanisms can take place at Fermilab, where instead of electrons the initial states are the  $u$  and  $d$  quarks at the quark-parton level [27]. Therefore, the necessary ingredients for our numerical discussion following below are the analytic expressions for the radiatively-corrected Higgs-boson masses and the effective Higgs-boson couplings to the gauge bosons. These analytic expressions pertaining to the MNSSM and NMSSM have been presented in Sections 3 and 4, respectively.

There are several possible combinations in choosing the independent kinematic parameters for the two supersymmetric extensions of the MSSM, the MNSSM and the NMSSM. For definiteness, for the MNSSM case, we consider

$$t_\beta, \quad M_{H^+}^2, \quad \mu, \quad \lambda, \quad \frac{\lambda t_S}{\mu} \quad \text{and} \quad m_{12}^2, \quad (5.1)$$

as free phenomenological parameters of the Higgs sector. As for the NMSSM, we take as input parameters

$$t_\beta, \quad M_{H^+}^2, \quad \mu, \quad \lambda, \quad \kappa \quad \text{and} \quad \frac{\kappa\mu A_\kappa}{\lambda}. \quad (5.2)$$

For both SUSY models, the stop-related parameters are chosen to have the typical values:

$$\widetilde{M}_Q = \widetilde{M}_t = 0.5 \text{ TeV}, \quad A_t = 1 \text{ TeV}. \quad (5.3)$$

Here, we should remark that  $m_{12}^2$  in Eq. (5.1) could in principle be absent, without spoiling the renormalizability of the theory. In this case, the  $U(1)_{\text{PQ}}$  symmetry of the MNSSM gets broken explicitly by the effectively generated tadpole parameter  $t_S$ , which is a term of the lowest possible dimension, namely of dimension 1. Such a reduction of the renormalizable parameters is not possible in the NMSSM because of the presence of  $\widehat{S}^3$  which violates  $U(1)_{\text{PQ}}$  hardly. Therefore, it is fair to conclude that in the admissible limit  $m_{12}^2 \rightarrow 0$ , the MNSSM under investigation represents the most economic, renormalizable scenario among the proposed non-minimal supersymmetric standard models.

In Fig. 2 we display the dependence of the lightest Higgs boson  $H_1$  in the MNSSM with  $m_{12}^2 = 0$  on the would-be  $\mu$ -parameter, for different values of the charged Higgs-boson mass, i.e. for  $M_{H^+} = 0.1, 0.3, 0.7$  and  $1 \text{ TeV}$ . In Fig. 2(a), we choose the tadpole-parameter value  $\lambda t_S/\mu = 1 \text{ TeV}^2$ . As we are interested in maximal values for the lightest Higgs-boson mass  $M_{H_1}$  which occur for low values of  $\tan\beta$ , i.e. for  $\tan\beta = 2$ , we consider the largest allowed coupling  $\lambda = 0.65$ , for which the MNSSM stays perturbative up to the gauge unification scale  $M_U \sim 10^{16} \text{ GeV}$  (see also discussion in Section 4). As can be seen from Fig. 2(a), the  $H_1$ -boson mass varies between 120 and 145 GeV depending on  $M_{H^+}$  for a wide range of  $\mu$  values, which is significantly larger than the current experimental lower bound of 113.3 GeV on the SM-type Higgs boson. Furthermore, we observe an asymmetry of order 5 GeV in  $M_{H_1}$  for large  $|\mu| \gtrsim 300 \text{ GeV}$  between positive and negative values of  $\mu$ . This is because stop-radiative effects on  $M_{H_1}$  get enhanced for larger values of the stop-mixing parameter  $|X_t| = |A_t - \mu/\tan\beta|$  which obviously result from large negative values of  $\mu$ , provided  $|X_t|/\max(\widetilde{M}_Q, \widetilde{M}_t) \lesssim \sqrt{6}$  (cf. Eq. (3.55)).

In Fig. 2(b) we consider a smaller value for the tadpole parameter, i.e.  $\lambda t_S/\mu = 0.04 \text{ TeV}^2$ . As in Fig. 2(a), we present numerical estimates of  $M_{H_1}$  as a function of  $\mu$ , for the same discrete values of the charged Higgs-boson mass:  $M_{H^+} = 0.1, 0.3, 0.7$  and  $1 \text{ TeV}$ . We find that the allowed range of  $\mu$  becomes much smaller, but the maximum values of  $M_{H_1}$  are still very close to those obtained in Fig. 2(a). Most interestingly, we observe that the maxima of  $M_{H_1}$  are located at almost the same  $\mu$  values found for the tadpole parameter of  $1 \text{ TeV}^2$ ; the maxima are practically independent of the tadpole parameter, for all relevant values of  $\lambda t_S/\mu = 0.01\text{--}1 \text{ TeV}^2$ . This feature that the allowed range of  $\mu$  values shrinks as

$\lambda t_S/\mu$  gets smaller is in good agreement with our discussion in Section 4 concerning the CP-even Higgs-boson mass matrix in the PQ-symmetric limit. Specifically, for small values of  $\lambda t_S/\mu$ , the allowed  $|\mu|$ -ranges can be accurately determined by Eqs. (4.13) and (4.15). In particular, the mean values of the allowed  $|\mu|$ -ranges, which are approximately given by  $s_\beta c_\beta M_{H^+}$  and are almost independent of  $\lambda t_S/\mu$ , appear to describe well the location of the maxima of  $M_{H_1}$ .

It is now very interesting to analyze a scenario within the context of the MNSSM, in which the charged Higgs boson has a relatively low mass, in the range  $M_{H^+} = 80\text{--}160$  GeV, and may be accessed in next-round experiments at LEP2 and/or at the upgraded Tevatron collider. For this purpose, in Fig. 3 we display numerical estimates of the two lightest Higgs bosons  $H_1$  and  $H_2$  and their corresponding squared couplings to the  $Z$  boson as functions of the parameter  $\mu$ , for  $M_{H^+} = 80, 120$  and  $160$  GeV. The other kinematic parameters are chosen to be the same as in Fig. 2(a):  $\tan\beta = 2$ ,  $\lambda = 0.65$  and  $\lambda t_S/\mu = 1$  TeV<sup>2</sup>. Let us first consider the lowest experimentally allowed value for the charged Higgs-boson mass  $M_{H^+} = 80$  GeV [1,15]. Then, in Fig. 3(a) we notice that the  $H_1$ -boson mass cannot become larger than 105 GeV, whilst the next-to-lightest  $H_2$  boson can be as heavy as 146 GeV. As can be seen from Fig. 3(b), such a scenario is not excluded experimentally, since the  $H_1 ZZ$ -coupling gets suppressed, i.e.  $g_{H_1 ZZ}^2 \lesssim 0.2$ , for  $|\mu| \lesssim 350$  GeV. In this scenario, the  $H_2$  boson becomes SM type ( $H_2 \equiv H_{\text{SM}}$ ), and is much heavier than  $H^+$ . This novel prediction of the MNSSM for viable scenarios with  $M_{H^+} \lesssim M_{H_{\text{SM}}}$  and low-values of  $\tan\beta < 5$  cannot be realized within the MSSM, even if CP-violating loop effects are included in the Higgs sector of the MSSM [28,18].<sup>¶</sup> In fact, as we will see later on, neither the NMSSM can naturally accommodate scenarios with  $M_{H^+} \lesssim M_{H_{\text{SM}}}$ , for the experimentally allowed values of  $|\mu| \gtrsim 90$  GeV [15].

As the charged Higgs boson becomes heavier in the MNSSM, the  $H_1$  boson also gets heavier and resembles the SM Higgs boson  $H_{\text{SM}}$ . Thus, from Fig. 3 we see that for  $M_{H^+} = 120$  GeV,  $M_{H_1} \lesssim 132$  GeV, with  $g_{H_1 ZZ}^2 \sim 0.5$ , while for  $M_{H^+} = 160$  GeV, it is  $M_{H_1} \lesssim 142$  GeV, with  $g_{H_1 ZZ}^2 \approx 1$ . Furthermore, as we have already discussed in Section 3.1, for the considered values of  $M_{H^+}$  much smaller than  $\lambda t_S/\mu$ , the Higgs states  $A_2$  and  $H_3$  decouple and are almost degenerate with  $M_{A_2}^2 \approx M_{H_3}^2 \approx \lambda t_S/\mu$ . In particular, our numerical estimates confirm the relations:  $M_{A_1}^2 \approx M_{H^+}^2 - M_W^2 + \frac{1}{2}\lambda^2 v^2$  (cf. Eq. (3.16)), and  $g_{H_1 ZZ}^2 \approx g_{H_2 A_1 Z}^2$  and  $g_{H_2 ZZ}^2 \approx g_{H_1 A_1 Z}^2$  (cf. Eq. (3.54)), which are only valid in the above specific decoupling regime of the  $A_2$  and  $H_3$  bosons in the MNSSM. From Fig. 3(a), we see finally that for  $M_{H^+} = 160$  GeV, the  $H_2$ -boson mass is nearly  $\mu$ -independent and equals

---

<sup>¶</sup>Using the code `cph` [29] based on [18], one finds that only for extreme values of  $|\mu| \gtrsim 5$  TeV and for  $\tan\beta > 20$ , such a scenario might be made viable [30].

the  $A_1$ -boson mass  $M_{A_1} \approx 179$  GeV. This result is just a consequence of the expected decoupling property of a heavy charged Higgs boson, with  $M_{H^+} = 160$  GeV  $\gg M_Z$ .

In Fig. 4 we display predicted values for  $M_{H_1}$  and  $M_{H_2}$ , as well as for  $g_{H_1 ZZ}^2$  and  $g_{H_2 ZZ}^2$  in the MNSSM, using the same input parameters as in Fig. 3, but with  $\tan \beta = 20$ , i.e.  $\lambda = 0.65$  and  $\lambda t_S/\mu = 1$  TeV<sup>2</sup>. We encounter a functional dependence of the evaluated kinematic parameters on  $\mu$ , for  $M_{H^+} = 80, 120$  and  $160$  GeV, which is qualitatively similar to the one presented in Fig. 3. Again, we see that the charged Higgs boson  $H^+$  can be lighter than the  $H_1$  boson, even for large values of  $\tan \beta$ . Yet, we observe that for larger  $H^+$ -boson masses, the squared  $H_1$ -boson coupling to the  $Z$  boson,  $g_{H_1 ZZ}^2$ , goes more rapidly to unity than in the  $\tan \beta = 2$  case. Here, we should emphasize again that as  $M_{H^+}$  becomes much larger than  $M_Z$ , the predicted values for  $M_{H_1}$  approach the one given by the square root of the RHS of Eq. (3.55), where, of course, the term proportional to  $\lambda^2 \sin^2 2\beta$  is negligible. Therefore, only in this kinematic regime where both  $\tan \beta$  and  $M_{H^+}$  are large, the predictions of the MNSSM will coincide with those of the MSSM.

In our numerical analysis in connection with Fig. 3, we have already observed that for large values of  $\lambda t_S/\mu$  but small values of  $M_{H^+}$ , the  $H_1$  boson does not couple strongly to the  $Z$  boson, but it is rather the  $H_2$  boson which is SM-type. Actually, this kind of behaviour is encountered even for larger values of  $M_{H^+}$ , provided  $\lambda t_S/\mu$  is sufficiently small. As was already discussed in Section 4, the latter reflects the fact that the model approaches the PQ-symmetric limit in this case. In Fig. 5, we present numerically the  $\mu$ -dependence of the two lightest CP-even Higgs-boson masses,  $M_{H_1}$  and  $M_{H_2}$ , and their respective couplings to the  $Z$  boson,  $g_{H_1 ZZ}^2$  and  $g_{H_2 ZZ}^2$ , in the MNSSM with  $m_{12}^2 = 0$ , for  $M_{H^+} = 200, 400, 600$  and  $800$  GeV. In addition, we have selected the value of the tadpole parameter  $\lambda t_S/\mu = 0.01328$  TeV<sup>2</sup>. For this specific value of the tadpole parameter and for  $M_{H^+} = 400$  GeV, we see that there is a value of  $\mu$  where the Higgs states  $H_1$  and  $H_2$  interchange their couplings to the  $Z$  boson, while being nearly degenerate having a mass close to the upper bound of  $M_{H_1}$ . We shall denote by  $\mu_*$  this specific value of  $\mu$  at which a level crossing in the couplings of  $H_1$  and  $H_2$  occurs. Thus, for values of  $|\mu|$  smaller than  $|\mu_*|$ , it is  $g_{H_1 ZZ}^2 > g_{H_2 ZZ}^2$ , while this inequality of the squared couplings gets inverted for  $|\mu| > |\mu_*|$ . If we now consider smaller values for  $M_{H^+} = 200$  GeV for the chosen value of  $\lambda t_S/\mu$ , we observe from Fig. 5 that as  $|\mu|$  grows,  $g_{H_1 ZZ}^2$  starts higher than  $g_{H_2 ZZ}^2$ , and the crossing point of these two squared couplings is before  $M_{H_1}$  reaches its highest value. If we now take larger values for  $M_{H^+}$ , e.g.  $M_{H^+} = 600, 800$  GeV, we see that  $g_{H_1 ZZ}^2$  starts again higher, becomes almost unity with  $M_{H_1}$  close to its largest allowed value, according to the mass-coupling sum rule (3.55), and intersects  $g_{H_2 ZZ}^2$  at a smaller value of  $M_{H_1}$ . The very special value of  $\lambda t_S/\mu$ , for a given value of  $M_{H^+}$ , for which  $M_{H_1}$  and  $M_{H_2}$  become equal



at the highest possible value for  $M_{H_1}$  and  $g_{H_1ZZ}^2 \approx g_{H_2ZZ}^2 \approx 0.5$  should be regarded as a critical point. Generically speaking, for values of  $\lambda t_S/\mu$  lower than the one corresponding to the critical point, the  $H_2$  boson couples predominantly to the  $Z$  boson. Instead, if  $\lambda t_S/\mu$  is higher than its critical value, it is then the  $H_1$  boson that couples with SM strength. In addition, in Fig. 5 we see that almost independently of  $M_{H^+}$ , the squared couplings  $g_{H_1ZZ}^2$  and  $g_{H_2ZZ}^2$  remain comparable for a wide range of  $\mu$  values. The latter is an indication of the fact that the critical value of  $\lambda t_S/\mu$  depends only weakly on the charged Higgs-boson mass  $M_{H^+}$  and has a value close to  $0.01 \text{ TeV}^2$ , for  $0.3 \text{ TeV} \lesssim M_{H^+} \lesssim 1 \text{ TeV}$ , where the remaining independent kinematic parameters are held fixed.

We shall now analyze the predictions of the MNSSM for relatively small values of the tadpole parameter  $\lambda t_S/\mu$ . In Fig. 6, we display numerical estimates of  $M_{H_1}$  and  $M_{H_2}$ , as well as of  $g_{H_1ZZ}^2$  and  $g_{H_2ZZ}^2$ , as functions of the  $\mu$ -parameter, for  $\lambda t_S/\mu = 0.0026 \text{ TeV}^2$ . As for charged Higgs-boson masses, we choose  $M_{H^+} = 0.3, 0.5, 0.7$  and  $1 \text{ TeV}$ . It is easy to see that, to a good approximation, the functional dependence of the masses of the two lightest CP-even Higgs bosons  $H_1$  and  $H_2$  are insensitive to the value of  $M_{H^+}$ . In this scenario of the MNSSM, the  $H_2$  boson has always the strongest coupling to the  $Z$  boson. Although not displayed in Fig. 6, the mass of the lightest CP-odd scalar  $A_1$  is found to be  $M_{A_1} \approx 50 \text{ GeV}$  and is almost independent of  $M_{H^+}$ . In addition, the CP-odd Higgs scalar  $A_1$  has suppressed couplings to the  $Z$  and  $H_1$  bosons, i.e.  $g_{H_1A_1Z}^2 \lesssim 10^{-2}$ , and therefore can escape detection at LEP2. In Fig. 6 we notice finally that the allowed intervals of  $\mu$  values become even shorter than those found in the previous scenarios of the MNSSM. These results are all consequences of our choice of a relatively small value for the tadpole parameter and are in good qualitative agreement with our discussion in Section 4 pertaining to the PQ-symmetric limit.

It is very interesting to examine the consequences of the presence of a non-vanishing effective  $F_S$ -tadpole term  $m_{12}^2$  on the Higgs-boson mass spectrum of the MNSSM. Therefore, in Fig. 7 we plot the dependence of the CP-even Higgs-boson masses  $M_{H_1}$  and  $M_{H_2}$  and the squared couplings  $g_{H_1ZZ}^2$  and  $g_{H_2ZZ}^2$ , as functions of the  $\mu$ -parameter, for  $t_S = -1 \text{ TeV}^3$  and  $m_{12}^2 = 0.325 \text{ TeV}^2$ . Because of the close relationship between  $t_S$  and  $m_{12}^2$ , we are now compelled to treat  $t_S$  as a  $\mu$ -independent constant. In fact, for  $M_{\text{SUSY}} = 1 \text{ TeV}$ , we can easily compute from Eq. (3.4) that the adopted values for  $t_S$  and  $m_{12}^2$  correspond to the typical values of  $\xi_S$  and  $\xi_F$ :  $\xi_S = -1$  and  $\xi_F = 1/2$ . To enable a direct comparison with Fig. 3, we choose the same values as in Fig. 3 for the remaining kinematic parameters of the theory. From Fig. 7, we see that the presence of a non-vanishing, positive tadpole term  $m_{12}^2$  can shift the maxima of  $M_{H_1}$  and  $M_{H_2}$  towards larger values of  $|\mu|$ , whereas all other features found in Fig. 3 are retained. In Fig. 7(a), we have also displayed the

dependence of the mass  $M_{A_1}$  of the lightest CP-odd scalar  $A_1$ , as a function of  $\mu$ . We see that  $M_{A_1}$  decreases with  $|\mu|$  decreasing. This kinematic behaviour originates from the fact that the contribution of the off-diagonal terms to the CP-odd mass matrix becomes rather significant for smaller values of  $|\mu|$ . Instead, for larger values of  $|\mu|$ , the corresponding contribution of the off-diagonal terms is smaller, and leads to the mass relation  $M_{A_1} \approx M_a$ .

Unlike the MSSM, the charged Higgs-boson  $H^+$  cannot be arbitrarily heavy in the MNSSM for fixed given values of  $\tan \beta$  and  $\lambda$ , and for natural choices of  $\lambda t_S/\mu$  and the soft squark masses, i.e. for  $\lambda t_S/\mu$ ,  $\widetilde{M}_Q^2$ ,  $\widetilde{M}_t^2 \lesssim 1 \text{ TeV}^2$ . Figure 8 displays the dependence of the maximum of the lightest Higgs-boson mass,  $\max(M_{H_1})$ , as a function of  $M_{H^+}$ , for  $\tan \beta = 2$ ,  $\lambda = 0.65$  and for two different values of the tadpole parameter:  $\lambda t_S/\mu = 0.04$  and  $1 \text{ TeV}^2$ . The coupling of the  $H_1$  scalar to the  $Z$  boson becomes SM-type, for  $M_{H^+} \gtrsim 150 \text{ GeV}$ . From Fig. 8, it is then easy to see that the current LEP2 lower bound on  $\max(M_{H_1})$  implies the approximate upper limit on  $M_{H^+}$ :  $M_{H^+} \lesssim 2.7 \text{ TeV}$ , almost independently of  $\lambda t_S/\mu$ . This result may be understood as follows. As the mass of the charged Higgs boson increases, the maximum of  $M_{H_1}$  occurs for larger values of  $|\mu|$ , which is a consequence of the tree-level structure of the CP-even Higgs-boson mass matrix in Eq. (3.15). On the other hand, the larger the value of  $|\mu|$  becomes the larger the stop-mixing parameter  $|X_t| = |A_t - \mu/t_\beta|$  is getting. Thus, when  $|X_t|/\max(\widetilde{M}_Q, \widetilde{M}_t) \gtrsim \sqrt{6}$ , the contributions of the stop-radiative effects to the lightest Higgs-boson mass  $M_{H_1}$  become negative, and so drive  $\max(M_{H_1})$  to unphysical values. For the very same reasons, a similar dependence of  $\max(M_{H_1})$  on  $M_{H^+}$  is found to apply to the NMSSM case as well.

For comparison, we shall now investigate a few representative scenarios within the context of the NMSSM. As a first example, we consider the scenario with  $\tan \beta = 2$ ,  $\lambda = 0.65$ ,  $\kappa = 0.01$  and  $(\kappa \mu A_\kappa)/\lambda = 0.0026 \text{ TeV}^2$ . Figure 9 exhibits the numerical predictions for the two lightest Higgs-boson masses,  $M_{H_1}$  and  $M_{H_2}$ , and their corresponding squared couplings to the  $Z$  boson,  $g_{H_1 ZZ}^2$  and  $g_{H_2 ZZ}^2$ , as functions of the  $\mu$ -parameter. We also vary the charged Higgs-boson mass in a discrete manner, i.e.  $M_{H^+} = 0.3, 0.5, 0.7$  and  $1 \text{ TeV}$ . We observe that  $M_{H_1}$  and  $M_{H_2}$  are practically independent of  $M_{H^+}$ , with  $M_{H_1}$  consistently below  $80 \text{ GeV}$ . Such low values of  $M_{H_1}$  are still acceptable at LEP2, in the range of  $\mu$  values where  $g_{H_1 ZZ}^2 \lesssim 0.07$ . In this scenario, the  $H_2$  boson has a SM-type coupling to the  $Z$  boson. Also, the mass of the lightest CP-odd Higgs scalar  $M_{A_1}$  is almost independent of  $M_{H^+}$  and comes out to be slightly higher than  $M_{H_1}$ . The NMSSM under discussion, with the chosen low value of  $\kappa \approx 0.01$ , may be considered to adequately describe the limiting scenario where  $\kappa \rightarrow 0$  and  $\kappa A_\kappa$  is held fixed. This last fact enables one to directly compare the present scenario of the NMSSM with the MNSSM where the tadpole parameter  $\lambda t_S/\mu$  is set to the same value with that of  $(\kappa \mu A_\kappa)/\lambda$ , i.e.  $\lambda t_S/\mu = 0.0026 \text{ TeV}^2$ . Such a scenario

in connection with the MNSSM has already been analyzed above in Fig. 6. Thus, if we now compare Fig. 9 with Fig. 6, we observe resembling numerical predictions for the Higgs-boson masses and couplings in the two models. The only visible difference between them is that in the MNSSM, the lightest CP-even Higgs boson  $H_1$  is consistently 30 GeV heavier than the corresponding one in the NMSSM, while the mass  $M_{A_1}$  of the lightest CP-odd scalar is about 30 GeV lower. These findings are in excellent agreement with our discussion in Section 4.

We shall now analyze in Fig. 10 a second scenario of the NMSSM, in which the Yukawa-type coupling  $\kappa$  is larger, but with the expression  $(\kappa\mu A_\kappa)/\lambda$  being held fixed again, i.e.  $\kappa = 0.1$  and  $(\kappa\mu A_\kappa)/\lambda = 0.0026 \text{ TeV}^2$ . In Fig. 10, we also vary the charged Higgs-boson mass in the same way as in Fig. 9:  $M_{H^\pm} = 0.3, 0.5, 0.7$  and  $1 \text{ TeV}$ . In this scenario, the ratio  $|A_\kappa/\mu|$  varies from 1.69 for  $|\mu| = 100 \text{ GeV}$  up to 0.096 for  $|\mu| = 420 \text{ GeV}$ , namely the ratio  $|A_\kappa/\mu|$  is no longer much larger than 1 for all relevant values of  $|\mu|$ . Furthermore, as  $|\mu|$  increases, the strong inequality  $|A_\kappa/\mu| \gg |\kappa/\lambda|$  gets gradually violated as well. As a consequence, as the charged Higgs-boson mass  $M_{H^\pm}$  takes higher values, the picture starts changing in comparison with Fig. 9. To be precise, as  $M_{H^\pm}$  becomes larger, we observe a progressive enhancement of the maximum of the  $H_1$ -boson mass  $M_{H_1}$  and of its respective squared coupling to the  $Z$  boson  $g_{H_1 ZZ}^2$ ; the values of  $M_{H_1}$  and  $g_{H_1 ZZ}^2$  approach those of  $M_{H_2}$  and  $g_{H_2 ZZ}^2$ , respectively. In particular, when  $M_{H^\pm}$  approaches  $1 \text{ TeV}$ , a level crossing effect in the masses and couplings of the  $H_1$  and  $H_2$  bosons takes place and the  $H_1$  boson becomes SM-type. In addition, the mass of the lightest CP-odd Higgs scalar  $M_{A_1}$  gets very small, i.e.  $M_{A_1} \sim 15 \text{ GeV}$ , resulting from a partial cancellation of the first two terms on the RHS of Eq. (4.19). It is obvious that with increasing  $|\kappa|$  and  $|\mu|$ , the predictions of the NMSSM start slowly resembling those of the MNSSM with  $\lambda t_S/\mu$  being in the vicinity of its critical value.

On the other hand, as the charged Higgs-boson mass decreases, we notice in Fig. 10 that viable scenarios occur for smaller values of  $|\mu|$ . In fact, within the specific NMSSM with  $\kappa = 0.1$  that we have been considering here, the experimental constraint,  $|\mu| \gtrsim 90 \text{ GeV}$  [15], implies that  $M_{H^\pm}$  cannot be lighter than  $180 \text{ GeV}$ . Of course, such a scenario could be directly excluded from the fact that for small positive values of  $\kappa \sim 0.1$ , the lightest singlino state contributes significantly to the  $Z$ -boson invisible width (see also discussion after Eq. (4.9)). For this reason, we present in Fig. 11 numerical estimates for a related scenario with negative  $\kappa$ , i.e.  $\kappa = -0.1$ . We also choose a smaller value for  $(\kappa\mu A_\kappa)/\lambda$ , i.e.  $(\kappa\mu A_\kappa)/\lambda = -0.0021 \text{ TeV}^2$ , so as to obtain a light CP-odd Higgs state  $A_1$ . In Fig. 11, we observe again the same characteristics as in Fig. 10, namely as the charged Higgs-boson mass decreases, viable scenarios take place for smaller values of  $|\mu|$ , leading to a similar

lower bound of about 180 GeV on  $M_{H^+}$ . In fact, after having carefully explored all the relevant parameter space of the NMSSM with  $\tan\beta = 2$ , we found that this is a general feature of the NMSSM for any perturbative value of  $\lambda$  and  $\kappa$  (see also discussion below). Consequently, as in the MSSM, the SM-type Higgs boson in the NMSSM is also predicted to be lighter than the charged Higgs boson.

To get a better understanding of this last phenomenological feature of the NMSSM, it is very instructive to analyze a scenario where the Yukawa-type couplings  $\kappa$  and  $\lambda$  are comparable in size. Specifically, we choose  $\lambda = 0.5$  and  $\kappa = -0.45$ . According to our discussion in Section 4, the parameters of this model have been chosen in a way such that the charged Higgs boson might be allowed to become lighter than the one predicted in the previous scenarios of the NMSSM. Furthermore, in order to obtain the largest possible values for the masses of the CP-even Higgs scalars, we always fix  $A_\kappa$  by the requirement that the  $A_1$  boson be extremely light of the order of a few GeV.<sup>||</sup> Having the above in mind, we present in Fig. 12 numerical estimates of  $M_{H_1}$  and  $M_{H_2}$ , and  $g_{H_1 ZZ}^2$  and  $g_{H_2 ZZ}^2$ , as functions of the  $\mu$ -parameter, for charged Higgs-boson masses  $M_{H^+} = 120, 400$  and 800 GeV. We observe that for  $|\mu| \gtrsim 100$  GeV, the  $H_1$  boson is always SM-type. In addition, for  $M_{H^+} = 120$  GeV, the mass of the  $H_1$  boson has a maximum of  $\sim 113$  GeV at  $|\mu| = 100$  GeV with  $g_{H_1 ZZ}^2 = 0.5$ , which is close to the present experimental lower bound of LEP2 [1]. In this scenario, the next-to-lightest CP-even Higgs boson  $H_2$  has a smaller coupling to the  $Z$  boson and its mass varies between 120–130 GeV. For larger values of  $M_{H^+}$ , the  $H_1$  boson is always SM-type, with  $M_{H_1} \approx 120$ –130 GeV for a wide range of  $|\mu|$  values, whilst the  $H_2$  boson is very heavy and decoupled from the lightest Higgs sector.

Our numerical analysis as presented above in Fig. 12 explicitly demonstrates that for  $M_{H^+} = 120$  GeV, the mass  $M_{H_1}$  of the lightest CP-even Higgs boson becomes acceptable only within a very narrow interval of  $|\mu|$ , which is, however, close to its current lowest bound as set by LEP2 [15]. Thus, even within this optimized scenario of the NMSSM with  $|\kappa/\lambda| \sim 1$ , the  $H_1$  boson cannot become heavier than the charged Higgs boson. Therefore, we reach the conclusion that a possible discovery of a charged Higgs boson lighter than 120–130 GeV and a SM-type Higgs boson heavier than 130–140 GeV can only be naturally accounted for within the MNSSM.

---

<sup>||</sup>Despite its similarity, our scenario differs from the one discussed in [31] very recently. In our case, the tree-level values of  $A_\lambda$  and  $A_\kappa$ , required for  $M_{A_1} \approx 0$ , are not forced to be suppressed. The latter turns out to be the case only within a very narrow range of  $\mu$  values close to the upper-end of the interval given by Eq. (4.22).

## 6 Conclusions

We have considered the simplest extension of the minimal supersymmetric standard model, in which the  $\mu$ -parameter has been promoted to a dynamical variable by means of a gauge-singlet superfield  $\hat{S}$ , with the linear, quadratic and cubic singlet-superfield terms,  $\hat{S}$ ,  $\hat{S}^2$  and  $\hat{S}^3$ , absent from the superpotential. Moreover, we have assumed that the breaking of SUSY in the observable sector is communicated gravitationally by a set of hidden-sector superfields which break  $N = 1$  supergravity spontaneously. In such a supergravity scenario, the absence of harmful destabilizing tadpole divergences at lower loop levels can be assured by forcing the complete superpotential and Kähler potential to respect specific discrete  $R$  symmetries. In particular, we have been able to show that with the imposition of the discrete  $R$  symmetries  $\mathcal{Z}_5^R$  and  $\mathcal{Z}_7^R$ , the potentially dangerous tadpole divergences first appear at the six- and seven-loop levels, respectively, and hence are naturally suppressed to the order of the electroweak scale, without destabilizing the gauge hierarchy.

The MNSSM we have been studying in this paper has a number of appealing field-theoretic and phenomenological features, which may be summarized as follows:

- The model provides a natural solution to the so-called  $\mu$ -problem of the MSSM, since the value of the  $\mu$ -parameter can now be directly set by the VEV of the gauge-singlet superfield  $\hat{S}$  which is of the required order of  $M_{\text{SUSY}}$ , as a consequence of the  $\mathcal{Z}_5^R$  and  $\mathcal{Z}_7^R$  symmetries.
- The presence of the effectively generated tadpole terms linear in  $S$  and  $F_S$  (or  $\hat{S}$ ) breaks explicitly the continuous  $U(1)_{\text{PQ}}$  and its discrete subgroup  $\mathcal{Z}_3$ . Thus, the model offers a natural solution to the visible axion and cosmological domain-wall problems.
- Depending on the underlying mechanism of SUSY breaking, the effective tadpole proportional to  $F_S$  could in principle be absent from the model. Such a reduction of the renormalizable operators does not thwart the renormalizability of the theory. The resulting renormalizable low-energy scenario has one parameter less than the frequently-discussed NMSSM with the cubic singlet-superfield term  $\frac{\kappa}{3}\hat{S}^3$  present; it therefore represents the most economic, renormalizable version among the non-minimal supersymmetric models proposed in the literature.
- As opposed to the NMSSM, the MNSSM satisfies the tree-level mass sum rule (3.19), which is very analogous to the corresponding one of the MSSM [16]. This striking analogy to the MSSM allows us to advocate that the Higgs sector of the MNSSM

differs indeed minimally from the one of the MSSM, i.e. the introduced model truly constitutes the minimal supersymmetric extension of the MSSM. In the NMSSM, the violation of the mass sum rule can become much larger than the one induced by the one-loop stop/top effects, especially for relatively large values of  $|\kappa|$ ,  $|\mu|$  and  $|A_\kappa|$ .

- A generic prediction of the non-minimal supersymmetric standard models is that for low values of  $\tan\beta$ , the lightest CP-even Higgs-boson mass  $M_{H_1}$  increases significantly with growing  $|\lambda|$  [cf. Eq. (3.18)]. Since in the MNSSM  $\lambda$  can take its maximum allowed value naturally corresponding to the NMSSM with  $\kappa = 0$ , the value of  $M_{H_1}$  is predicted to be the highest, after the dominant stop-loop effects have been included, i.e.  $M_{H_1} \lesssim 145$  GeV. Therefore, such a scenario can only be decisively tested by the upgraded Tevatron collider at Fermilab and by the Large Hadron Collider (LHC) at CERN.
- The MNSSM can comfortably predict viable scenarios, where the mass of the charged Higgs boson  $H^+$  is in the range:  $80 \text{ GeV} < M_{H^+} \lesssim 3 \text{ TeV}$ , for phenomenologically relevant values of  $|\mu| \gtrsim 90 \text{ GeV}$ . In particular, numerical estimates in Section 5 reveal that a possible discovery of a charged Higgs boson, with  $M_{H^+} \lesssim 120 \text{ GeV}$ , and a neutral Higgs boson, with  $M_{H_1} \gtrsim 130 \text{ GeV}$ , can only be naturally accounted for within the MNSSM, whereas the NMSSM would be highly disfavoured. This important phenomenological feature of the MNSSM, which is very helpful to discriminate it from the NMSSM, is a reflection of a new non-trivial decoupling limit due to a large tadpole  $|t_S|$ , which is only attainable in the MNSSM (see also discussion of the paragraph that includes Eq. (3.16)).
- For scenarios with  $M_{H^+} \gtrsim 200 \text{ GeV}$ , the distinction between the MNSSM and the NMSSM becomes more difficult. In this case, additional experimental information would be necessary to distinguish the two SUSY extensions of the MSSM, resulting from a precise determination of the masses, the widths, the branching ratios and the production cross sections of the CP-even and CP-odd Higgs bosons. Nevertheless, if the tadpole parameter  $\lambda t_S/\mu$  becomes much larger than  $M_{H^+}^2$  with the remaining kinematic parameters held fixed, the Higgs states  $H_3$  and  $A_2$  will be predominantly singlets. As an important phenomenological consequence of this, the complementarity relations (3.54) between the  $H_{1,2}ZZ$ - and  $H_{2,1}A_1Z$ - couplings will then hold approximately true in the MNSSM. However, these relations will be generically violated in the NMSSM, as there is no analogous decoupling limit in the latter model, in which the states  $H_3$  and  $A_2$  could decouple as singlets.

The MNSSM also predicts the existence of a light neutralino, the axino. The axino

is predominantly a singlet field, for  $|\mu| \gtrsim 120$  GeV. LEP limits on the  $Z$ -boson invisible width lead to the additional constraint:  $200 \lesssim |\mu| \lesssim 250$  GeV, for  $\lambda \approx 0.65$ . However, such a constraint disappears completely for smaller values of  $\lambda$ , namely for  $\lambda \lesssim 0.45$ . In fact, the axino may become the LSP in the MNSSM. In this paper we shall not address the issues associated with the cosmological consequences of the axino on the reheating temperature of the Universe [32] and on the dark-matter problem. A detailed discussion of these issues may be given elsewhere.

The present study has shown that the MNSSM is a viable scenario, which departs minimally from the MSSM, having a large number of appealing field-theoretic and phenomenological features. Even though further refinements of our treatment of loop effects might be very useful, such as the inclusion of one-loop  $D$ -term contributions to the effective potential and the computation of two-loop leading logarithmic corrections, our predictions for the Higgs-boson mass spectrum as well as the results of our comparative analysis between the MNSSM studied here and the frequently-discussed NMSSM are not expected to modify dramatically. In particular, we find that the MNSSM can naturally predict viable scenarios in which the charged Higgs boson  $H^+$  is much lighter than the neutral Higgs boson with SM-type coupling to the  $Z$  boson. The planned colliders, i.e. the upgraded Tevatron collider and the LHC, have the potential capabilities to test such interesting scenarios with a relatively light  $H^+$ , as well as probe large domains of the Higgs-sector structure of this truly minimal supersymmetric extension of the MSSM, the MNSSM.

## Acknowledgements

We thank Carlos Wagner for illuminating discussions and Alexandros Kehagias for a useful suggestion.

## A Non-destabilizing tadpole divergences

Employing standard power counting rules [9,10], we shall show the absence of harmful tadpole divergences up to a sufficiently high loop order  $n$ , i.e.  $n \leq 5$ , within the context of the supergravity scenarios described in Section 2.

It is useful to briefly review first the sufficient conditions that govern the absence of harmful tadpole divergences. To this end, let us consider a supergraph with one external leg, i.e. a tadpole graph. The tadpole graph may involve a number  $V_d$  of superpotential vertices of dimension  $d + 3$ , which are of the form  $z^{d+3}/M_{\text{P}}^d$  where  $z$  represents a generic chiral superfield, and a number  $U_d$  of Kähler-potential vertices of dimension  $d + 2$ , which have the form  $z^{d+2}/M_{\text{P}}^d$ . Then, the superficial degree of divergence of the tadpole graph, e.g. that of  $\hat{S}$ , is given by

$$D = 1 + \sum_d d V_d + \sum_d d U_d, \quad (\text{A.1})$$

which leads to a contribution to the effective potential

$$V_{\text{tad}} \sim \frac{1}{(16\pi^2)^n} \frac{\Lambda^D M_{\text{SUSY}}^{3-D+\sum_d d V_d + \sum_d d U_d}}{M_{\text{P}}^{\sum_d d V_d + \sum_d d U_d}} S + \text{h.c.} \sim \frac{1}{(16\pi^2)^n} M_{\text{P}} M_{\text{SUSY}}^2 S + \text{h.c.}, \quad (\text{A.2})$$

where  $n$  counts the number of loops and  $M_{\text{SUSY}}$  is the soft SUSY-breaking scale. In obtaining the last step of Eq. (A.2), we have used  $\Lambda \sim M_{\text{P}}$  as a natural energy cut-off scale. This very last step in Eq. (A.2) shows that a tadpole contribution to the effective potential is proportional to one power of  $M_{\text{P}}$  at most. Such tadpole contributions which remain proportional to  $M_{\text{P}}$  will be referred to as “harmful” to be distinguished from the “harmless” ones in which the cut-off dependence disappears. In this context, an additional requirement for a tadpole graph to be harmful is that  $D$  be an even number. Finally, the degree of divergence can also be determined by the number of loops  $n$  and superpotential vertices  $V_d$  through the relation

$$D = 2n - \sum_d V_d. \quad (\text{A.3})$$

In summary, one finds that a set of vertices produces a harmful tadpole divergence if the following equalities are all simultaneously satisfied:

$$D = 1 + \sum_d d V_d + \sum_d d U_d = 2n - \sum_d V_d = \text{even}, \quad (\text{A.4})$$

with  $D \geq 2$ .

In the next two subsections, we shall apply the power counting rule of superficial divergences, stated in Eq. (A.4), to the two models based on the discrete  $R$ -symmetries  $Z_5^R$  and  $Z_7^R$ .



## A.1 The $Z_5^R$ case

Here, we shall show that the potentially harmful tadpole divergences are absent up to five loops. Alternatively, we shall prove that it is impossible to construct a tadpole diagram from the sets of vertices which satisfy the condition (A.4) for  $n \leq 5$ , corresponding to  $D \leq 10$ . Suppose now that at least one superpotential vertex is involved in a tadpole supergraph. Based on Eq. (A.3), we see that we need at least two superpotential vertices to form a tadpole graph with  $D$  even, i.e.  $\sum_d V_d \geq 2$ . Thus, for  $n = 5$ , one has  $D \leq 8$ , and by virtue of Eq. (A.1), it is  $\sum_d d V_d \leq 7$  and  $d \leq 7$ . In the case that no superpotential vertices are involved, we have the relation  $D = 1 + \sum_d d U_d \leq 10$  or  $\sum_d d U_d \leq 9$  on account of Eq. (A.1). We consider it obvious that it is impossible to form a tadpole graph with only one Kähler-potential vertex of  $d = 9$ . This observation excludes Kähler-potential operators of  $d = 9$ . Furthermore, as we will see below, the imposition of  $Z_5^R$  on the complete Kähler potential does not permit operators of  $d = 1$ . If we now wish to satisfy the above constraint  $\sum_d d U_d \leq 9$  with two vertices, we then need one operator of  $d = 2$  and another one of  $d = 7$ ; the latter is the Kähler-potential term of the highest dimensionality that could participate into a harmful divergent tadpole graph with  $n \leq 5$ . Consequently, we reach the conclusion that only superpotential and Kähler-potential vertices with  $d \leq 7$  will be of relevance here.

We shall confine ourselves to a minimal model, in which only the superfields  $\widehat{H}_1$ ,  $\widehat{H}_2$  and  $\widehat{S}$  are present and ignore quark and lepton superfields, as they do not couple directly to  $\widehat{S}$ ; the inclusion of the fermion superfields is straightforward and does not alter our results. Moreover, we shall not include in the list of Kähler-potential terms those obtained by multiplying the latter with any power of  $\widehat{H}_1^\dagger \widehat{H}_1$ ,  $\widehat{H}_2^\dagger \widehat{H}_2$ ,  $\widehat{S}^* \widehat{S}$ . The reason is that the omitted terms generate graphs of higher loop order than the included ones.

Having the above in mind, we are now able to list all superpotential and Kähler-potential terms of  $d \leq 7$ , respecting the discrete  $R$ -symmetry  $Z_5^R$  (cf. Eq. (2.6)):

$$\begin{aligned}
W : \quad W_0 &\equiv \widehat{S}(\widehat{H}_1^T i\tau_2 \widehat{H}_2) \delta(\bar{\theta}) + \text{h.c.}, & W_1 &\equiv \frac{\widehat{S}^4}{M_P} \delta(\bar{\theta}) + \text{h.c.}, \\
W_3 &\equiv \frac{(\widehat{H}_1^T i\tau_2 \widehat{H}_2)^3}{M_P^3} \delta(\bar{\theta}) + \text{h.c.}, & W_4 &\equiv \frac{\widehat{S}^3(\widehat{H}_1^T i\tau_2 \widehat{H}_2)^2}{M_P^4} \delta(\bar{\theta}) + \text{h.c.}, \\
W_5 &\equiv \frac{\widehat{S}^6(\widehat{H}_1^T i\tau_2 \widehat{H}_2)}{M_P^5} \delta(\bar{\theta}) + \text{h.c.}, & W_6 &\equiv \frac{\widehat{S}^9}{M_P^6} \delta(\bar{\theta}) + \text{h.c.}, \\
W_7 &\equiv \frac{\widehat{S}^2(\widehat{H}_1^T i\tau_2 \widehat{H}_2)^4}{M_P^7} \delta(\bar{\theta}) + \text{h.c.} & & \quad (A.5)
\end{aligned}$$

$$K : \quad K_0^{(1)} \equiv \widehat{H}_1^\dagger \widehat{H}_1, \quad K_0^{(2)} \equiv \widehat{H}_2^\dagger \widehat{H}_2, \quad K_0^{(3)} \equiv \widehat{S}^* \widehat{S},$$

$$\begin{aligned}
K_2 &\equiv \frac{\widehat{S}^2(\widehat{H}_1^T i\tau_2 \widehat{H}_2)}{M_{\text{P}}^2} + \text{h.c.}, & K_3^{(1)} &\equiv \frac{\widehat{S}^5}{M_{\text{P}}^3} + \text{h.c.}, \\
K_3^{(2)} &\equiv \frac{\widehat{S}^{*3}(\widehat{H}_1^T i\tau_2 \widehat{H}_2)}{M_{\text{P}}^3} + \text{h.c.}, & K_3^{(3)} &\equiv \frac{\widehat{S}^*(\widehat{H}_1^T i\tau_2 \widehat{H}_2)^2}{M_{\text{P}}^3} + \text{h.c.}, \\
K_5 &\equiv \frac{\widehat{S}(\widehat{H}_1^T i\tau_2 \widehat{H}_2)^3}{M_{\text{P}}^5} + \text{h.c.}, & K_6 &\equiv \frac{\widehat{S}^4(\widehat{H}_1^T i\tau_2 \widehat{H}_2)^2}{M_{\text{P}}^6} + \text{h.c.}, \\
K_7 &\equiv \frac{\widehat{S}^7(\widehat{H}_1^T i\tau_2 \widehat{H}_2)}{M_{\text{P}}^7} + \text{h.c.}, & &
\end{aligned} \tag{A.6}$$

where  $\delta(\bar{\theta})$  is the usual Grassmann-valued  $\delta$ -function. Notice that the terms  $K_0^{(1)}$ ,  $K_0^{(2)}$  and  $K_0^{(3)}$  represent the usual Higgs-superfield propagators and have no direct effect on our power counting rules. These terms are merely needed to contract the superfields in propagator lines and so form a loop supergraph. Furthermore, from Eqs. (A.5) and (A.6), we observe that  $\mathcal{Z}_5^R$  forbids the appearance of superpotential operators of  $d = 2$  ( $W_2$ ) and of Kähler-potential terms of  $d = 1, 4$  ( $K_1, K_4$ ).

In the following, we shall systematically analyze all possible sets of vertices compatible with the conditions in Eq. (A.4) up to five loops. At the one-loop level ( $n = 1$ ), with  $\sum_d V_d = 0$ , we readily find from Eq. (A.1) that  $\sum_d dU_d = 1$ , entailing the absence of contributing operators. The situation becomes increasingly more involved for  $n = 2, 3, 4$  and 5. More explicitly, our systematic search for the existence of possible harmful tadpoles may be summarized as follows:

**I.  $n = 2$  :**

$$\begin{aligned}
\text{a)} \quad & D = 2, \quad \sum_d V_d = 2, \quad \sum_d dV_d + \sum_d dU_d = 1 : \\
& \{W_0, W_1\}; \\
\text{b)} \quad & D = 4, \quad \sum_d V_d = 0, \quad \sum_d dU_d = 3 : \\
& \{K_3^{(i)}\}.
\end{aligned} \tag{A.7}$$

**II.  $n = 3$  :**

$$\begin{aligned}
\text{a)} \quad & D = 2, \quad \sum_d V_d = 4, \quad \sum_d dV_d + \sum_d dU_d = 1 : \\
& \{3W_0, W_1\}; \\
\text{b)} \quad & D = 4, \quad \sum_d V_d = 2, \quad \sum_d dV_d + \sum_d dU_d = 3 : \\
& \{W_0, W_3\}, \quad \{W_0, W_1, K_2\}, \quad \{2W_0, K_3^{(i)}\}; \\
\text{c)} \quad & D = 6, \quad \sum_d V_d = 0, \quad \sum_d dU_d = 5 : \\
& \{K_5\}, \quad \{K_2, K_3^{(i)}\}.
\end{aligned} \tag{A.8}$$

**III.**  $n = 4 :$

- a)  $D = 2, \quad \sum_d V_d = 6, \quad \sum_d dV_d + \sum_d dU_d = 1 :$   
 $\{5W_0, W_1\};$
- b)  $D = 4, \quad \sum_d V_d = 4, \quad \sum_d dV_d + \sum_d dU_d = 3 :$   
 $\{3W_0, W_3\}, \quad \{W_0, 3W_1\}, \quad \{3W_0, W_1, K_2\},$   
 $\{4W_0, K_3^{(i)}\};$
- c)  $D = 6, \quad \sum_d V_d = 2, \quad \sum_d dV_d + \sum_d dU_d = 5 :$   
 $\{W_0, W_5\}, \quad \{W_1, W_4\}, \quad \{W_0, W_3, K_2\}, \quad \{W_0, W_1, 2K_2\},$   
 $\{2W_1, K_3^{(i)}\}, \quad \{2W_0, K_5\}, \quad \{2W_0, K_2, K_3^{(i)}\};$
- d)  $D = 8, \quad \sum_d V_d = 0, \quad \sum_d dU_d = 7 :$   
 $\{2K_2, K_3^{(i)}\}, \quad \{K_2, K_5\}, \quad \{K_7\}.$  (A.9)

**IV.**  $n = 5 :$

- a)  $D = 2, \quad \sum_d V_d = 8, \quad \sum_d dV_d + \sum_d dU_d = 1 :$   
 $\{7W_0, W_1\};$
- b)  $D = 4, \quad \sum_d V_d = 6, \quad \sum_d dV_d + \sum_d dU_d = 3 :$   
 $\{3W_0, 3W_1\}, \quad \{5W_0, W_3\}, \quad \{5W_0, W_1, K_2\}, \quad \{6W_0, K_3^{(i)}\};$
- c)  $D = 6, \quad \sum_d V_d = 4, \quad \sum_d dV_d + \sum_d dU_d = 5 :$   
 $\{3W_0, W_5\}, \quad \{2W_0, W_1, W_4\}, \quad \{W_0, 2W_1, W_3\},$   
 $\{3W_0, W_3, K_2\}, \quad \{W_0, 3W_1, K_2\}, \quad \{2W_0, 2W_1, K_3^{(i)}\},$   
 $\{3W_0, W_1, 2K_2\}, \quad \{4W_0, K_5\}, \quad \{4W_0, K_2, K_3^{(i)}\};$
- d)  $D = 8, \quad \sum_d V_d = 2, \quad \sum_d dV_d + \sum_d dU_d = 7 :$   
 $\{W_0, W_7\}, \quad \{W_1, W_6\}, \quad \{W_3, W_4\}, \quad \{W_0, W_5, K_2\},$   
 $\{W_1, W_4, K_2\}, \quad \{W_0, W_4, K_3^{(i)}\}, \quad \{W_1, W_3, K_3^{(i)}\},$   
 $\{W_0, W_3, 2K_2\}, \quad \{2W_1, K_5\}, \quad \{2W_1, K_2, K_3^{(i)}\},$   
 $\{W_0, W_1, K_6\}, \quad \{W_0, W_1, 3K_2\}, \quad \{W_0, W_1, K_3^{(i)}, K_3^{(j)}\},$   
 $\{2W_0, K_7\}, \quad \{2W_0, K_2, K_5\}, \quad \{2W_0, 2K_2, K_3^{(i)}\};$
- e)  $D = 10, \quad \sum_d V_d = 0, \quad \sum_d dU_d = 9 :$   
 $\{K_2, K_7\}, \quad \{2K_2, K_5\}, \quad \{3K_2, K_3^{(i)}\}, \quad \{K_6, K_3^{(i)}\},$

$$\{K_3^{(i)}, K_3^{(j)}, K_3^{(k)}\}. \quad (\text{A.10})$$

Here  $i, j, k = 1, 2, 3$ . The remaining task is to show that the sets of vertices listed above do not produce tadpole graphs. This can be best verified case by case algebraically in the following manner. First, we multiply all the vertices belonging to a set and formally substitute  $\widehat{H}_1^\dagger \widehat{H}_1$ ,  $\widehat{H}_2^\dagger \widehat{H}_2$  and  $\widehat{S}^* \widehat{S}$  with 1 into the product of vertices. Then, we examine whether terms linear in  $\widehat{S}$  or  $\widehat{S}^*$  survive in the resulting expression. In this way, we have carefully checked that there are no such terms linear in  $\widehat{S}$  or  $\widehat{S}^*$  for all sets of vertices listed in Eqs. (A.7)–(A.10), thus implying the absence of harmful tadpole graphs up to five loops.

At a higher loop level, we can construct tadpole supergraphs by making free use of the renormalizable superpotential vertex  $W_0$  in Eq. (A.5) together with some of the above vertices e.g., the higher-dimensional Kähler-potential vertices  $K_2$  and  $K_5$  defined in Eq. (A.6). Specifically, we find that the set of vertices

$$\{4W_0, K_2, K_5\} \quad (\text{A.11})$$

leads to the typical six-loop tadpole graph depicted in Fig. 1(a). Also, it is not difficult to see that the above graph is actually a harmful divergent one since the set of vertices in (A.11) satisfies the global constraint of Eq. (A.4), with  $n = 6$ ,  $D = 8 = \text{even}$ ,  $\sum_d V_d = 4$ , and  $\sum_d dV_d + \sum_d dU_d = \sum_d dU_d = 7$ .

## A.2 The $Z_7^R$ case

In this section we shall show that the symmetry  $Z_7^R$  prohibits the presence of all possible harmful tadpole divergences up to six loops. Following a line of arguments similar to the  $Z_5^R$  case, we conclude that only superpotential and Kähler-potential operators with  $d \leq 9$  are of interest in this case. Therefore, we list all possible vertices of  $d \leq 9$ , respecting the discrete  $R$ -symmetry  $\mathcal{Z}_7^R$  (cf. Eq. (2.9)):

$$\begin{aligned} W : \quad W_0 &\equiv \widehat{S}(\widehat{H}_1^T i\tau_2 \widehat{H}_2) \delta(\bar{\theta}) + \text{h.c.}, & W_2 &\equiv \frac{\widehat{S}^5}{M_{\text{P}}^2} \delta(\bar{\theta}) + \text{h.c.}, \\ W_3 &\equiv \frac{(\widehat{H}_1^T i\tau_2 \widehat{H}_2)^3}{M_{\text{P}}^3} \delta(\bar{\theta}) + \text{h.c.}, & W_5 &\equiv \frac{\widehat{S}^4(\widehat{H}_1^T i\tau_2 \widehat{H}_2)^2}{M_{\text{P}}^5} \delta(\bar{\theta}) + \text{h.c.}, \\ W_7 &\equiv \frac{\widehat{S}^8(\widehat{H}_1^T i\tau_2 \widehat{H}_2)}{M_{\text{P}}^7} \delta(\bar{\theta}) + \text{h.c.}, & W_8 &\equiv \frac{\widehat{S}^3(\widehat{H}_1^T i\tau_2 \widehat{H}_2)^4}{M_{\text{P}}^8} \delta(\bar{\theta}) + \text{h.c.}, \\ W_9 &\equiv \frac{\widehat{S}^{12}}{M_{\text{P}}^9} \delta(\bar{\theta}) + \text{h.c.} \end{aligned} \quad (\text{A.12})$$

$$K : \quad K_0^{(1)} \equiv \widehat{H}_1^\dagger \widehat{H}_1, \quad K_0^{(2)} \equiv \widehat{H}_2^\dagger \widehat{H}_2, \quad K_0^{(3)} \equiv \widehat{S}^* \widehat{S},$$

$$\begin{aligned}
K_3^{(1)} &\equiv \frac{\widehat{S}^3(\widehat{H}_1^T i\tau_2 \widehat{H}_2)}{M_{\text{P}}^3} + \text{h.c.}, & K_3^{(2)} &\equiv \frac{\widehat{S}^*(\widehat{H}_1^T i\tau_2 \widehat{H}_2)^2}{M_{\text{P}}^3} + \text{h.c.}, \\
K_4 &\equiv \frac{\widehat{S}^{*4}(\widehat{H}_1^T i\tau_2 \widehat{H}_2)}{M_{\text{P}}^4} + \text{h.c.}, & K_5 &\equiv \frac{\widehat{S}^7}{M_{\text{P}}^5} + \text{h.c.}, \\
K_6 &\equiv \frac{\widehat{S}^2(\widehat{H}_1^T i\tau_2 \widehat{H}_2)^3}{M_{\text{P}}^6} + \text{h.c.}, & K_8^{(1)} &\equiv \frac{\widehat{S}^6(\widehat{H}_1^T i\tau_2 \widehat{H}_2)^2}{M_{\text{P}}^8} + \text{h.c.}, \\
K_8^{(2)} &\equiv \frac{\widehat{S}^{*2}(\widehat{H}_1^T i\tau_2 \widehat{H}_2)^4}{M_{\text{P}}^8} + \text{h.c.}, & K_9^{(1)} &\equiv \frac{\widehat{S}(\widehat{H}_1^T i\tau_2 \widehat{H}_2)^5}{M_{\text{P}}^9} + \text{h.c.}, \\
K_9^{(2)} &\equiv \frac{\widehat{S}^{*5}(\widehat{H}_1^T i\tau_2 \widehat{H}_2)^3}{M_{\text{P}}^9} + \text{h.c.} .
\end{aligned} \tag{A.13}$$

Note that the symmetry  $\mathcal{Z}_7^R$  forbids the occurrence of superpotential operators of  $d = 1, 4, 6$  ( $W_1, W_4, W_6$ ) as well as of Kähler-potential terms of  $d = 1, 2, 7$  ( $K_1, K_2, K_7$ ).

As we did for the  $Z_5^R$  case, we shall determine all possible sets of vertices compatible with the conditions in Eq. (A.4) up to six loops. Again, it is not difficult to see that at the one-loop level ( $n = 1$ ), with  $\sum_d V_d = 0$  and  $\sum_d dU_d = 1$ , one is unable to find contributing operators. Furthermore, the absence of  $d = 1$  operators leads to the constraint

$$\sum_d dV_d + \sum_d dU_d = D - 1 > 1, \tag{A.14}$$

i.e.  $D > 2$ . This observation simplifies further the search for the existence of possible harmful tadpoles. Thus, for  $n = 2, 3, 4, 5$  and 6, we find the set of vertices:

**I.**  $n = 2$  :

$$\begin{aligned}
\text{a)} \quad D = 4, \quad \sum_d V_d = 0, \quad \sum_d dU_d = 3 : \\
\{K_3^{(i)}\}.
\end{aligned} \tag{A.15}$$

**II.**  $n = 3$  :

$$\begin{aligned}
\text{a)} \quad D = 4, \quad \sum_d V_d = 2, \quad \sum_d dV_d + \sum_d dU_d = 3 : \\
\{W_0, W_3\}, \quad \{2W_0, K_3^{(i)}\}; \\
\text{b)} \quad D = 6, \quad \sum_d V_d = 0, \quad \sum_d dU_d = 5 : \\
\{K_5\}.
\end{aligned} \tag{A.16}$$

**III.**  $n = 4$  :

$$\begin{aligned}
\text{a)} \quad D = 4, \quad \sum_d V_d = 4, \quad \sum_d dV_d + \sum_d dU_d = 3 : \\
\{3W_0, W_3\}, \quad \{4W_0, K_3^{(i)}\}; \\
\text{b)} \quad D = 6, \quad \sum_d V_d = 2, \quad \sum_d dV_d + \sum_d dU_d = 5 :
\end{aligned}$$

$$\begin{aligned}
& \{W_0, W_5\}, \quad \{W_2, W_3\}, \quad \{W_0, W_2, K_3^{(i)}\}, \quad \{2W_0, K_5\}; \\
\text{c)} \quad & D = 8, \quad \sum_d V_d = 0, \quad \sum_d dU_d = 7 : \\
& \{K_3^{(i)}, K_4\}.
\end{aligned} \tag{A.17}$$

IV.  $n = 5$  :

$$\begin{aligned}
\text{a)} \quad & D = 4, \quad \sum_d V_d = 6, \quad \sum_d dV_d + \sum_d dU_d = 3 : \\
& \{5W_0, W_3\}, \quad \{6W_0, K_3^{(i)}\}; \\
\text{b)} \quad & D = 6, \quad \sum_d V_d = 4, \quad \sum_d dV_d + \sum_d dU_d = 5 : \\
& \{3W_0, W_5\}, \quad \{2W_0, W_2, W_3\}, \quad \{3W_0, W_2, K_3^{(i)}\}, \quad \{4W_0, K_5\}; \\
\text{c)} \quad & D = 8, \quad \sum_d V_d = 2, \quad \sum_d dV_d + \sum_d dU_d = 7 : \\
& \{W_0, W_7\}, \quad \{W_2, W_5\}, \quad \{W_0, W_2, K_5\}, \\
& \{W_0, W_3, K_4\}, \quad \{2W_2, K_3^{(i)}\}, \quad \{2W_0, K_3^{(i)}, K_4\}; \\
\text{d)} \quad & D = 10, \quad \sum_d V_d = 0, \quad \sum_d dU_d = 9 : \\
& \{K_9^i\}, \quad \{K_4, K_5\}, \quad \{K_3^{(i)}, K_6\}, \quad \{K_3^{(i)}, K_3^{(j)}, K_3^{(k)}\};
\end{aligned}$$

V.  $n = 6$  :

$$\begin{aligned}
\text{a)} \quad & D = 4, \quad \sum_d V_d = 8, \quad \sum_d dV_d + \sum_d dU_d = 3 : \\
& \{7W_0, W_3\}, \quad \{8W_0, K_3^{(i)}\}; \\
\text{b)} \quad & D = 6, \quad \sum_d V_d = 6, \quad \sum_d dV_d + \sum_d dU_d = 5 : \\
& \{5W_0, W_5\}, \quad \{4W_0, W_2, W_3\}, \quad \{5W_0, W_2, K_3^{(i)}\}, \quad \{6W_0, K_5\}; \\
\text{c)} \quad & D = 8, \quad \sum_d V_d = 4, \quad \sum_d dV_d + \sum_d dU_d = 7 : \\
& \{3W_0, W_7\}, \quad \{2W_0, W_2, W_5\}, \quad \{W_0, 2W_2, W_3\}, \\
& \{2W_0, 2W_2, K_3^{(i)}\}, \quad \{3W_0, W_3, K_4\}, \quad \{3W_0, W_2, K_5\}, \\
& \{4W_0, K_3^{(i)}, K_4\}; \\
\text{d)} \quad & D = 10, \quad \sum_d V_d = 2, \quad \sum_d dV_d + \sum_d dU_d = 9 : \\
& \{W_0, W_9\}, \quad \{W_2, W_7\}, \quad \{2W_0, K_9^{(i)}\}, \\
& \{W_0, W_3, K_6\}, \quad \{2W_2, K_5\}, \quad \{W_0, W_5, K_4\}, \\
& \{W_2, W_3, K_4\}, \quad \{2W_3, K_3^{(i)}\}, \quad \{W_0, W_2, K_3^{(i)}, K_4\}, \\
& \{2W_0, K_3^{(i)}, K_6\}, \quad \{2W_0, K_4, K_5\}, \quad \{W_0, W_3, K_3^{(i)}, K_3^{(j)}\},
\end{aligned}$$

$$\begin{aligned}
& \{2W_0, K_3^{(i)}, K_3^{(j)}, K_3^{(k)}\}; \\
\text{e)} \quad & D = 12, \quad \sum_d V_d = 0, \quad \sum_d dU_d = 11 : \\
& \{K_3^{(i)}, K_8^{(j)}\}, \quad \{K_5, K_6\}, \quad \{K_3^{(i)}, 2K_4\}, \\
& \{K_3^{(i)}, K_3^{(j)}, K_5\}.
\end{aligned} \tag{A.18}$$

The indices  $i, j, k$  take admissible values according to Eq. (A.13). Again, we have carefully checked that terms linear in  $\hat{S}$  or  $\hat{S}^*$  do not survive when the product of all vertices within each set listed in Eqs. (A.15)–(A.18) is formed by formally replacing the bilinears  $\widehat{H}_1^\dagger \widehat{H}_1$ ,  $\widehat{H}_2^\dagger \widehat{H}_2$  and  $\widehat{S}^* \widehat{S}$  with 1.

Nevertheless, at the seven-loop level, we can still construct tadpole supergraphs by combining the renormalizable superpotential vertex  $W_0$  four times with the higher-dimensional Kähler-potential vertices  $K_3^{(1)}$  and  $K_6$  in Eq. (A.13). In other words, the set of vertices

$$\{4W_0, K_3^{(1)}, K_6\} \tag{A.19}$$

gives rise to the typical seven-loop tadpole graph of Fig. 1(b). Finally, we can check that the global constraint of Eq. (A.4) is satisfied, with  $n = 7$ ,  $D = 10 = \text{even}$ ,  $\sum_d V_d = 4$ , and  $\sum_d dV_d + \sum_d dU_d = \sum_d dU_d = 9$ .

## B The Peccei–Quinn-symmetric limit

In this appendix we shall derive the analytic expressions for the Higgs-boson masses and couplings pertinent to the two gauge-singlet SUSY extensions of the MSSM in the PQ-symmetric limit, i.e.  $\kappa/\lambda$ ,  $t_S$ ,  $m_{12}^2 \rightarrow 0$ . Of course, a kinematic situation close to the PQ-symmetric limit can more naturally be realized in the NMSSM rather than in the MNSSM where  $\lambda t_S/\mu$  is expected to be unsuppressed of order  $M_{\text{SUSY}}^2$ . Additionally, we shall assume that  $M_{H^+} \gg M_W$ . For notational simplicity, we have everywhere dropped the superscript (0), e.g. from  $M_{H^+}^{2(0)}$ ,  $M_a^{2(0)}$  etc., as all quantities involved in this appendix are evaluated at the tree level.

In the limit of a heavy  $H^+$ , the quantity  $\delta = \sqrt{\lambda^2 v^2 / (2M_a^2)}$  defined in Eq. (4.14) is much less than 1 and therefore serves as an expansion parameter in our calculations. In this limit, it is a reasonable approximation to set  $\mu$  to its value in the middle of the allowed  $\mu^2$ -interval determined by Eq. (4.13), i.e.  $\mu^2 = \mu_{\text{mid}}^2 = s_\beta^2 c_\beta^2 M_a^2$ , at which  $M_{H_1}$  is expected to approximately acquire its maximum. Then, the tree-level CP-even Higgs-boson mass

matrix  $M_S^2$  may be cast, up to terms of order  $\delta^2 M_a^2$ , into the approximately diagonal form:

$$(O^H)^T M_S^2 O^H = \begin{pmatrix} \frac{1}{2} \lambda^2 v^2 s_{2\beta}^2 & 0 & 0 \\ 0 & M_Z^2 c_{2\beta}^2 + \frac{1}{2} \lambda^2 v^2 s_{2\beta}^2 & \left(\frac{1}{2} \lambda^2 v^2 - M_Z^2\right) s_{2\beta} c_{2\beta} \\ 0 & \left(\frac{1}{2} \lambda^2 v^2 - M_Z^2\right) s_{2\beta} c_{2\beta} & M_a^2 + \frac{1}{2} \lambda^2 v^2 c_{2\beta}^2 - \left(\frac{1}{2} \lambda^2 v^2 - M_Z^2\right) s_{2\beta}^2 \end{pmatrix}, \quad (\text{B.1})$$

by virtue of the orthogonal matrix  $O^H$

$$O^H = \begin{pmatrix} \text{sign}(\lambda\mu) \delta s_{\beta} c_{2\beta} & c_{\beta} & -s_{\beta} (1 - \frac{1}{2} \delta^2 c_{2\beta}^2) \\ -\text{sign}(\lambda\mu) \delta c_{\beta} c_{2\beta} & s_{\beta} & c_{\beta} (1 - \frac{1}{2} \delta^2 c_{2\beta}^2) \\ 1 - \frac{1}{2} \delta^2 c_{2\beta}^2 & 0 & \text{sign}(\lambda\mu) \delta c_{2\beta} \end{pmatrix} + \mathcal{O}(\delta^3), \quad (\text{B.2})$$

where we have used the short-hand notation  $s_{2\beta} = \sin 2\beta$  and  $c_{2\beta} = \cos 2\beta$ .

Likewise, the orthogonal matrix  $O^A$ , which diagonalizes the CP-odd Higgs-boson mass matrix  $M_P^2$  in the PQ-symmetric limit, is easily found to be

$$O^A = \frac{1}{\sqrt{1 + \delta^2}} \begin{pmatrix} -\text{sign}(\lambda\mu) \delta & 1 \\ -1 & -\text{sign}(\lambda\mu) \delta \end{pmatrix}. \quad (\text{B.3})$$

In the PQ-symmetric limit, the CP-odd mass matrix  $M_P^2$  has one massless eigenstate  $A_1$  and one massive one  $A_2$ , with  $M_{A_2}^2 = M_a^2 + \frac{1}{2} \lambda^2 v^2$ .

Substituting Eqs. (B.2) and (B.3) into Eqs. (3.51) and (3.52), we obtain, up to order  $\delta^2$ , all the couplings  $H_i Z Z$  and  $H_i A_j Z$ :

$$\begin{aligned} g_{H_1 Z Z} &= 0, & g_{H_2 Z Z} &= 1, & g_{H_3 Z Z} &= 0, \\ g_{H_1 A_1 Z} &= -\delta^2 c_{2\beta}, & g_{H_2 A_1 Z} &= 0, & g_{H_3 A_1 Z} &= -\text{sign}(\lambda\mu) \delta, \\ g_{H_1 A_2 Z} &= \text{sign}(\lambda\mu) \delta c_{2\beta}, & g_{H_2 A_2 Z} &= 0, & g_{H_3 A_2 Z} &= 1 - \frac{\delta^2}{2} (1 + c_{2\beta}^2). \end{aligned} \quad (\text{B.4})$$



## References

- [1] A. Read, LEPC presentation on 20 July 2000, <http://lephiggs.web.cern.ch/LEPHIGGS>.
- [2] For recent studies, see G. Degrossi, P. Gambino, M. Passera and A. Sirlin, Phys. Lett. **B418** (1998) 209; S. Bauberger and G. Weiglein, Phys. Lett. **B419** (1998) 333; G. D'Agostini and G. Degrossi, Eur. Phys. J. **C10** (1999) 663.
- [3] J. Ellis, G. Ridolfi and F. Zwirner, Phys. Lett. **B257** (1991) 83; M.S. Berger, Phys. Rev. **D41** (1990) 225; Y. Okada, M. Yamaguchi and T. Yanagida, Prog. Theor. Phys. **85** (1991) 1; Phys. Lett. **B262** (1991) 54; H.E. Haber and R. Hempfling, Phys. Rev. Lett. **66** (1991) 1815; R. Barbieri, M. Frigeni and F. Caravaglios, Phys. Lett. **B258** (1991) 167; P.H. Chankowski, S. Pokorski and J. Rosiek, Phys. Lett. **B274** (1992) 191; J.R. Espinosa and M. Quirós, Phys. Lett. **B266** (1991) 389; J.L. Lopez and D.V. Nanopoulos, Phys. Lett. **B266** (1991) 397; M. Carena, K. Sasaki and C.E.M. Wagner, Nucl. Phys. **B381** (1992) 66; P.H. Chankowski, S. Pokorski and J. Rosiek, Phys. Lett. **B281** (1992) 100; Nucl. Phys. **B423** (1994) 437; D.M. Pierce, A. Papadopoulos and S.B. Johnson, Phys. Rev. Lett. **68** (1992) 3678; A. Brignole, Phys. Lett. **B281** (1992) 284; M. Drees and M.M. Nojiri, Phys. Rev. **D45** (1992) 2482; H.E. Haber and R. Hempfling, Phys. Rev. **D48** (1993) 4280; V. Barger, M.S. Berger and P. Ohmann, Phys. Rev. **D49** (1994) 4908; G.L. Kane, C. Kolda, L. Roszkowski and J.D. Wells, Phys. Rev. **D49** (1994) 6173; R. Hempfling and A.H. Hoang, Phys. Lett. **B331** (1994) 99; P. Langacker and N. Polonsky, Phys. Rev. **D50** (1994) 2199; J. Kodaira, Y. Yasui and K. Sasaki, Phys. Rev. **D50** (1994) 7035; J.A. Casas, J.R. Espinosa, M. Quirós and A. Riotto, Nucl. Phys. **B436** (1995) 3; (E) **B439** (1995) 466; M. Carena, J.R. Espinosa, M. Quirós and C.E.M. Wagner, Phys. Lett. **B355** (1995) 209; M. Carena, M. Quiros and C.E.M. Wagner, Nucl. Phys. **B461** (1996) 407; H.E. Haber, R. Hempfling and A.H. Hoang, Z. Phys. **C75** (1997) 539; S. Heinemeyer, W. Hollik and G. Weiglein, Phys. Lett. **B440** (1998) 96 and Phys. Rev. **D58** (1998) 091701; R.-J. Zhang, Phys. Lett. **B447** (1999) 89; J.R. Espinosa and R.-J. Zhang, JHEP **0003** (2000) 026 and hep-ph/0003246; M. Carena, S. Mrenna and C.E.M. Wagner, Phys. Rev. **D60** (1999) 075010; M. Carena, H.E. Haber, S. Heinemeyer, W. Hollik, C.E.M. Wagner and G. Weiglein, Nucl. Phys. **B580** (2000) 29.
- [4] L. Hall, J. Lykken and S. Weinberg, Phys. Rev. **D27** (1983) 2359; J.E. Kim and H.-P. Nilles, Phys. Lett. **B138** (1984) 150; G.F. Giudice and A. Masiero, Phys. Lett. **B206**

- (1988) 480; E.J. Chun, J.E. Kim and H.-P. Nilles, Nucl. Phys. **B370** (1992) 105; I. Antoniadis, E. Gava, K.S. Narain and T.R. Taylor, Nucl. Phys. **B432** (1994) 187.
- [5] P. Fayet, Nucl. Phys. **B90** (1975) 104; H.-P. Nilles, M. Srednicki and D. Wyler, Phys. Lett. **B120** (1983) 346; J.-M. Frere, D.R.T. Jones and S. Raby, Nucl. Phys. **B222** (1983) 11; J.-P. Derendinger and C.A. Savoy, Nucl. Phys. **B237** (1984) 307; B.R. Greene and P.J. Miron, Phys. Lett. **B168** (1986) 226; J. Ellis, K. Enqvist and D.V. Nanopoulos, K.A. Olive, M. Quiros and F. Zwirner, Phys. Lett. **B176** (1986) 403; L. Durand and J.L. Lopez, Phys. Lett. **B217** (1989) 463; M. Drees, Int. J. Mod. Phys. **A4** (1989) 3635; J. Ellis, J. Gunion, H. Haber, L. Roszkowski and F. Zwirner, Phys. Rev. **D39** (1989) 844; U. Ellwanger, Phys. Lett. **B303** (1993) 271; U. Ellwanger, M. Rausch de Taubenberg and C.A. Savoy, Phys. Lett. **B315** (1993) 331; Z. Phys. **C67** (1995) 665; Nucl. Phys. **B492** (1997) 21; P.N. Pandita, Phys. Lett. **B318** (1993) 338; Z. Phys. **C59** (1993) 575; T. Elliott, S.F. King and P.L. White, Phys. Lett. **B305** (1993) 71; Phys. Rev. **D49** (1994) 2435; Phys. Lett. **B351** (1995) 213; S.F. King and P.L. White, Phys. Rev. **D52** (1995) 4183; F. Franke and H. Fraas, Int. J. Mod. Phys. **A12** (1997) 479; U. Ellwanger and C. Hugonie, hep-ph/9909260; D.A. Demir, E. Ma and U. Sarkar, hep-ph/0005288; M. Bastero-Gil, C. Hugonie, S.F. King, D.P. Roy and S. Vempati, hep-ph/0006198; U. Ellwanger and C. Hugonie, hep-ph/0006222.
- [6] For example, see E.W. Kolb and M.S. Turner, “The Early Universe,” Addison-Wesley Publishing Co., 1990.
- [7] S.A. Abel, S. Sarkar and P.L. White, Nucl. Phys. **B454** (1995) 663.
- [8] H.-P. Nilles, M. Srednicki and D. Wyler, Phys. Lett. **B124** (1983) 337; A. B. Lahanas, Phys. Lett. **B124** (1983) 341; U. Ellwanger, Phys. Lett. **B133** (1983) 187.
- [9] J. Bagger and E. Poppitz, Phys. Rev. Lett. **71** (1993) 2380; J. Bagger, E. Poppitz and L. Randall, Nucl. Phys. **B455** (1995) 59; V. Jain, Phys. Lett. **B351** (1995) 481; C. Kolda, S. Pokorski and N. Polonsky, Phys. Rev. Lett. **80** (1998) 5263.
- [10] S.A. Abel, Nucl. Phys. **B480** (1996) 55.
- [11] C. Panagiotakopoulos and K. Tamvakis, Phys. Lett. **B446** (1999) 224.
- [12] C. Panagiotakopoulos and K. Tamvakis, Phys. Lett. **B469** (1999) 145.
- [13] P. Ciafaloni and A. Pomarol, Phys. Lett. **B404** (1997) 83.
- [14] J.C. Romao, Phys. Lett. **B173** (1986) 309.

- [15] Review of Particle Physics (D.E. Groom et al.), Eur. Phys. J. **C15** (2000) 1.
- [16] J.F. Gunion and H.E. Haber, Nucl. Phys. **B272** (1985) 1; J.F. Gunion and A. Turski, Phys. Rev. **D40** (1989) 2333.
- [17] S. Coleman and E. Weinberg, Phys. Rev. **D7** (1973) 1888.
- [18] M. Carena, J. Ellis, A. Pilaftsis and C.E.M. Wagner, hep-ph/0003180.
- [19] T. Elliott, S.F. King and P.L. White, Phys. Lett. **B305** (1993) 71; Phys. Rev. **D49** (1994) 2435.
- [20] J.F. Gunion, B. Grzadkowski, H.E. Haber and J. Kalinowski, Phys. Rev. Lett. **79** (1997) 982.
- [21] J.M. Moreno, D.H. Oaknin and M. Quirós, Nucl. Phys. **B483** (1997) 267; M. Carena, S. Mrenna and C.E.M. Wagner, Phys. Rev. **D62** (2000) 055008. A similar relation, although stated in a form of inequality, was also observed by J.R. Espinosa and D. Comelli, Phys. Lett. **B388** (1996) 793; J.R. Espinosa and J.F. Gunion, Phys. Rev. Lett. **82** (1999) 1084.
- [22] K.S. Babu and S.M. Barr, Phys. Rev. **D49** (1994) R2156; N. Haba, M. Matsuda and M. Tanimoto, Phys. Rev. **D54** (1996) 6928; S.W. Ham, S.K. Oh and H.S. Song, Phys. Rev. **D61** (2000) 055010.
- [23] S. Bertolini, F. Borzumati, A. Masiero and G. Ridolfi, Nucl. Phys. **B353** (1991) 591; R. Barbieri and G.F. Giudice, Phys. Lett. **B309** (1993) 86; R. Garisto and J.N. Ng, Phys. Lett. **B315** (1993) 372.
- [24] For example, see M. Carena, S. Pokorski and C.E.M. Wagner, Nucl. Phys. **B406** (1993) 59.
- [25] P. Binetruy and C. Savoy, Phys. Lett. **B327** (1992) 453; S.P. Martin and M.T. Vaughn, Phys. Rev. **D50** (1994) 2282.
- [26] G.K. Yegyan, hep-ph/9904488.
- [27] See, e.g. Report of the SUGRA Working Group Collaboration for Run II of the Tevatron, hep-ph/0003154.
- [28] A. Pilaftsis, Phys. Rev. **D58** (1998) 096010 and Phys. Lett. **B435** (1998) 88; A. Pilaftsis and C.E.M. Wagner, Nucl. Phys. **B553** (1999) 3; D.A. Demir, Phys. Rev. **D60**

- (1999) 055006; S.Y. Choi, M. Drees and J.S. Lee, Phys. Lett. **B481** (2000) 57; G.L. Kane and L.-T. Wang, hep-ph/0003198; T. Ibrahim and P. Nath, hep-ph/0008237.
- [29] The Fortran code `cph.f` is available from <http://home.cern.ch/p/pilaftsi/www/>.
- [30] Carlos Wagner, private communication.
- [31] B.A. Dobrescu and K.T. Matchev, hep-ph/0008192.
- [32] G.F. Giudice, E.W. Kolb and A. Riotto, hep-ph/0005123.

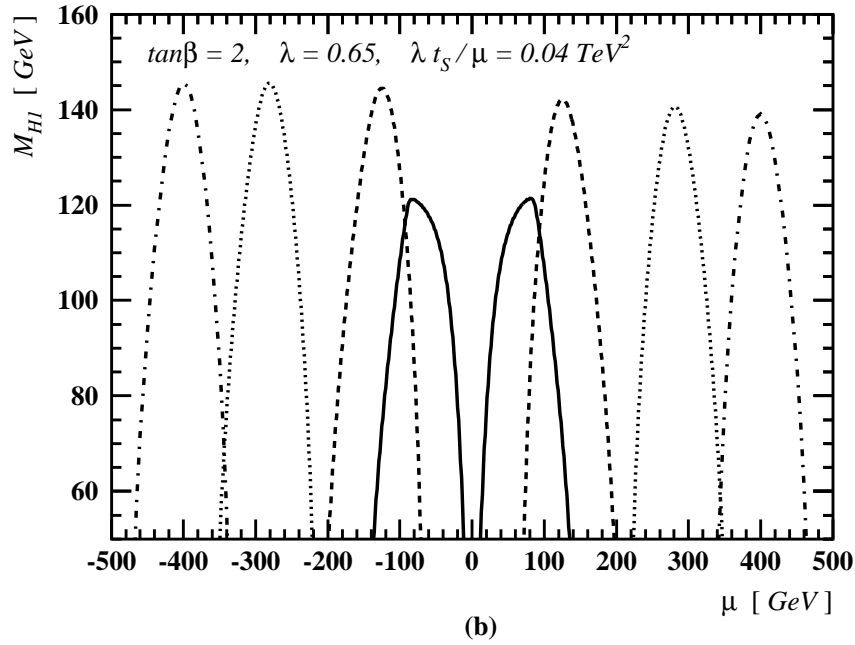
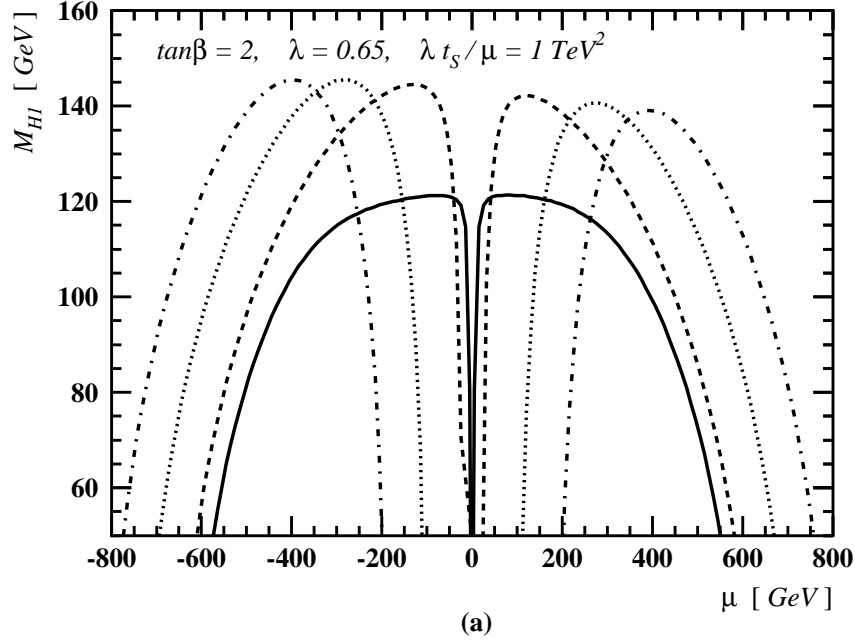


Figure 2: Numerical predictions for  $M_{H_1}$  as a function of  $\mu$  in the MNSSM with  $m_{12}^2 = 0$ , for  $M_{H^\pm} = 0.1$  (solid line),  $0.3$  (dashed line),  $0.7$  (dotted line),  $1$  (dash-dotted line) TeV.

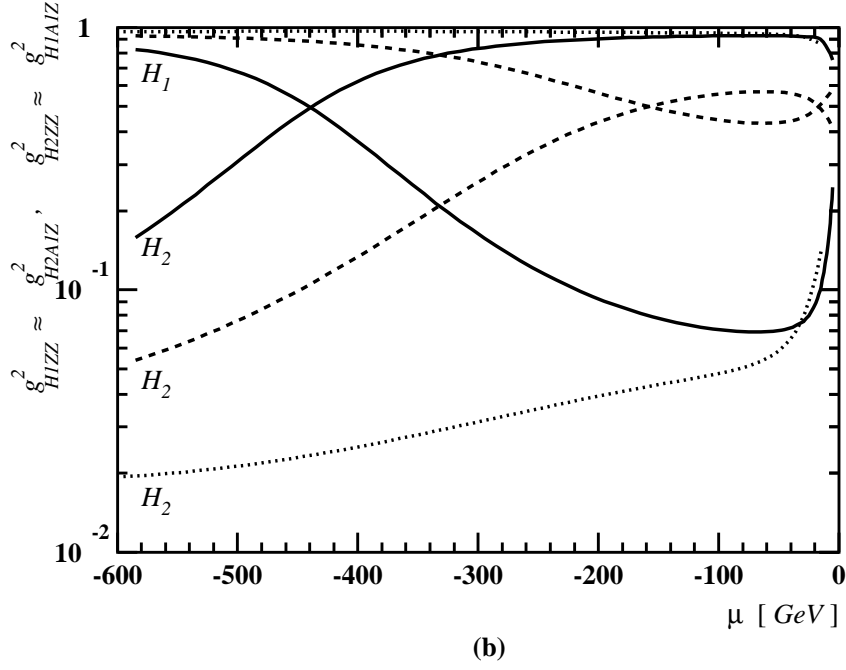
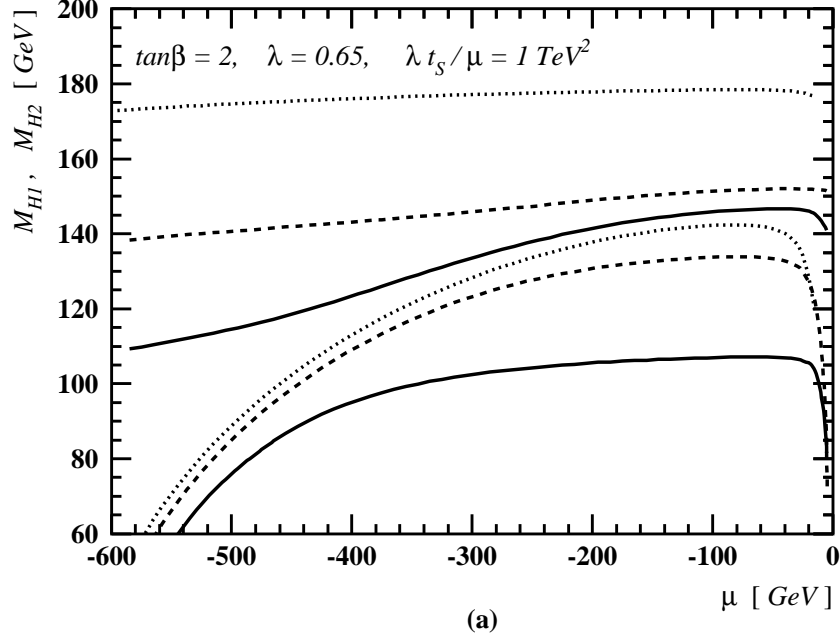


Figure 3: Numerical estimates of (a)  $M_{H_1}$  and  $M_{H_2}$  and of (b)  $g_{H_1 ZZ}^2$  and  $g_{H_2 ZZ}^2$ , as functions of  $\mu$  in the MNSSM with  $m_{12}^2 = 0$ , for  $M_{H^+} = 80$  (solid line), 120 (dashed line) and 160 (dotted line) GeV.

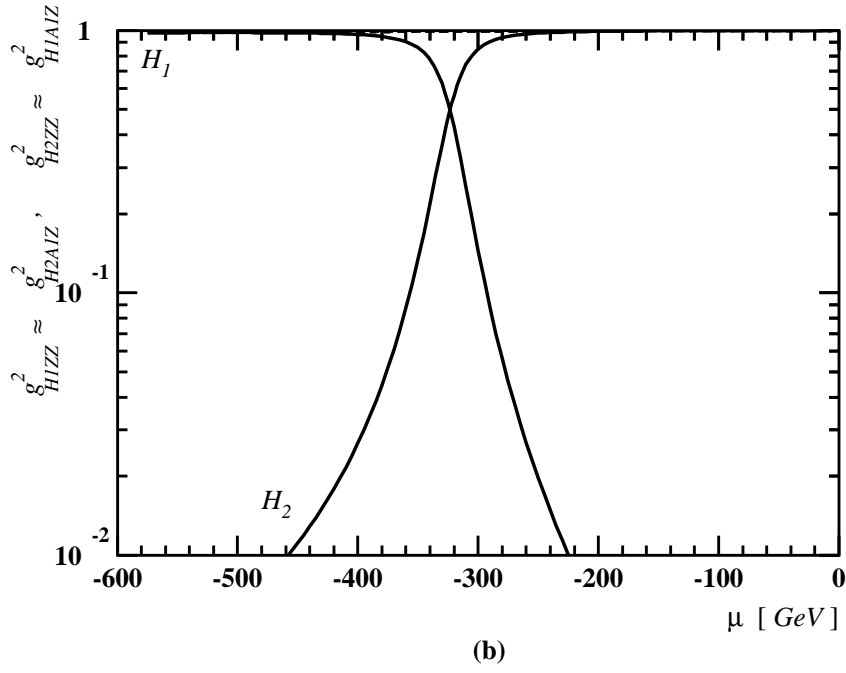
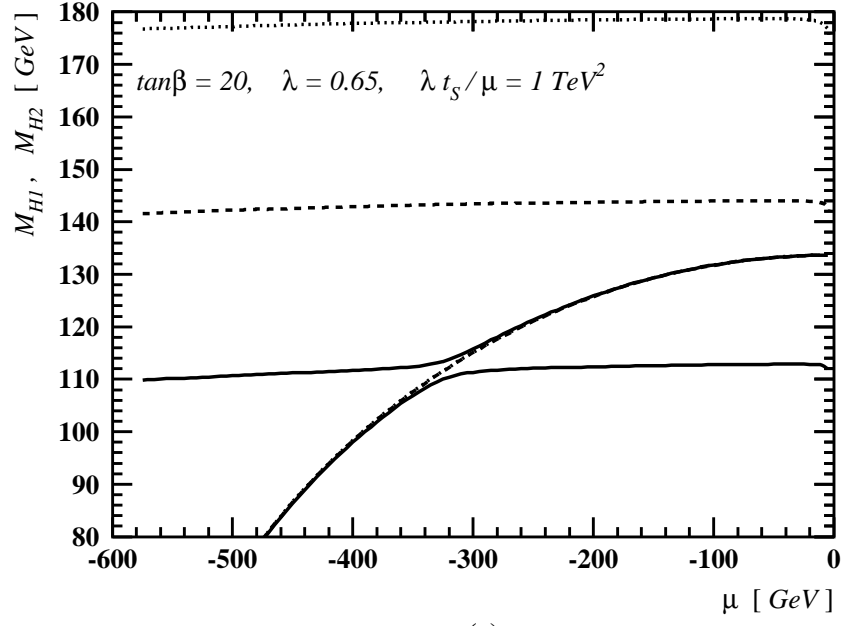
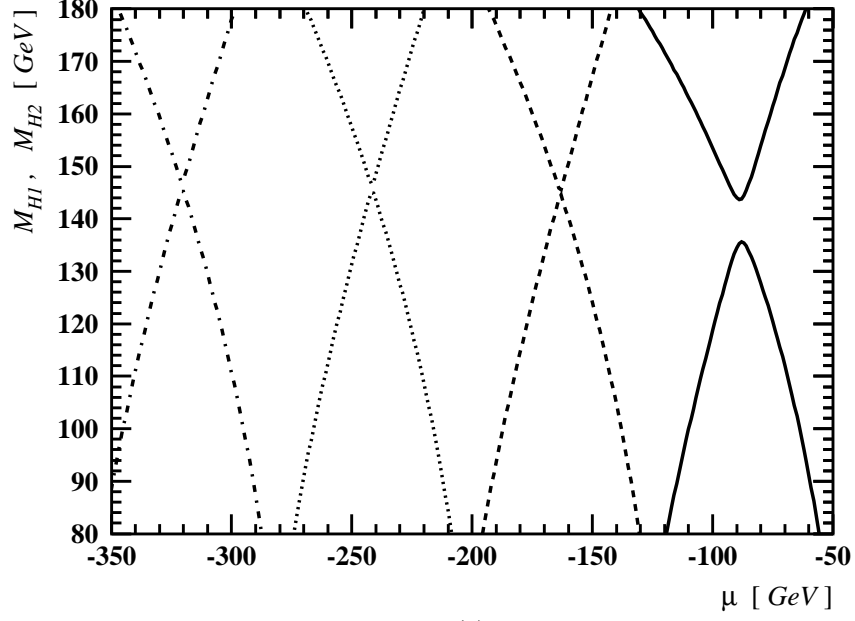
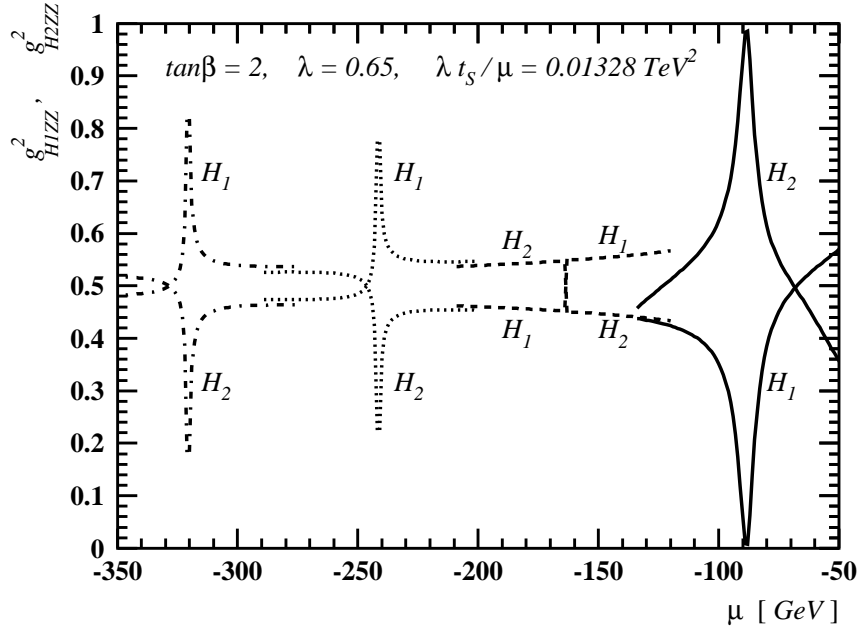


Figure 4: The same as in Fig. 3, but with  $\tan \beta = 20$ .



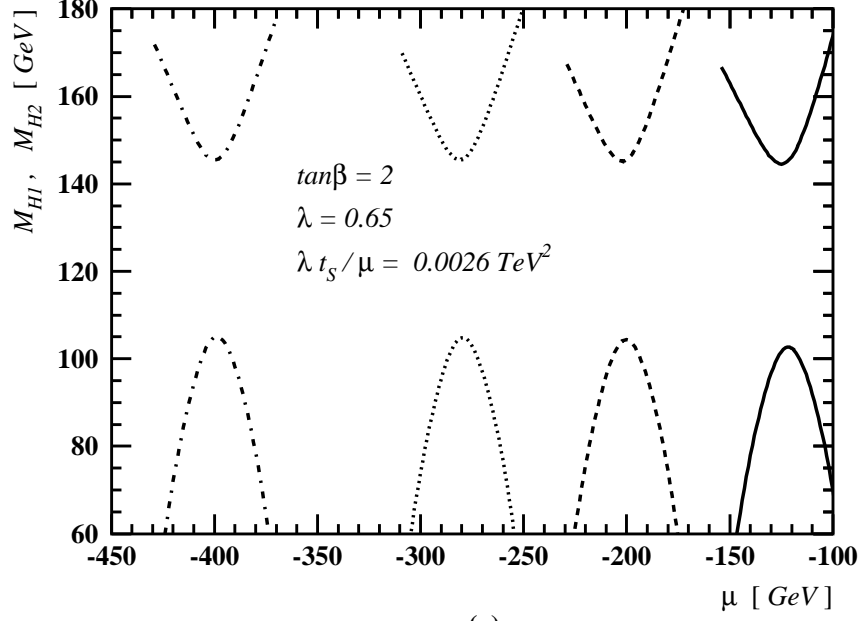
(a)



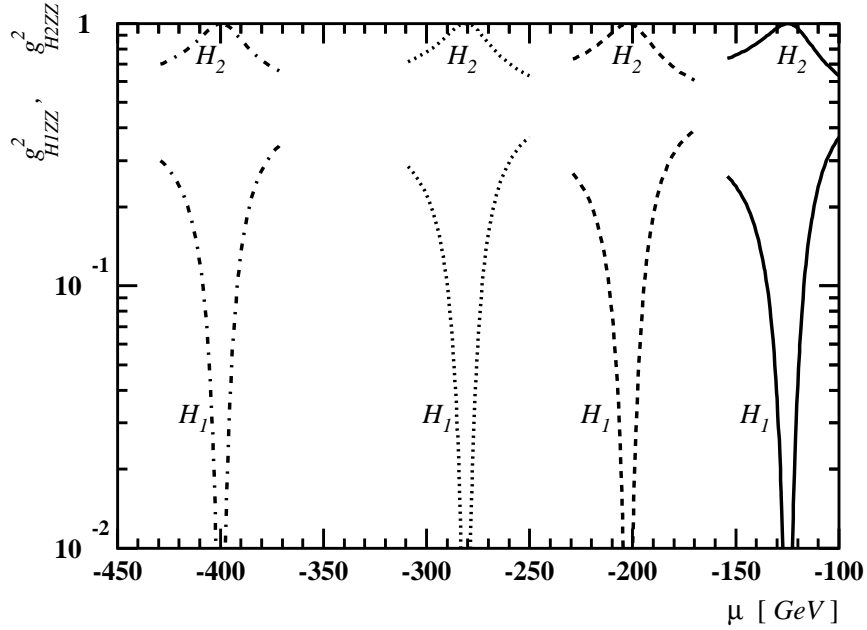
(b)

Figure 5: Numerical estimates of (a)  $M_{H_1}$  and  $M_{H_2}$  and of (b)  $g_{H_1ZZ}^2$  and  $g_{H_2ZZ}^2$ , as functions of  $\mu$  in the MNSSM with  $m_{12}^2 = 0$ , for  $M_{H^+} = 0.2$  (solid line), 0.4 (dashed line), 0.6 (dotted line) and 0.8 (dash-dotted line) TeV.





(a)



(b)

Figure 6: Numerical predictions for (a)  $M_{H_1}$  and  $M_{H_2}$  and for (b)  $g_{H_1ZZ}^2$  and  $g_{H_2ZZ}^2$ , as functions of  $\mu$  in the MNSSM with  $m_{12}^2 = 0$ , for  $M_{H^+} = 0.3$  (solid line), 0.5 (dashed line), 0.7 (dotted line) and 1 (dash-dotted line) TeV.

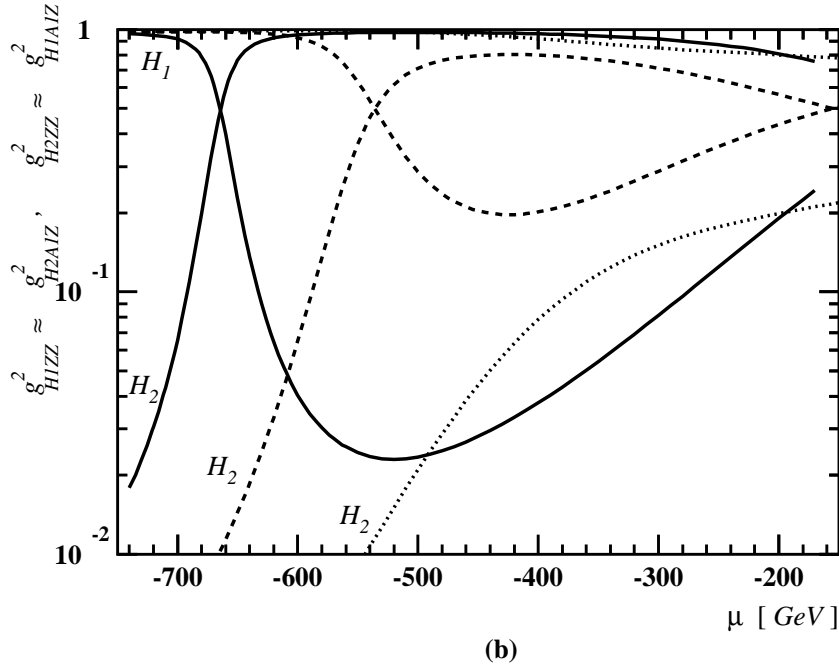
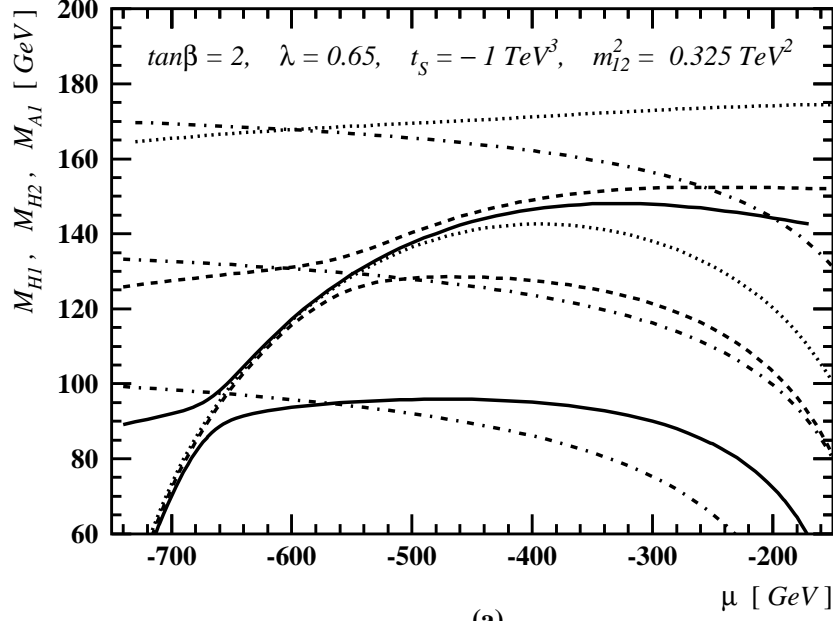


Figure 7: Numerical predictions for (a)  $M_{H_1}$ ,  $M_{H_2}$  and  $M_{A_1}$ , and for (b)  $g_{H_1ZZ}^2$  and  $g_{H_2ZZ}^2$ , as functions of  $\mu$  in the MNSSM, for  $M_{H^+} = 80$  (solid line), 120 (dashed line) and 160 (dotted line) GeV. Numerical estimates of  $M_{A_1}$  are indicated by dash-dotted lines.

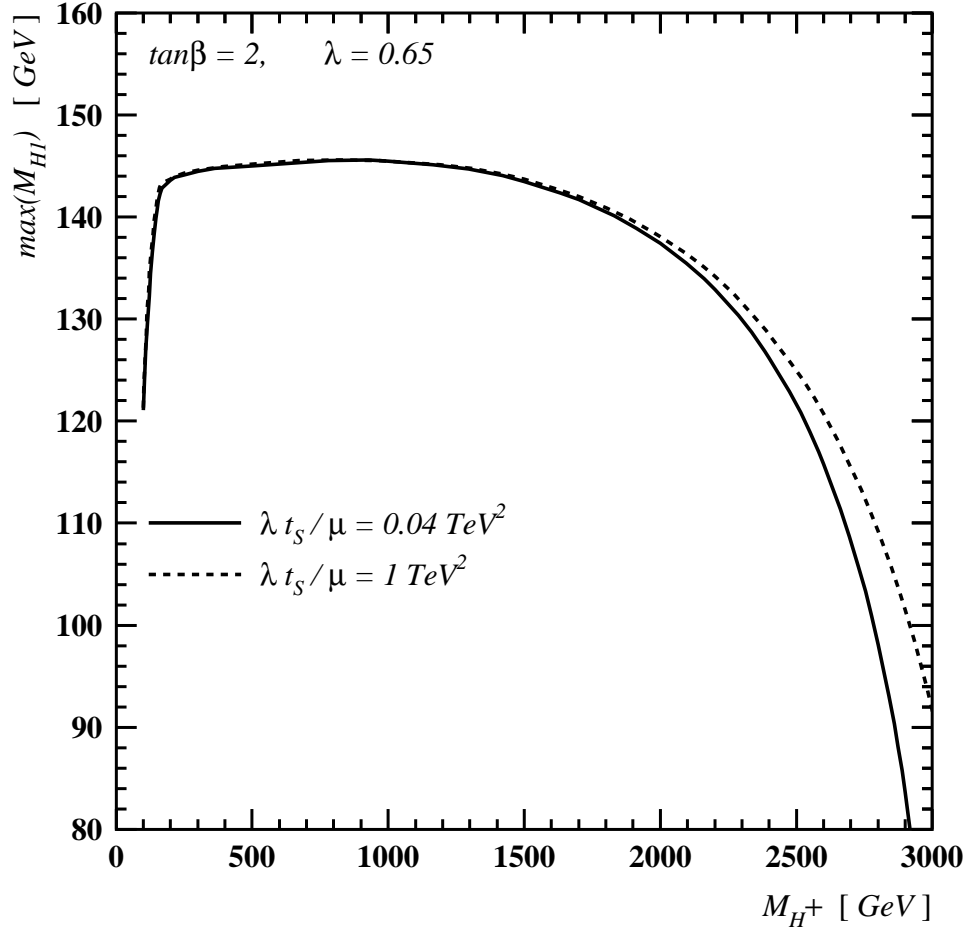


Figure 8: The maximal predicted value of  $M_{H_1}$  as a function of the charged Higgs-boson mass  $M_{H^+}$  in the MNSSM with  $m_{12}^2 = 0$ .

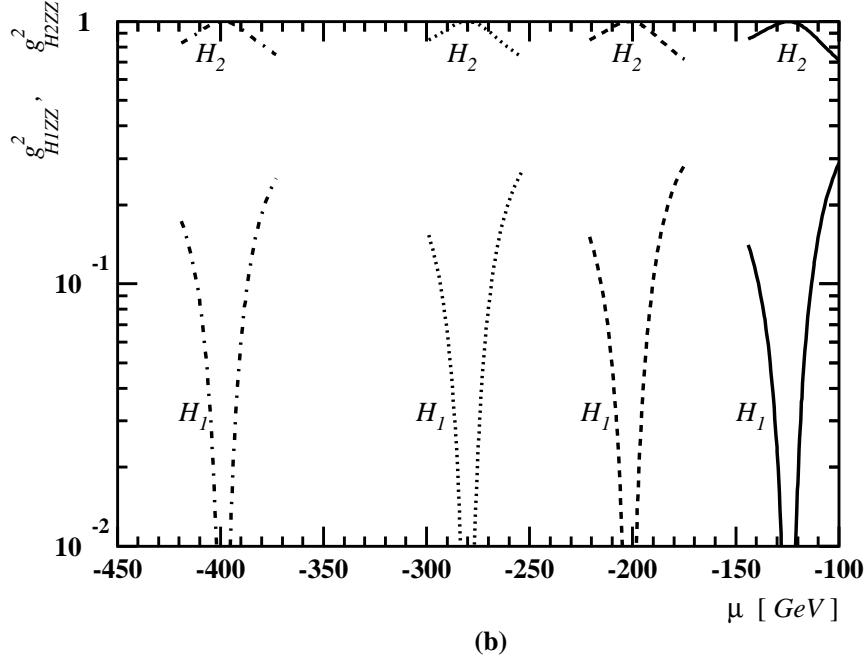
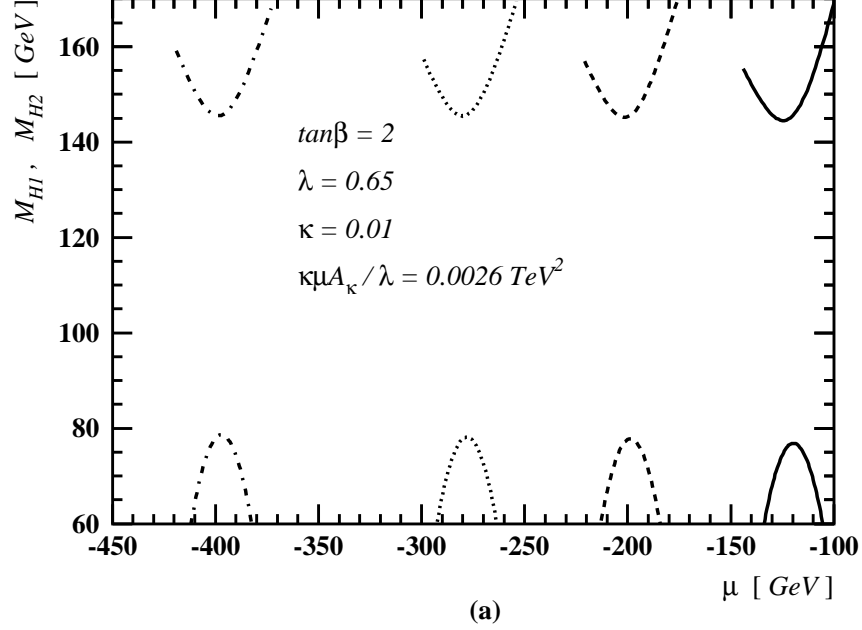
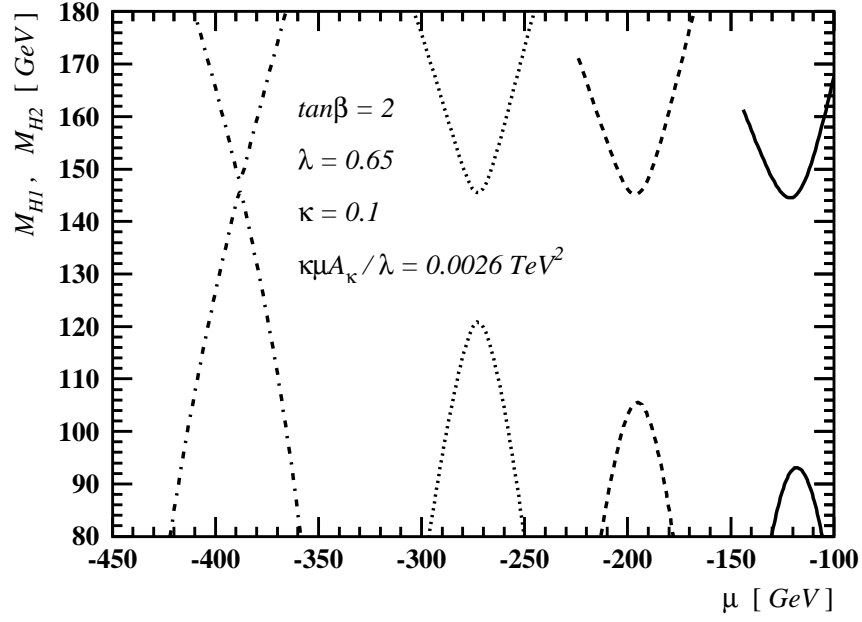
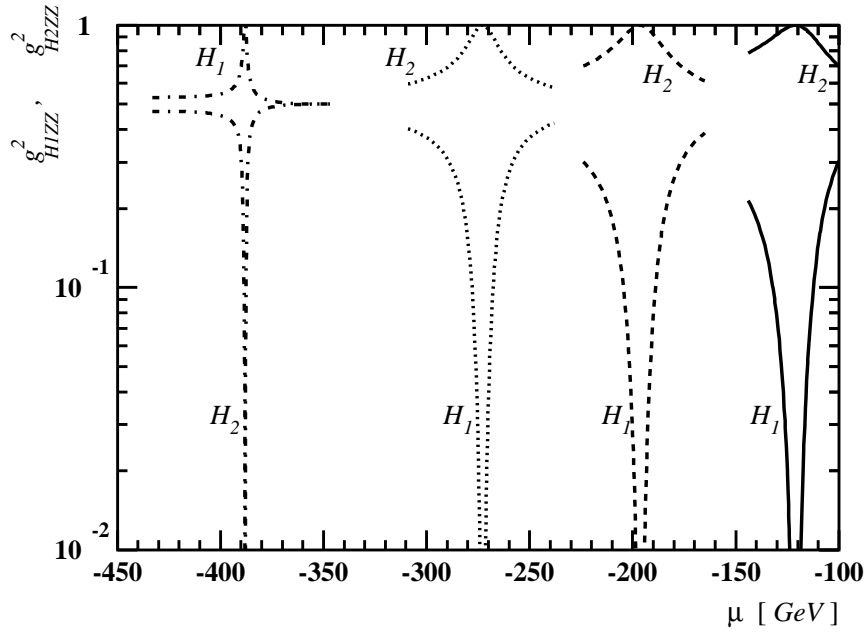


Figure 9: Numerical estimates of (a)  $M_{H_1}$  and  $M_{H_2}$  and of (b)  $g_{H_1ZZ}^2$  and  $g_{H_2ZZ}^2$  as functions of  $\mu$  in the NMSSM, for  $M_{H^+} = 0.3$  (solid line), 0.5 (dashed line), 0.7 (dotted line) and 1 (dash-dotted line) TeV.

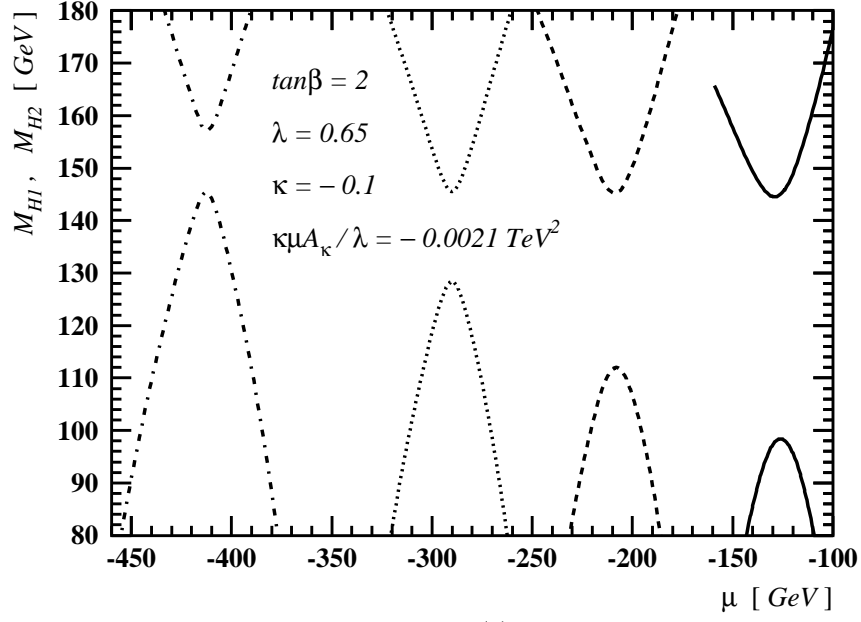


(a)

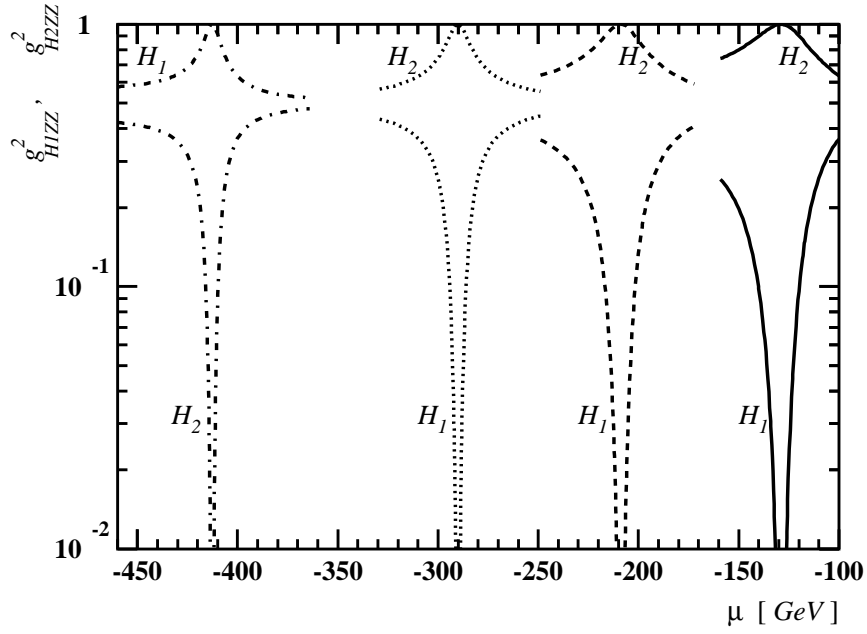


(b)

Figure 10: The same as in Fig. 9, but with  $\kappa = 0.1$ .



(a)



(b)

Figure 11: The same as in Fig. 9, but with  $\kappa = -0.1$  and  $\kappa\mu A_\kappa/\lambda = -0.0021 \text{ TeV}^2$ .

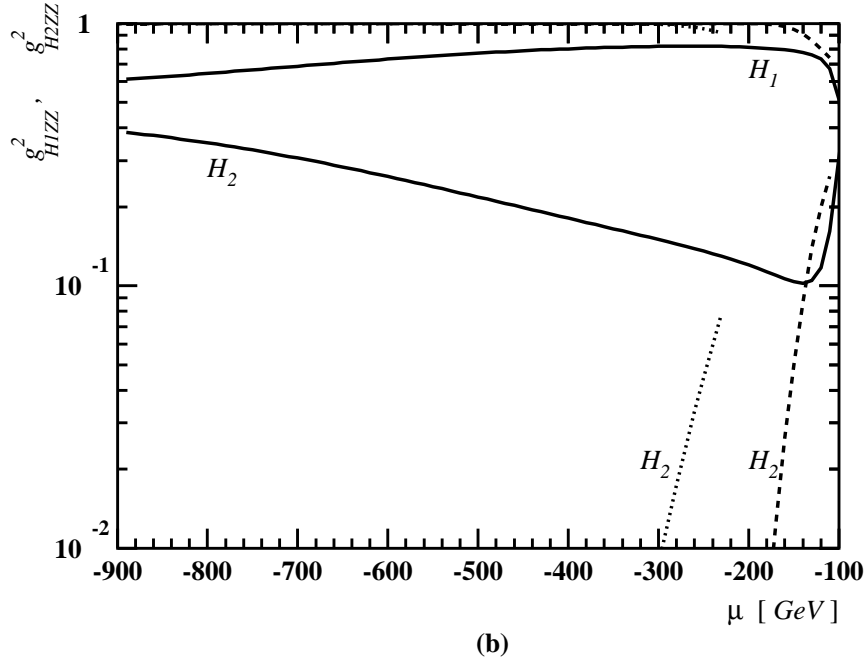
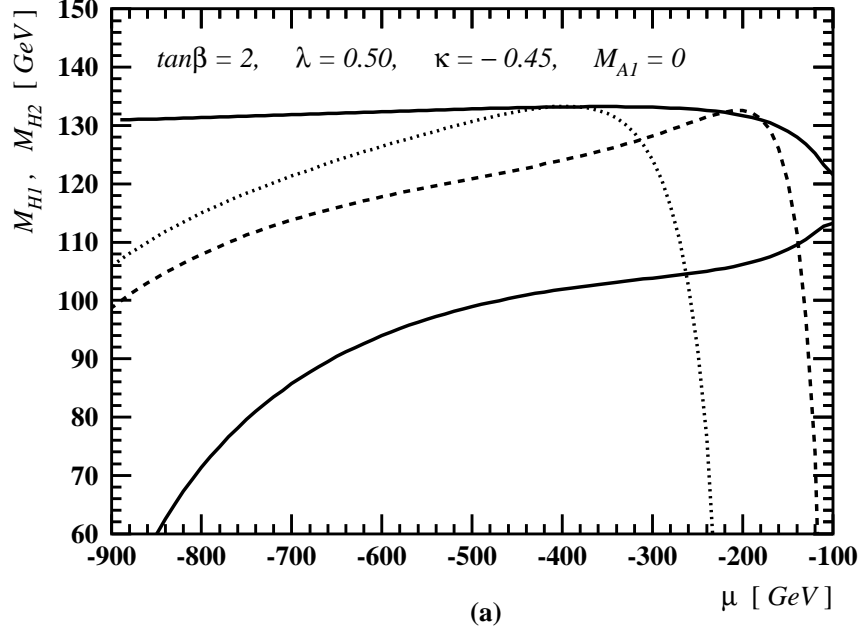


Figure 12: Numerical estimates of (a)  $M_{H_1}$  and  $M_{H_2}$  and of (b)  $g_{H_1ZZ}^2$  and  $g_{H_2ZZ}^2$  as functions of  $\mu$  in the NMSSM, with the constraint  $M_{A_1} = 0$ , for  $M_{H^+} = 120$  (solid line), 400 (dashed line) and 800 (dotted line) GeV.